

POLITECNICO DI TORINO

FACOLTÀ DI INGEGNERIA

Corso di Laurea in Ingegneria Biomedica

Tesi di Laurea Magistrale

**3D microfluidic model of Small Cell Lung
Carcinoma to validate targeted therapies against
B7-H3 positive tumor cells and vasculature**



Advisor

Prof. Valeria Chiono

Co-advisors

Dr. Marco Campisi

Dr. Navin Mahadevan

Prof. David A. Barbie

Candidate

Carla Stornante

December 2023

A mia nonna Franca, le profonde radici

A mio nipote Marco, nuovo bocciolo

del mio albero della vita

Contents

Abstract.....	9
----------------------	----------

Chapter I

Introduction.....	11
--------------------------	-----------

1.1 Introduction to Lung Cancer	11
---------------------------------------	----

1.2 Background and Significance of Small Cell Lung Cancer (SCLC).....	12
---	----

1.3 Lung Tumor Microenvironment.....	13
--------------------------------------	----

1.3.1 Anatomy of Lung	13
-----------------------------	----

1.3.2 SCLC origins within the lungs	15
---	----

1.3.3 Cellular components.....	15
--------------------------------	----

1.3.3.1 Tumor cells: molecular subtypes and emerging biomarkers	16
---	----

1.3.3.2 Vascular and stromal cells.....	17
---	----

1.3.3.3 Immune cells	20
----------------------------	----

1.4 Different types of TIME and vascular effect	23
---	----

1.5 Current challenges in SCLC treatment and patient outcomes	25
---	----

1.5.1 Standard of care for SCLC	26
---------------------------------------	----

1.5.2 Novel treatments (cell therapies and targeted therapies).....	26
---	----

1.5.2.1 Cell immunotherapy (adoptive therapies, CAR-T, CAR-NK)	27
--	----

1.5.2.2 Targeted therapies	28
----------------------------------	----

1.5.2.3 CD276/B7H3 as a promising target for SCLC	34
---	----

1.6 <i>In vitro</i> and <i>in vivo</i> pre-clinical models and introduction to microfluidic technology.....	37
--	----

1.6.1 The 3R principle and the need for reliable <i>in vitro</i> models in cancer research.....	38
--	----

1.6.2 Introduction to microfluidics.....	40
--	----

1.6.3 <i>In vitro</i> SCLC TME modeling using a microfluidic device	43
---	----

1.6.4 Microfluidic device as a platform for testing anticancer therapies	44
---	----

1.7 Research aims: study rationale, significance, purposes and objectives	45
---	----

Chapter II

Materials and methods	49
2.1 Cell culture.....	49
2.2 2D Viability assay	54
2.2.1 NK cell-mediated cytotoxicity	54
2.2.2 B7H3-ADC - mediated cytotoxicity.....	55
2.3 ELISA	57
2.4 Flow-cytometry.....	58
2.5 Design and fabrication of microfluidic device.....	58
2.6 3D TIME models	59
2.6.1 Tumor spheroids culture.....	59
2.6.2 Tumor spheroids – NK cells coculture	60
2.7 Blood vessel formation: 3D macrovessel.....	61
2.7.1 Tumor spheroids culture - vascular barrier – NK cells	62
2.8 Blood vessel formation: vasculogenesis model	63
2.9 Immunofluorescent (IF) microscope imaging.....	67
2.10 3D Viability assay using a microfluidic device.....	69
2.11 3D Migration assay: measurements and quantification	69
2.12 3D permeability assay using a microfluidic device	70

Chapter III

Results	73
3.1 Evaluation of B7H3 expression in SCLC TME: B7H3 is mainly upregulated on Non-Neuroendocrine SCLC and vasculature.....	73
3.2 Evaluation of the B7H3-ADC's ability to selectively bind the target: B7H3-ADC selectively binds to B7H3 ⁺	74
3.3 Evaluation of B7H3-ADC's tumoricidal effect: B7H3-ADC is cytotoxic on Non-NE SCLC and vascular components in 2D viability assay.....	75

3.4 Evaluation of B7H3-ADC's effect on <i>in vivo</i> -like vasculature: B7H3-ADC is effective on microvascular network in a 3D viability assay	76
3.5 Evaluation of the B7H3-ADC effect on the vascular structure: B7H3-ADC enhances vascular permeability in a 3D permeability assay	77
3.6 Investigation of the role of the vasculature in immune cell trafficking: The vasculature acts as a barrier to NK cell infiltration in a 3D migration assay.	85
3.7 Evaluation of NK cells' cytotoxic effect on SCLC molecular subtypes in a 2D co-culture: Neuroendocrine-SCLC is sensitive to NK-cell mediated cytotoxicity in a 2D viability assay	85
3.8 Evaluation of NK cells' cytotoxic effect on SCLC molecular subtypes in a 3D MPS: Neuroendocrine-SCLC is sensitive to NK-cell mediated cytotoxicity in a 3D viability assay	86

Chapter IV

Discussion.....	90
------------------------	-----------

Conclusion.....	98
------------------------	-----------

References	101
-------------------------	------------

Acknowledgements

I would like to express my sincere appreciation to my esteemed supervisor, Professor Valeria Chiono, for her unwavering patience, constant support, and trust in me during the course of my thesis project. I am immensely grateful for her enthusiastic embrace of this project, which has inspired in me a deep passion for the field of biomedical engineering that has persisted throughout my entire tenure at Politecnico di Torino. Her steadfast commitment to the discipline of biomedical engineering has been a source of inspiration for me, and I am truly grateful for the opportunity to learn from her expertise and experience.

I am deeply grateful to my mentors, Marco Campisi and Navin Mahadevan, for their outstanding guidance and unwavering support throughout my research journey for this thesis. Their remarkable patience, dedicated attention, and words of encouragement during difficult moments have been instrumental in shaping the quality of my research. Their exceptional commitment and expertise have greatly enriched my academic experience, providing invaluable insights and wise counsel at every stage of the process.

Last but not least, I extend my sincere appreciation to Professor David A. Barbie for his steadfast commitment and inspiring guidance, which has fostered my interest in the area of study. Since my initiation into the Barbie Lab, I have been warmly welcomed experiencing a sense of comfort and inclusivity. I was always been supported through the challenges, which has resulted in one of the most rewarding experiences of my life. His trust and dedication have significantly enriched my learning experience, and I am eager to apply the skills I have acquired in my future professional endeavors.

List of figures

FIGURE 1.1 Schematic of SCLC masses within the bronchi in the lungs.	15
FIGURE 1.2 MHC I expression in SCLC patients with non-neuroendocrine features..	17
FIGURE 1.3 Schematic of SCLC TME	18
FIGURE 1.4 Schematic of T cells and NK cells' mechanism of tumor cell targeting and killing.....	22
FIGURE 1.5 Schematic of the different types of TIME	24
FIGURE 1.6 Mechanism of action of an ADCC.....	30
FIGURE 1.7 Clinically Tested ADCs.....	31
FIGURE 1.8 Structure of a generic ADC.....	31
FIGURE 1.9 Schematic of ADC's mechanism of action	32
FIGURE 1.10 Schematic of the aim of the study.....	48
FIGURE 2.1 Screenshot from Countess Cell Counter	51
FIGURE 2.2 2D viability assay.....	57
FIGURE 2.3 Schematic of the microfluidic device used in this study	59
FIGURE 2.4 Schematics of 3D culture models in microfluidic device	66
FIGURE 2.5 Region of interest (ROIs = yellow bordered rectangles) of the IF images considered in the quantification analysis.	72
FIGURE 3.1 Flow cytometry of the B7-H3 expression.....	78
FIGURE 3.2 Flow cytometry of anti-hIgG expression for the binding assay.....	78
FIGURE 3.3 Plots of the CTG viability assay quantification analysis	79
FIGURE 3.4 Optical microscope representative images of the different target cells cultures	81
FIGURE 3.5 3D Viability assay on the MVN model after 6 days treatments. ...	82

FIGURE 3.6 IF representative images of the MVN models after 6 days under the different treatments.....	83
FIGURE 3.7 3D permeability assay on the macrovessel model after 6 days treatments	84
FIGURE 3.8 3D migration assay.	87
FIGURE 3.9 HLA-ABC expression (representative of the MHC I) on our cell lines panel and 2D viability assay quantification analysis.	88
FIGURE 3.10 3D viability assay on Tumor cells – NK cells co-culture	89

List of tables

TABLE 1.1 Fabrication technique used for the design of microfluidic device... 42	42
TABLE 2.1 Panel of the cell lines used in this study	53
TABLE 2.2 List of antibodies used for flow cytometry and FACS.	58
TABLE 2.3 NK cell tracker reagents used in this study and experimental conditions.....	60
TABLE 2.4 IF staining reagents and experimental conditions	68

Abstract

Small cell lung carcinoma (SCLC) is a type of lung cancer that accounts for about 15% of all lung cancer cases. Although SCLC patients initially respond to chemotherapy and immune checkpoint blockade (ICB), however, resistance invariably emerges. Currently, there are no predictive biomarkers of response, and patients with SCLC continue to have a poor prognosis with limited treatment options.

Recent multiparametric profiling of SCLC cell lines and patient samples has revealed significant inter-tumoral and intra-tumoral heterogeneity. Non-neuroendocrine (Non-NE) SCLC exhibits increased innate immune signaling and robust upregulation of antigen presentation on MHC-I, whereas neuroendocrine (NE) SCLC subpopulations downregulate MHC-I. Based on this, MHC-I low SCLC was predicted to be vulnerable to NK cell-mediated control. However, the MHC-I low SCLC tumor-immune microenvironment (TIME) is characterized by a scarcity of immune cells, possibly due to the vascular barrier in the absence of sufficient chemokine gradients.

In the context of novel therapeutic approaches, Antibody-Drug Conjugate (ADC)-based therapies are focused on targeting cell-surface proteins selectively expressed by malignant cells. Recently, there has been increased interest in B7-H3/CD276, whose dual overexpression on tumor and tumor-associated vasculature provides an opportunity for the development of therapies that simultaneously target and destroy both the tumor cells and the tumor vasculature, preserving healthy tissues.

In this thesis, we developed an advanced MicroPhysiological System (MPS) using a microfluidic technology, that is highly adaptable and precisely controlled, enabling it to replicate TIME biology. Through this platform, we modeled the interaction between solid tumor (in terms of SCLC spheroids) and immune cells in the presence of a vascular barrier and external stimuli, and we used it to explore various strategies to test cell therapies and explore the mechanisms of B7-H3 targeted ADC-based therapy, which drug is currently in phase 1/2 clinical trial.

Firstly, the CD276/B7H3 protein is mainly upregulated in non-NE SCLC and vasculature, we tested the efficacy of an ADC designed to target CD276/B7H3 positive cells. The compound demonstrated cytotoxicity against non-NE SCLC spheroids in a 2D viability assay. Furthermore, B7H3-ADC cytotoxicity was tested on vascular elements in a self-assembled 3D microvascular network assay. The impact on disrupting vasculature was confirmed by 3D permeability assay on a macrovessel model. Then, using a 3D model of vascular extravasation, we have confirmed that vascular priming leads to enhanced vascular permeability and the promotion of NK cell extravasation. Similarly, since B7H3 causes vascular disruption, lead us to believe that it could stimulate immune cell infiltration. We then demonstrated that NE-SCLC appears to be vulnerable to natural killer (NK) cell-mediated cytotoxicity triggered by natural killer (NK) cells in a 2D and 3D viability co-culture assay, suggesting that once NK cells can cross the vascular barrier, they are able to eradicate the tumor.

Our MPS platform has proven to be a promising tool for exploring and testing strategies testing novel targeted therapies, offering a bridge for translational medicine purposes toward better outcomes for cancer patients.

Chapter I

Introduction

1.1 Introduction to Lung Cancer

Lung cancer represents one of the most prevalent and lethal malignancies worldwide, contributing significantly to cancer-related morbidity and mortality, with an incidence rate of 11.4% and 18% of cancer-related deaths [1]. It arises from the uncontrolled growth of cells in the lung tissues, leading to the formation of malignant metastasis, most commonly in the brain, bone, and liver, and it is commonly categorized into two main histological types: Small Cell Lung Carcinoma (SCLC) and Non-Small Cell Lung Carcinoma (NSCLC) [2]. These subtypes exhibit distinct biological characteristics, clinical behavior, and treatment approaches.

SCLC accounts for approximately 10-15% of all lung cancer cases and is characterized by its rapid growth, early metastasis, strong association with smoking and poor prognosis. Histologically, SCLC is characterized by small, round cells with neuroendocrine features. It is often classified into limited-stage (LS) and extensive-stage disease (ES) based on the extent of metastasis [3]. Despite its initial sensitivity to chemotherapy, SCLC frequently becomes resistant to treatment, necessitating novel therapeutic strategies [4].

NSCLC comprises the majority of lung cancer cases (approximately 85-90%) and is further divided into three main histological subtypes: adenocarcinoma, squamous cell carcinoma, and large cell carcinoma. Adenocarcinoma is the most prevalent type, constituting 40% of all lung cancers and is commonly found in individuals who do not smoke. In contrast, squamous cell carcinomas, accounting for 25-30% of all lung cancers, are primarily linked to those with a smoking history. Large cell carcinoma is the least frequent form and comprises only 10-15% of instances [5]. Each subtype has distinct morphological features, genetic alterations, and clinical behavior. NSCLC groups together subtypes that start from different types of lung cells due to their similar treatment and prognosis. Advancements in molecular profiling have led to identifying specific driver mutations and genetic alterations that guide targeted therapies in NSCLC [6]. In this context, the most recurrent are KRAS mutations (25%), EGFR mutations (15%) and ALK rearrangements (5%-7%) [7].

From the clinical significance point of view, the distinction between SCLC and NSCLC subtypes is crucial for treatment decisions, prognosis estimation, and research endeavors. SCLC's rapid progression and limited treatment options underscore the need for innovative therapeutic approaches [8]. At the same time, NSCLC's diverse subtypes highlight the importance of personalized treatment strategies based on genetic and molecular profiles [9].

1.2 Background and Significance of Small Cell Lung Cancer (SCLC)

Small Cell Lung Carcinoma (SCLC) occupies a distinct position within the spectrum of lung cancer due to its aggressive behavior, rapid progression, and unique biological characteristics, and represents a formidable challenge in oncology [4]. The epidemiological landscape of SCLC is closely intertwined with the prevalence of tobacco use. Smoking, a well-established risk factor for lung cancer, particularly predisposes individuals to SCLC development, reflecting the significant impact of environmental factors on its etiology [10].

Patients with SCLC face an exceptionally poor prognosis, with a five-year overall survival (OS) of 7% [11].

SCLC is a high-grade neuroendocrine carcinoma that arises the breathing tubes (bronchi) in the center of the chest, and virtually all tumors display a loss of some tumor suppressor genes. Compared to NSCLCs, SCLCs are genomically homogeneous and almost always have functional inactivation of RB1 and TP53 genes without actionable mutations [12]. Although cytotoxic chemotherapy may yield a positive response initially, resistance inevitably develops, leading to a poor 5-year survival rate [13]. Moreover, the Tumor Mutational Burden (TMB), highly associated with smoking, has been revealed as a predictable biomarker for immunotherapy effectiveness. Despite high TMB in SCLC, Immune Checkpoint Blockade (ICB)-based therapy results in only 12.6% of patients being progression-free after 1 year [14]. Therefore, it is absolutely crucial to prioritize the research and development of effective treatments for this aggressive cancer.

1.3 Lung Tumor Microenvironment

The SCLC ecosystem consists of several different cell populations that coexist together. The TME (tumor microenvironment) is a rapidly growing area of cancer research closely related to the occurrence and development of tumors. It comprises tumor cells, supporting cells (like cancer associated fibroblasts (CAFs), stromal cells, and endothelial cells), immune cells, metabolites, and cytokines [15].

Moreover, SCLC has a poorly differentiated vasculature[15], [16], which makes nutrient and oxygen delivery inefficient and waste removal slow. This creates a challenging environment as the rapidly proliferating cancer cells and activated immune cells compete for nutrients. As a result, SCLC faces an adverse TME with poor vascular exchange and high bioenergy demands of various cells. Accumulating evidence on the TME suggests a directed role of the adverse environment on tumor immune evasion [17].

1.3.1 Anatomy of Lung

The respiratory system in humans is a complex network of organs and tissues that work together to facilitate breathing. At the core of this system are lungs, which are highly efficient and intricately designed organs. The lungs are divided into lobes,

with the right lung having three and the left lung having two. Situated in the mediastinum, the lungs are surrounded by the heart, trachea, esophagus, and numerous lymph nodes. To protect the lungs from external forces and infections, they are enveloped by a robust and resilient membrane called the pleura. Separating the lungs from the abdominal cavity is the muscular diaphragm, which expands and contracts during respiration.

The lung is a highly intricate organ that comprises various cell types and is divided into two significant zones: the conducting zone and the respiratory zone. The respiratory zone is where gas exchange takes place. The process of breathing commences with inhalation, where air enters the body through the nose or mouth and travels down the trachea and bronchi. The bronchi branch off into smaller air passages, eventually leading to tiny air sacs called alveoli. These sacs are arranged in clusters and are enclosed by a network of capillaries. Here, oxygen from the air is transferred through the walls of the alveoli and into the bloodstream, where it is transported by red blood cells to all parts of the body.

As oxygen is delivered to the body's tissues, carbon dioxide, a waste product, is produced. This carbon dioxide is absorbed by the blood cells and transported back to the lungs. During exhalation, carbon dioxide is expelled from the body through the trachea and bronchi. This process of inhalation and exhalation is repeated countless times each day, ensuring that our bodies receive the necessary oxygen to function correctly.

Notably, the epithelial sheet covering the airway differs in cellular composition and morphology between the conducting and respiratory zones. In this microenvironment, lung cancers typically start in the cells lining the airways of the bronchus, bronchioles or alveoli [18].

Even though the lung microenvironment has a protective role against pathogens and particulates (thanks to the presence of goblet cells and ciliated cells along the epithelium) it may still contribute to cancer development in inflammatory states [19].

1.3.2 SCLC origins within the lungs

Carcinoid tumors, which are low-grade neuroendocrine lung tumors, are often linked to their precursor lesion known as diffuse idiopathic pulmonary neuroendocrine cell hyperplasia. In contrast, in human SCLC, there is no well-defined precursor lesion. However, it's important to note that carcinoids are not associated with smoking and have a genetic profile distinct from SCLC [20].

SCLC primarily occurs in the central airways and almost always involves mediastinal lymph nodes. Initially, pulmonary neuroendocrine cells were believed to be the origin of SCLCs.

Approximately 5% of cases, however, arise peripherally in the lungs [20]. In fact, SCLC typically originates in the bronchi located at the center of the chest, and it is characterized by the presence of small, tightly packed cells that spread quickly, making early detection challenging (Figure 1.1).

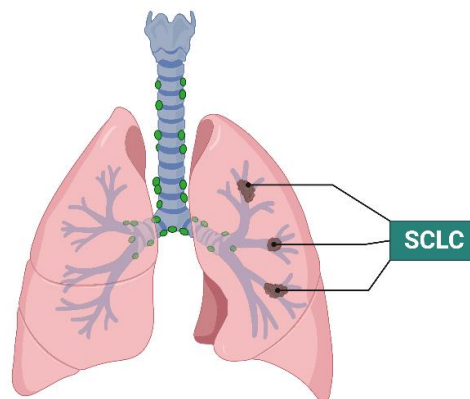


FIGURE 1.1 | Schematic of SCLC masses within the bronchi in the lungs. (schematic created with BioRender.com)

The lungs are a complex organ with a large surface area, which creates multiple pathways for SCLC cells to infiltrate and spread: this is the main reason why metastasis occurs early, with up to two-thirds of patients having widespread disease at the initial presentation [16], [20].

Identifying the precise regions of the lungs affected by SCLC is crucial for developing effective treatment options tailored to the individual's needs.

1.3.3 Cellular components

Lung cancer is a complex ecosystem with a variety of cells and noncellular factors that work together. The cellular and mutational diversity of human lung carcinomas is reflected in their distinct subtypes. This diversity extends beyond the tumor epithelial cells to encompass the vasculature, CAFs, extracellular matrix (ECM), and infiltrating immune cells in the TME. In this complexity, the interaction

between the tumor and non-malignant cells plays a critical role in shaping antitumor immune responses, while stromal and vascular components can promote tumor growth [21].

1.3.3.1 Tumor cells: molecular subtypes and emerging biomarkers

SCLC is named for its distinctive small, oval-shaped cancer cells under a microscope, which are characterized by their diminutive to intermediate size, high ratio of nuclear-to-cytoplasmic matter, distinct nuclear appearance, and presence of nuclear molding. Moreover, SCLC tumors are highly malignant and display a high proliferation rate, apoptosis, and necrosis. These characteristics make them different from other types of lung cancer [22].

The 2021 World Health Organization (WHO) classification of lung tumors recognizes SCLC as one of four lung tumors of neuroendocrine origin [23]. It has been discovered by recent transcriptomic profiling of SCLC cell lines and patient samples are characterized by significant intertumoral and intratumoral heterogeneity.

The recent classification of SCLC into molecular subtypes has provided an essential step in searching for new therapeutic targets for the disease. This classification system identifies two main subtypes: neuroendocrine and non-neuroendocrine.

- Neuroendocrine SCLC accounts for 71-72% of all SCLCs and is characterized by morphology of small, fast-dividing and nonadherent cells [24]. Others divide this neuroendocrine subtype into two categories defined by the transcription factors ASCL1 and NEUROD1, each marking a different path of neuroendocrine differentiation [25]–[27]. SCLC has been known to be poorly immunogenic, displaying intrinsically low levels of Major Histocompatibility Complex (MHC) I (20–22) (MHC^{lo/neg}), which has recently been suggested to be the consequence of epigenetic programming.
- Non-neuroendocrine SCLC account for approximately 10% to 15% of all SCLCs. It has a mesenchymal, non-neuroendocrine morphology and tends to show adherent *in vitro* growth. This subtype consistently exhibits high expression of MHC Class I (MHC^{hi}) and neuroendocrine markers, which are essential for presenting peptides to CD8⁺ T cells in all nucleated cell

compartments for immunosurveillance [9]. Non-neuroendocrine SCLC shows a higher expression of POU2F4, YAP1, and c-MYC [10]-[12]. Previous studies have shown that these cells derepress specific endogenous retroviruses and STING, promoting intrinsic innate immune signaling.

Genetically engineered mouse models of SCLC and profiling of human SCLC have revealed that neuroendocrine and non-neuroendocrine cells can coexist within a single tumor, and these tumor cells are plastic enough to transdifferentiate between the two subtypes [3].

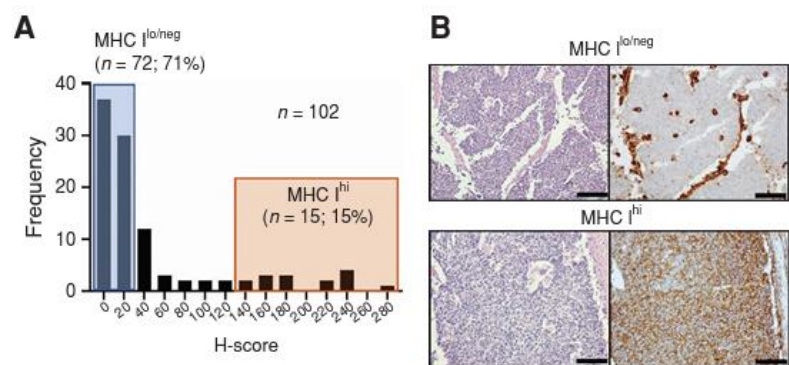


FIGURE 1.2 | MHC I expression in SCLC patients with non-neuroendocrine features. (A) Frequency distribution of MHC I expression expressed as H-score in patient SCLC tumors ($n = 102$). **(B)** Representative micrographs of hematoxylin and eosin (H&E) and MHC I IHC in (top) MHC I low/negative (MHC I^{lo/neg}) and (bottom) MHC I uniformly high (MHC I^{hi}) patient SCLC tumors. Scale bar, 100 μm . Source: Mahadevan, N., Knelson E. et al. (Reproduced with permission from [156])

1.3.3.2 Vascular and stromal cells

In normal tissue, the stroma acts as the primary defense mechanism against the initiation of tumors. Nevertheless, the infiltration of transformed tumor cells triggers significant alterations capable of changing this setting into a supportive milieu for cancer development. The coordination of these modifications involves enlisting fibroblasts, the migration of immune cells, restructuring of the extracellular matrix, and the eventual establishment of vascular networks. Tumor development results from the interaction and mutual adaptation of neoplastic cells with several elements, such as the extracellular matrix, tumor vasculature, and immune cells [28], [29]. The growth of cancerous cells leads to the formation of the tumor niche. However, other non-transformed cells in the environment also evolve along tumor cells, actively participating in tumorigenesis.

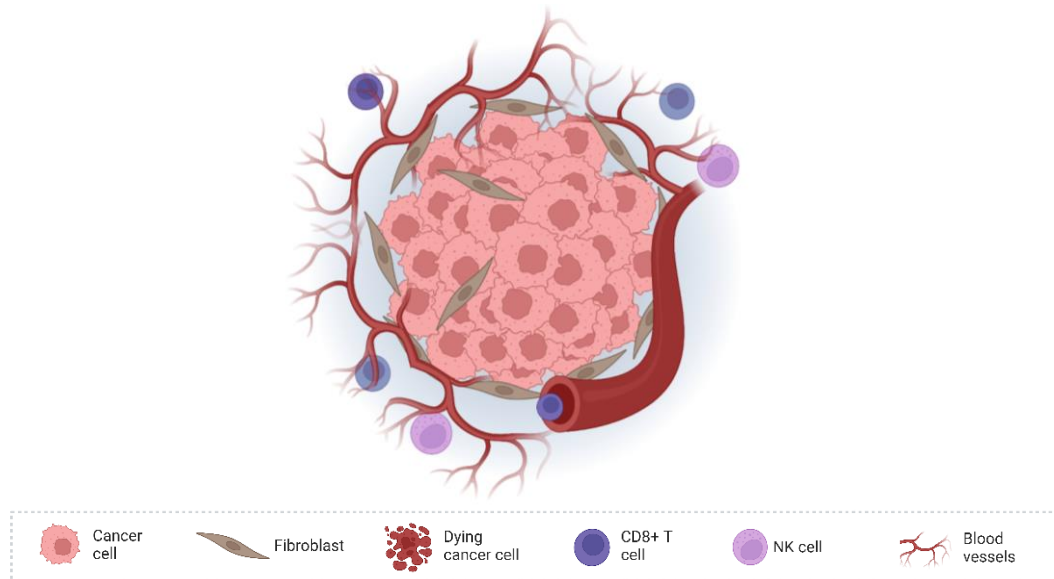


FIGURE 1.3 | Schematic of SCLC TME. Being a solid tumor, tumor cells are organized as aggregates and are surrounded by stroma and infiltrated blood vessels. The immune components are confined at the boundaries, not being able to infiltrate the tumor bed. (Schematic created with BioRender.com)

- Fibroblasts, which come from mesenchyme, are a crucial cell type in the human body that helps maintain the structural framework of tissues. Usually, they prevent the formation of tumors. However, cancer-associated fibroblasts (CAFs) can do the opposite and encourage tumorigenesis. The process of cancer cells activating and modifying these fibroblasts creates an environment that promotes tumor growth, angiogenesis, invasion, and immune evasion. In addition to this, CAFs can increase extracellular matrix production and release unique cytokines like stromal cell-derived factor 1 (SDF1), vascular endothelial growth factor (VEGF), platelet-derived growth factor (PDGF), and hepatocyte growth factor (HGF) [30]. Other mesenchyme-derived cell types, such as adipocytes, can also contribute to tumor growth and progression [28], [29].

Studies have revealed that CAFs, isolated from human lung cancer tissues, secrete interleukin-6 (IL-6), a cytokine that activates the JAK/STAT3 signaling pathway in both tumor cells and tumor-infiltrating immune cells. This activation can lead to tumor-cell proliferation, survival, invasiveness, and metastasis. Regrettably, the IL-6/JAK/STAT3 pathway is often hyperactivated in many types of cancer comprising SCLC, and such hyperactivation is typically associated with a poor clinical prognosis. [31].

- The dynamics of the tumor vascular network plays a crucial role in limiting tumor growth. Endothelial cells (ECs) line the inside of blood vessels, and they play a crucial role in both normal tissues and tumors. In tumors, ECs are highly abundant and are the first cells to come into contact with circulating blood components. Their importance is highlighted by their critical role in maintaining tissue health, which is closely linked with endothelial integrity. In the vascular system, quiescent ECs contribute to homeostasis by inhibiting local hyperplasia, angiogenesis, and inflammation. Conversely, when endothelial cells (ECs) become diseased or dysfunctional, they can contribute to cancer progression by enhancing processes that exacerbate tissue injury beyond mere structural support. Like other stromal cell types, ECs modulate cancer cell behavior, promoting equilibrium in a healthy state, fueling cancer progression when they malfunction, and activating stromal regulatory cells with unique access to the innermost regions of tumors [32]. Even minor changes in EC phenotype could have significant effects on cancer fate, as these changes can be easily transmitted to tumors, exerting profound effects on their development and progression [19].

Endothelial cells play a critical role in the complex landscape of cancer by serving as facilitators. In particular, they are major contributors to angiogenesis, responding to signals from the tumor microenvironment, promoting the growth of new blood vessels, and ensuring that tumors receive the necessary supply of nutrients and oxygen [33]. Additionally, these cells actively engage in the tumor microenvironment, interacting with cancer cells, and influencing tumor progression, invasion, and metastasis. This supportive niche created by endothelial cells enhances tumor adaptability [34][35]. The importance of endothelial cells in cancer progression underscores the need for further investigation to develop effective therapeutic strategies.
- Another essential constituent of the TME is the extracellular matrix (ECM), formed by collagens, proteoglycans, and glycosaminoglycans. It mediates the interactions between cellular components [36], provides structure and support for cells and contributes to paracrine signaling [37]. The density of the lung ECM has been correlated with less immune infiltration into the tumor in either NSCLC or SCLC, functioning as a barrier for immune cell trafficking [38].

1.3.3.3 Immune cells

The highly intricate Tumor Immune Microenvironment (TIME) is a sophisticated interplay of tumor, immune, and stromal cells [39]. Within this complex ecosystem, the interactions between tumor cells and the immune system profoundly influence various TIME characteristics. Moreover, this interplay can be regulated by tumor heterogeneity and individual immune response disparities, significantly shaping the landscape of the TIME [40]. Additionally, it encompasses a diverse array of cytokines and metabolites [41], [42].

T lymphocytes

The profound complexity of the TIME, driven by genomic and epigenetic alterations, categorizes SCLC as highly heterogeneous [43], which means that the interaction between tumor and immune cells can both promote and inhibit tumor growth and progression. This dynamic interaction could be summarized into three steps: neoantigen release, presentation, and T cell activation; T cell infiltration; and T cell recognition and killing [19]. As previously mentioned, 71% SCLC patients' tumor cells exhibit a significantly deficient MHC I antigen presentation mechanism, resulting in extremely low immunogenicity. This hinders the ability of cytotoxic T lymphocytes (CTLs) to recognize and destroy the tumor cells effectively. Patients with SCLC who express high MHC I levels can benefit over the long term from immunotherapy [24], and the antigen presentation protein transporter associated with antigen processing 1 (TAP1) is also universally absent in SCLC [44]. Studies investigating the mechanisms behind SCLC have discovered that certain epigenetic factors, such as enhancer of zeste homolog 2 (EZH2) and lysine-specific methylase 1 (LSD1), silence antigen presentation molecules in SCLC. Inhibiting their expression restores the MHC I antigen presentation pathway and reverses resistance to immunotherapy [45]. Tumor-infiltrating lymphocytes (TILs) CD8⁺ and CD4⁺ are responsible for the anti-tumor effects, and their presence correlates with the overall effectiveness of immunotherapy [46]. As will be explored further below, SCLC is classified as immune-cold tumor [47], [48], and TILs expression is lower than other lung carcinomas [49]. Moreover, the cytotoxic T lymphocytes (CTLs) density, which is in general scarce in SCLC, is much higher in the stroma than in the tumor parenchyma [50]. This suggests that the SCLC microenvironment has a common

mechanism that affects CTL recruitment and infiltration and, consequently, their cytotoxic effects. Indeed, since SCLC has defective expression of MHC I molecules, the ability of CD8⁺ and CD4⁺ T cells to exert their anti-tumor effects is limited, with a reduced infiltration of T cells. Combined with other factors, such as abnormal blood vessels, extracellular matrix and chemokine secretions, it leads to poor response to Immune Checkpoint Inhibitors (ICIs) in SCLC treatment. Conversely, such theoretically defects render tumor cells more susceptible to recognition by innate immune natural killer (NK) cells, that can recognize all non-self-components that lack MHC I [19] (Figure 1.4 A).

Natural killer cells

Natural killer (NK) cells are a crucial component of the innate immune system. Unlike other immune cells like T and B cells, NK cells can attack target cells swiftly without the need for prior sensitization. These cells, known as group I innate lymphoid cells (ILCs), express specific markers and produce important cytokines like interferon- γ (IFN- γ) [51]. NK cells release various signaling molecules, such as cytokines, growth factors, and chemokines, which help in directly combating infections. These molecules also play a crucial role in shaping adaptive immune responses by interacting with other immune cells [52].

The immune defense's frontline is aided by NK cells, as they target infected or malignant cells. Indeed, mature natural killer (NK) cells express a variety of transmembrane receptors that help them distinguish between normal and abnormal cells. The 'missing self' theory is the primary method of killing action. It involves NK cells targeting cells with reduced or aberrant expression of MHC or human leukocyte antigen (HLA) class I molecules, which are usually expressed on healthy tissues (Figure 1.4 B). The presence of MHC class I molecules hinders NK cell activation [53]. However, subsequent research has shown that NK cell activation is also influenced by the presence of ligands for NK cell-activating receptors. The 'induced self' model recognizes cellular stress ligands induced during malignant transformation or viral invasion. This model challenges the initial assumptions of the 'missing self' model by emphasizing the determining role of inhibitory signals for functional NK cell responses. The MHC class I chain-related gene

MICA/MICB, recognized by the NKG2D-activating receptor, exemplifies the induced expression of stress-related proteins under cellular stress, such as viral infections [55]. The dual perspective underscores the complexity of NK cell activation mechanisms, incorporating both inhibitory and activating signals in response to distinct cellular contexts [56]. In the context of cancer, NK cells are effective innate immune cells that actively monitor hematological malignancies and solid tumors, and prevent metastatic spreading. Interestingly, the presence of cytotoxic NK cells within tumors serves as a positive indicator for several types of cancer, including NSCLC. This infiltration of NK cells into tumor tissues highlights their potential therapeutic significance and underscores their crucial role in the body's immune surveillance and defense mechanisms. Conversely and interestingly, despite the majority of SCLC subtypes should be recognizable by NK cells, SCLC is characterized by low/absent NK cells infiltration among the TME. To resume, despite the presence of T cells in SCLC TME, the majority of the cases is characterized by the lack of MHC I expression, making tumor cells undetectable. Furthermore, even if this characteristic should make them sensitive to NK cell-mediated cytotoxicity, in this type of tumor the microenvironment appears low/absent of NK cell infiltration. This is probably due to several factors, such as the presence of a barrier constituted by abnormal vascularization and the lack of chemokine secretions. This results in a poor response to ICIs treatment and in the need to find a strategy to improve NK cells infiltration mechanisms.

Two Types of Tumor Cell Killing

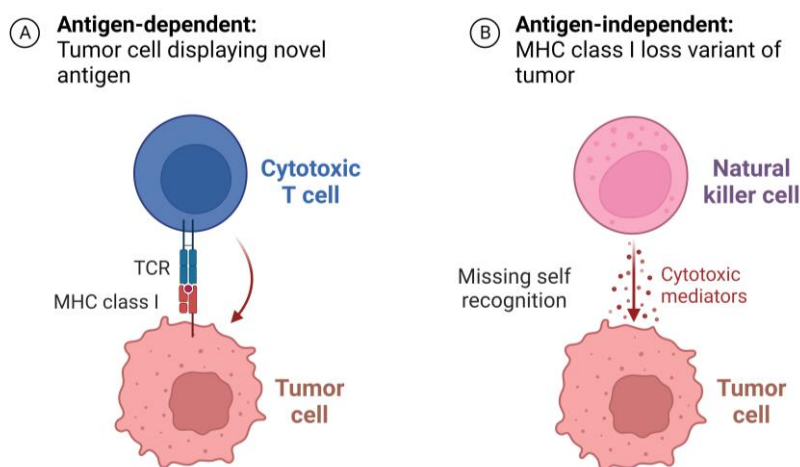


FIGURE 1.4 | Schematic of T cells and NK cells' mechanism of tumor cell targeting and killing. *The T cell is able to recognize the tumor cells by their expression of MHC class I, while the NK cells recognize the abnormal cells as non-self by the lack of MHC class I. (Schematic created with BioRender.com)*

1.4 Different types of TIME and vascular effect

The TIME plays a pivotal role in cancer progression and response to immunotherapy. Understanding the diverse landscapes of TIME is crucial for tailoring effective treatments. The immune profiles of tumors that are unresponsive to immunotherapy have been classified into three categories: immune-inflamed, immune-excluded, and immune-desert tumor [27], [57]. Ranging from inflamed, where robust immune responses are present, to cold, where immune evasion dominates, is crucial for tailoring effective treatments.

Immune-inflamed tumors are characterized by the presence of CD4⁺ and CD8⁺ T cells within the tumor parenchyma, indicating the presence of a preexisting antitumor response that an immunosuppressive microenvironment or intrinsic T-cell anergy has quelled. This phenotype is associated with a type I IFN signature, highlighting the crucial role of innate immune signaling in successful T-cell priming against tumor antigens [57].

Both immune-excluded and immune-desert tumors fall under the category of cold tumors. Unlike inflamed tumors, cold tumors lack preexisting tumor-infiltrating lymphocytes (TILs). Immune-excluded tumors attract T cells to the periphery of the tumor but fail to infiltrate, while immune-desert tumors are entirely devoid of T-cell infiltrate.

It is crucial to understand that the immune profile of a person's tumors can vary significantly, both within the tumor area and between primary sites and metastases. Additionally, it may change over time with disease progression, recurrence, and medical treatment [57].

As previously discussed, the intricate interactions among tumor cells and the immune system sculpt various characteristics of the TIME. These characteristics are attributed to tumor heterogeneity and individual differences in immune systems. Genetic and epigenetic alterations that determine TIME complexity have resulted in SCLC being highly heterogeneous [58]. The relationship between immune and tumor cells is complex and changing constantly. It involves a constant interplay of dynamic interactions that can either promote or inhibit tumor growth and progression. Various factors, such as the type and state of immune cells, tumor cell characteristics, and environmental cues influence these interactions.

Hot Tumor

- CD8+ T cells and NK cells are present in tumor
- Suppression of immunosuppressive cell types
- Improved prognosis and killing of tumor cells with immunotherapy treatment

Cold Tumor

- Exclusion of CD8+ T cells and NK cells from the tumor bed
- Poor prognosis and response to immunotherapy

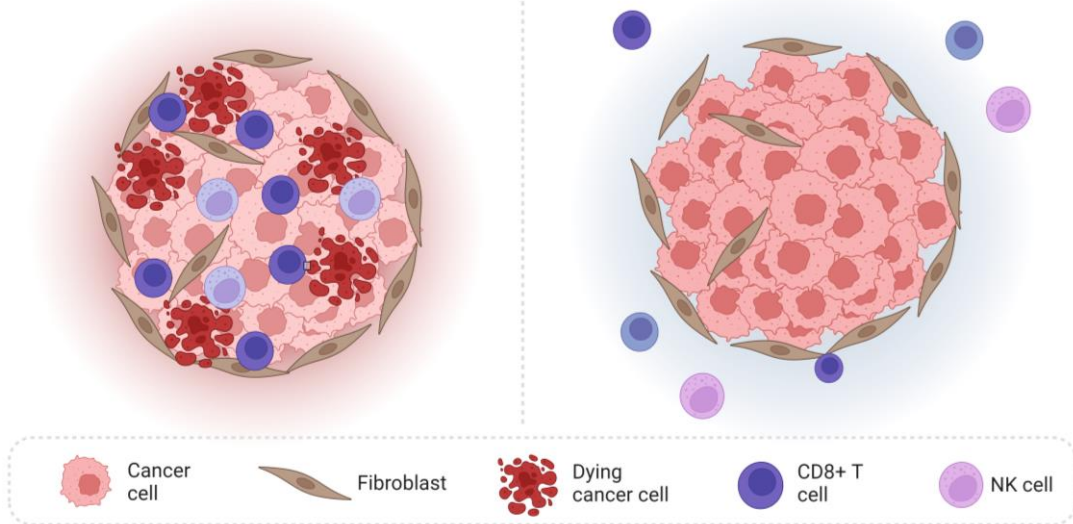


FIGURE 1.5 | Schematic of the different types of TIME. When the tumor bed appears infiltrated by immune cells, which are able to detect and kill target cells, the TIME is classified as hot tumor. When the immune cells are absent or not able to infiltrate, the TIME is classified as cold tumor. (Schematic created with BioRender.com)

The dynamics of the tumor vascular network plays a crucial role in limiting tumor growth. These networks develop through various mechanisms, including the formation of new vessels (angiogenesis), co-option and modification of existing vessels, or recruitment and differentiation of endothelial precursors from the bone marrow (vasculogenesis) [29]. These processes lead to diverse vascular structures within and among tumors, contributing to vascular heterogeneity. Additionally, the formation of vessels involves the degradation and reincorporation of existing vascular basement membranes, exhibiting tissue-specific variations. Normal organ homeostasis demonstrates tissue-specific vascular function and signaling, a phenomenon likely applicable in the context of tumors. These diverse vascular networks create distinct microenvironments within the tumor, contributing to both inter- and intratumor heterogeneity, ultimately impacting clinical outcomes.

Tumor-associated vasculature is a major obstacle that prevents immune effector cells from accessing the TIME. Endothelial cells, concurring in cancer progression, influencing angiogenesis, microenvironment interactions, vascular permeability, and metastasis, are the main responsible for the extravasation of immune cells into tissue microenvironments, express inducible ligands that facilitate leukocyte

tethering, rolling, and transmigration, such as selectins (E-, P-, and L-selectin), vascular cell adhesion molecule 1 (VCAM-1), and intracellular adhesion molecule 1 (ICAM-1). These adhesion molecules are usually absent in basal expression but are rapidly upregulated in response to inflammatory stimuli, such as TNF α and IL-1 β [59]. Inflammatory signaling via the cGAS/STING pathway can also activate the vasculature, leading to increased transmigration of immune effector cells [60]. This has been demonstrated in studies where activation of STING signaling in endothelial or immune cells within the TIME of KRAS/STK11 co-mutated lung adenocarcinoma or mesothelioma facilitated T and NK cell extravasation into the tumor microenvironment [61]–[63].

In cases where tumor cells lack intrinsic inflammatory signaling or do not respond to exogenous stimulators of these pathways (e.g. STING agonism), one strategy to improve the TIME is to stimulate inflammatory signaling in non-malignant cells that still have an intact STING expression [64].

1.5 Current challenges in SCLC treatment and patient outcomes

SCLC remains a challenge in oncology, characterized by its aggressive clinical course and limited treatment options. The diagnosis and treatment of SCLC pose unique challenges due to its molecular complexity. Histopathological examination remains the primary method for SCLC diagnosis, traditionally based on hematoxylin and eosin staining. Nevertheless, Immunohistochemistry (IHC) has become integral in pathology practice, although its interpretation can be challenging, especially in cases where morphology is poorly preserved.

Unlike NSCLC, identifying therapeutic targets in SCLC has been difficult, primarily because driver mutations often involve first-line loss of function or untargetable genes [65], [66].

As previously mentioned, a diagnostic strategy involves assessing the loss of RB and mutant TP53 staining, indicative of SCLC's genetic hallmark. Additionally, the identification of genetic alterations, including MYC mutations, in a significant percentage of SCLC patients, along with the exploration of biomarkers like PD-L1

and Tumor Mutational Burden (TMB) signifies crucial progress in developing targeted therapies and predicting responses to immune checkpoint inhibitors [65].

1.5.1 Standard of care for SCLC

In terms of disease staging, SCLC presents as localized (LD) or extended (ED) disease. LD-SCLC can be approached with loco-regional treatment (radiotherapy) combined with chemotherapy; surgical resection of the primary tumor is usually not performed. In the ED stage, systemic treatments only are recommended [67].

The extremely high proliferation rates of SCLC usually guarantee a good initial response to standard therapies including conventional cytotoxic chemotherapies and radiotherapy, but the prognosis is very poor with short survival [11]. The standard treatment strategies in the LD stages have not seen significant evolutions lately [65]. In the ED counterpart, after decades of lack of therapeutic improvement with only platinum/etoposide-based chemotherapy regimen in the first-line setting, immunotherapy with antibodies that inhibit of the PD-1/PD-L1 axis represent has defined a new standard of care. The combination of the mentioned cytotoxic drugs with either atezolizumab or durvalumab (both PD-L1 inhibitors) is now administered to patients diagnosed with ED SCLC, However, after a variable period of activity of chemo-immunotherapy, most patients show primary or acquired resistance to these anti-PD-L1 [68].

Unfortunately, disease recurrence and progression are the norm in terms of months after the end of the first-line treatment. The lack of effective drugs in the second-line setting concurs to the poor prognosis of these patients.

1.5.2 Novel treatments (cell therapies and targeted therapies)

For decades, improvements in treatment for SCLC patients were barely sufficient or inadequate [69]. However, recent research has uncovered new insights into SCLC's molecular underpinnings and has revealed possible therapeutic vulnerabilities [70].

Due to its high association with smoking, SCLC has an extremely high tumor mutational burden (TMB) but, unexpectedly, this does not translate to a high

immunogenicity [71], [72]. It has been demonstrated that immune checkpoint blockade (ICB) has significantly lower efficacy in SCLC when compared to other highly mutated cancer types, due to the downregulation of the antigen presenting machinery MHC I, as previously described. Over the past few decades, the importance of the TIME in determining disease progression and treatment outcomes has become increasingly evident [58]. It has become possible to identify different subclasses of the immune microenvironment that influence tumor initiation and response to therapy [51][59]. It remains to be understood how tumor-produced cytokines and chemokines, tumor oncogenes and mutation landscapes determine the composition of the TIME [51]. In the last few years, precision medicine has brought a revolutionary change in cancer treatment by adopting an individualized approach to therapy [73]. Precision medicine focuses on identifying specific molecular targets crucial for tumor growth and survival and developing drugs specifically targeting these gene alterations. This approach has shown great success in treating various types of cancer, such as NSCLC, prostate cancer, ovarian cancer, and cholangiocarcinoma [74]. However, progress in treating SCLC has been slower due to the lack of targetable biomarkers or molecular pathways that drive SCLC tumorigenesis [75]. The pathogenesis of SCLC involves the activation of multiple oncogenic drivers, some of which have been already investigated (MYC, TP53, RB1, PTEN, and NOTCH1) [75] but, despite their identification, there are limited targeted therapies that are available and effective for these drivers [59].

1.5.2.1 Cell immunotherapy (adoptive therapies, CAR-T, CAR-NK)

Adoptive cell therapy has exhibited great potential in treating hematological and solid malignancies with limited treatment options using engineered immune cells [76]. The exponential growth in interest in NK cells as a candidate for immunotherapy in recent years is due to the success of chimeric antigen receptor (CAR)-engineered adoptive T cell therapy and the advancement in technologies that can turn cells into powerful antitumor weapons [77].

While CAR T cell therapy has achieved notable successes, the intricate manufacturing process of CAR T cells escalates costs and requires the use of the patient's own cells as the primary material, limiting eligibility, particularly for

heavily pretreated and lymphopenic patients who may lack sufficient cells for a viable product [78]. To advance CAR T cell therapy and increase its accessibility to a broader patient population, it is crucial to address these challenges. NK cells offer a promising avenue for cellular immunotherapy due to their unique recognition mechanism. Unlike T cells, NK cells are immune to the risks associated with HLA-restricted recognition since they do not rely on specific human leukocyte antigen (HLA) matching [79]. The effector function of NK cells is finely tuned by a complex interplay of activating and inhibitory receptors that enable them to differentiate between healthy and stressed cells. While healthy cells are spared from NK cell attacks through the recognition of self-major histocompatibility complex (MHC) class I molecules, which bind to inhibitory killer cell immunoglobulin-like receptors (KIRs), signaling NK cells to halt their function, when self-cells, such as tumor cells, downregulate MHC class I molecules to evade T cell responses and upregulate activating ligands induced by stress like DNA damage or malignant transformation, NK cells identify these abnormalities and initiate an attack. This missing-self recognition mechanism highlights the potential of NK cells in targeting cancer cells and other diseased cells, making them attractive candidates for universal cellular immunotherapy [79], [80]. The main preparations are similar between NK-based and T-based adoptive immunotherapy: NK cells are collected from patients or healthy volunteers typically and undergo a series of processes *in vitro*, including purification, activation and expansion, quality control, and eventually infusion into patients. These NK cell products not only kill target cells directly *in vivo* but also control cancer recurrence and metastasis by activating and/or enhancing the body's immunity [81].

1.5.2.2 Targeted therapies

One of the major challenges in modern oncology is to maximize the effectiveness of treatments while minimizing off-target toxicities [82]. Traditional chemotherapy affects both cancerous and healthy cells, resulting in significant side effects. A new approach that aims to achieve a wide therapeutic window with minimal collateral damage is represented by targeted therapies, which are considered a promising turning point in cancer treatment [83]. Examples of targeted therapies are the

targeted kinase inhibitors (TKIs), which work by blocking the signals that promote the growth of cancer cells, and the angiogenesis inhibitors, which is a type of targeted therapy that prevents the formation of new blood vessels that supply nutrients to cancer cells [84].

During the 1970s, monoclonal antibodies (mAbs) started being investigated for chemotherapies. These antibodies bind to a specific antigen on cancerous cells, which reduces non-specific toxicities and targets tumor cells. This results in either altered signaling patterns towards a therapeutic outcome or directs an immune response towards the tumor cell. Over the next few decades, the technology was further developed by conjugating antibodies with various antitumor effector molecules (such as cytotoxic drugs, radiopharmaceuticals, and immunotoxins) [85]. The idea of using a chemical that targets microorganisms, known as "the magic bullet theory", has led to the development of mAb-based targeted therapies and immunotherapies [86]

Antibody-dependent Cellular Cytotoxicity (ADCC)

Tumor-targeting mAb therapies have shown that many mAbs are dependent on natural killer (NK) cells for their anti-tumor efficacy [87]. Cancer therapy is using tumor-specific mAbs that recognize antigens selectively present on the surface of tumor cells. These therapeutic mAbs work by attacking tumor cells through various mechanisms, such as directing toxic molecules to target cells, inhibiting target cell proliferation, blocking inhibitory signals for immune cells, and directing immune cells to kill targets through antibody-dependent cellular cytotoxicity (ADCC) [56].

There are several ways in which natural killer (NK) cells can kill tumors with the help of antibodies. They include exocytosis of cytotoxic granules, TNF family death receptor signaling, and pro-inflammatory cytokine release such as IFN γ [88], [89]. NK cells can cause target cell apoptosis through the uptake of perforin, granzyme, and TNF family death receptor signaling. Additionally, IFN γ produced by NK cells can activate immune cells around the target cell to promote antigen presentation and adaptive immune responses. Recent studies have shown that CD56dimCD16+ NK cells, the main cytotoxic NK subset responsible for mAb-mediated tumor killing, can also produce IFN γ following activation. This is important because IFN γ

can help inhibit cell proliferation and angiogenesis, as well as increasing MHC surface expression [56]. Furthermore, IFN γ treatment can cause NK-insensitive targets to become NK-sensitive through ICAM-1 upregulation, which can increase conjugate formation with NK cells. These mechanisms work together to eliminate tumor targets through both innate and adaptive immune responses [56].

The mechanism of ADCC involves specific steps: the antibodies attach to antigens on target cells; Fc receptors on immune cells (e.g., NK cells) bind to the antibody's Fc region; binding activates immune cells, triggering intracellular signaling; activated cells release cytotoxic granules containing perforin and granzymes, which respectively forms pores, and induce apoptosis in the target cell, leading to its elimination. (Figure 1.6).

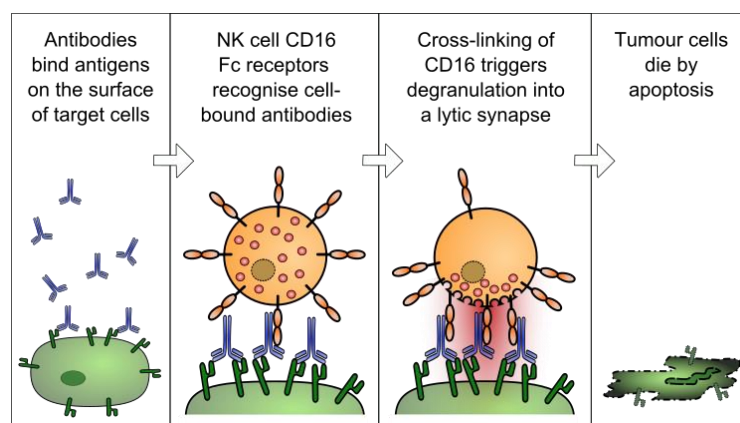


FIGURE 1.6 | Mechanism of action of an ADCC. (Reproduced with permission from Wikipedia.org)

Antibody Drug Conjugate (ADC)

Another powerful example of biopharmaceutical drugs arisen from the investigation of targeted therapies is the class of antibody-drug conjugates (ADCs).

ADCs are a new type of smart bio-pharmaceutical compounds which are rapidly gaining popularity in the field of oncology and some of them have already received approval from the US FDA [90] (Figure 1.7).

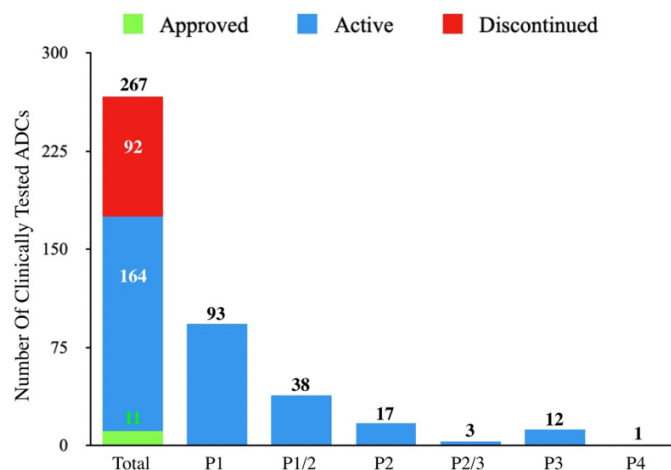


FIGURE 1.7 | Clinically Tested ADCs. This bar graph captures the 267 ADC that have undergone clinical testing of which: 11 are FDA Approved (green sector), 164 are in Active clinical testing (blue sectors), and 92 have been Discontinued (red sector). Additionally, for the Active ADCs, they have been broken down to highlight their highest development stage (Phase 1-Phase 4, P1-P4). The one candidate in this class listed in Phase 4 (P4), disitamab vedotin, has been approved in China and is not yet approved by the FDA.

Source: Maecker H, Jonnalagadda V, Bhakta S, Jammalamadaka V, Junutula JR. (Reproduced with permission from [91])

Apart from their proven effectiveness and low toxicity levels, they have a wide range of applications across different types of tumors. Moreover, their potential to be combined with other innovative molecules makes them even more attractive [83].

All ADCs are constituted by three main components: a monoclonal antibody (mAb), a linker, and a cytotoxic payload (Figure 1.8). These therapeutic agents are designed to exert potent antitumor effects by selectively delivering the cytotoxic payload into cancer cells expressing the target antigen: the antibody specifically targets

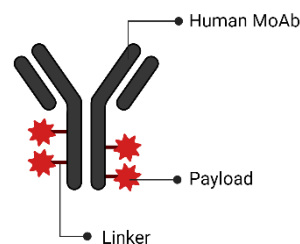


FIGURE 1.8 | Structure of a generic ADC (Schematic created with BioRender.com)

against a tumor-associated antigen, while the linker is used to bind the antibody to the cytotoxic payload. This design prevents premature release into the plasma, limiting systemic toxicity, and delivers it directly to tumor cells [86], [92]. Linkers usually fall into two categories: cleavable (hydrazone, disulfide, and dipeptide) and non-cleavable varieties [92]. The cytotoxic payload should be preferentially non-immunogenic, nontoxic when circulating in the blood, and highly potent at sub-

nanomolar concentrations. The overall goal is to widen the therapeutic window of these drugs by delivering them specifically to target cells.

The ideal target for the antibody is a cell-surface protein that is overexpressed by tumor cells but not on normal cells. This allows for more selective killing and less systemic toxicity [92], [93].

The ADC's monoclonal antibody specifically targets a particular antigen expressed on the surface of cancer cells; following binding to the cancer cell, the ADC-antigen complex is internalized through endocytosis, bringing the conjugate into the intracellular compartment; once inside the cancer cell, within lysosomes, the ADC is subjected to enzymatic degradation, resulting in the release of the cytotoxic payload in the cytosol, which induces cell death through DNA damage (Figure 1.9).

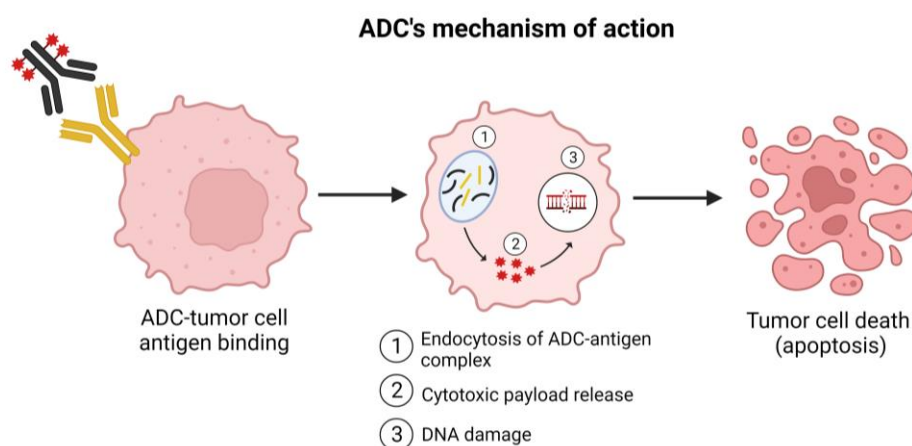


FIGURE 1.9 | Schematic of ADC's mechanism of action from the binding of target cell to the tumor cell death through apoptosis. (Schematic created with BioRender.com)

Over the years, numerous ADCs have been approved for the treatment of various types of cancers. However, ongoing clinical trials are still exploring novel ADCs to help improve treatment outcomes. One of the latest developments in this field is the DXd-ADC technology [94]. This technology utilizes an enzymatically cleavable tetra-peptide-based linker and a potent DXd payload to deliver targeted therapy. DXd is considered a breakthrough in ADC technology and offers a stable plasma linker and a payload with a short systemic half-life, which ensures that the targeted therapy is delivered precisely where it is needed.

One of the most promising treatments that utilizes DXd-ADC technology is Trastuzumab deruxtecan (T-DXd), a HER2-targeting ADC [95]. It has demonstrated potent antitumor activity in both preclinical and clinical settings, making it a highly effective treatment option. T-DXd has already gained approval for HER2-positive breast and gastric cancers in various regions.

DXd-ADC technology is now expanding to other cancer targets, with several programs in clinical development.

ADCs have proven to be highly effective in targeting tumor cells during cancer treatment. However, drug-resistant variants have emerged, presenting challenges that are often attributed to tumor heterogeneity. Indeed, when treating solid tumors, mAbs face several challenges that must be overcome for the therapy to be effective [84]:

1. accessibility: unlike blood cancers, solid tumors are enclosed within tissues and are not as easily accessible. Therapeutic agents need to penetrate through vascular endothelium, stromal barriers, and high interstitial pressure to reach the tumor cells.
2. heterogeneity: solid tumors are highly heterogeneous, meaning they consist of a variety of different cell types. This diversity makes it challenging to target all tumor cells effectively.
3. antigen loss: tumor cells can sometimes lose the antigens that are targeted by antibodies, leading to treatment resistance.

To address these issues, a novel strategy is being investigated, which aims to broaden the scope of ADCs and target the tumor vasculature, in order to overcome the limitations associated with tumor cell-centric approaches.

As previously described, the tumor vasculature plays a critical role in tumor progression and metastasis. Unlike tumor cells, endothelial cells lining the vasculature exhibit excellent genetic stability (less likelihood of antigen loss variants), and the ability to target multiple tumor cells regardless of their antigen-expression profile [96], reducing the risk of developing resistance through mutation. Additionally, ECs are more accessible to high molecular weight drugs, making them attractive targets for therapeutic interventions.

1.5.2.3 CD276/B7H3 as a promising target for SCLC

Despite the potential of ADCs targeting tumor vasculature [97], limited data exist to substantiate this concept. Challenges include the absence of validated ADCs for vascular targeting, uncertainties regarding optimal warheads for ECs, and the identification of suitable targets with the required specificity to target tumor vasculature selectively.

Anti-angiogenic therapies aim to inhibit the formation of new blood vessels in tumors, which is a process crucial for tumor growth. However, tumors can evade these therapies by utilizing existing non-angiogenic vessels and alternative pathways for neovascularization that do not depend on VEGF [98], [99]. Additionally, VEGF therapies can interfere with normal physiological angiogenesis, leading to unintended side effects [100].

In order to face these problems, researchers are investigating new methods that aim to target cell-surface proteins that are highly expressed during pathological angiogenesis, which is the growth of blood vessels in tumors, but are not present in normal, healthy angiogenesis [101]: this selective expression pattern makes these proteins an appealing target for destroying tumor vasculature specifically, without causing any harm to normal blood vessels. Advancements in proteomics, bioinformatics, and molecular imaging can identify proteins on tumor blood vessel endothelial cell surfaces and this knowledge could be used to design targeted therapies aimed at these specific endothelial cells, potentially improving the effectiveness of cancer treatments for solid tumors. In this context, B7-H3 is currently under clinical investigation for their potential in treating various solid tumors [102].

CD276/B7-H3

B7-H3, also known as CD276, is a member of the B7 family of immune checkpoint proteins. B7-H3 is a protein that is found to be expressed in limited amounts in normal tissues. However, it is found to be overexpressed in many types of cancer, including SCLC. This overexpression of B7-H3 has been linked to lower survival rates in patients with SCLC [102].

Immunologic functions of B7-H3

Emerging evidence has demonstrated that B7-H3 helps cancer cells to evade the surveillance of cytotoxic T-cells and natural killer cells, and have shown that B7-H3 is involved in tumor proliferation, metastasis, and treatment resistance, resulting in poor patient outcome [103]. Furthermore, its overexpression correlates with reduced levels of T-cells and interferon- γ . Consequently, blocking B7-H3 proves advantageous by encouraging an early influx of CD8⁺ T-cells, enhancing the body's ability to combat tumors [104]. Recent studies have underscored the promise of B7-H3 blockade, showcasing its effectiveness in various murine cancer models. Notably, B7-H3's functionality appears to be closely linked to NK cells and CD8⁺ T cells, suggesting its impact may vary depending on the tumor's origin. B7-H3's ability to inhibit both mouse and human NK-cell activation supports previous findings, emphasizing the need to comprehend its interactions with immune cells for targeted therapy development [105].

B7-H3 Involvement in angiogenesis

B7-H3 is shown to be implicated in angiogenesis in a variety of cancer diseases and promotes angiogenesis by stimulating the secretion of VEGF [103]. B7-H3 is even broadly overexpressed tumor-infiltrating blood vessels [101]: this dual overexpression on tumor and tumor vascular cells and not in normal tissues provides an opportunity for the development of therapies that simultaneously target and destroy both the tumor cells and the tumor vasculature, resulting in an approach potentially effective for multiple types of tumors.

Development of B7-H3 targeting drugs for cancer treatment

B7-H3 is expressed in tumors and not in normal tissues, making it a potential target for selective cancer cell killing with minimal side effects on normal cells. Research is currently being conducted on various approaches, including antibody-drug conjugates (ADCs), monoclonal antibodies (mAbs) mediating cellular cytotoxicity (ADCC), bispecific antibodies (BsAbs), chimeric antigen receptor (CAR) T-cell therapy, and radioimmunotherapy (RIT), to effectively target B7-H3 [106].

Overall, unlocking the potential of B7-H3 could lead to a revolutionary breakthrough in cancer immunotherapy, providing hope for a brighter future in the fight against cancer.

B7H3-ADC

As previously mentioned, ADCs have emerged as a promising approach for targeted cancer therapy, and the DXd-ADC technology is an innovative platform that features an enzymatically cleavable linker and a novel exatecan derivative (DXd) payload, known for its enhanced potency as a TOP1 inhibitor. The DXd-ADC technology has opened up new possibilities for cancer researchers, who can now explore the full potential of targeted cancer therapy.

A novel ADC targeting B7-H3 has been developed using DXd-ADC technology. The B7H3-ADC comprises a humanized anti-B7-H3 mAb designed to bind to B7-H3 on the surface of cancer cells [107]. Upon binding, the ADC is internalized into the cancer cells, where it releases DXd into the cytoplasm after linker cleavage through enzymatic processing. The released DXd inhibits TOP1 activity, which induces apoptosis in the target cancer cells. The DXd-ADC technology is a significant breakthrough in targeted cancer therapy, and the B7-H3 ADC is a promising candidate for cancer treatment.

1.6 *In vitro* and *in vivo* pre-clinical models and introduction to microfluidic technology

In the context of drug development process, clinical trials play a critical role by providing comprehensive and reliable evaluations of potential therapeutics prior to their release to the market. These trials are conducted in various phases, each serving a specific purpose in assessing safety and efficacy, with the ultimate aim of ensuring the safety and effectiveness of the new drug. The transition from preclinical to clinical trials is a carefully planned and highly regulated process that is essential for guaranteeing the safety and effectiveness of a drug candidate before it is tested on human subjects. Despite the meticulous planning and execution involved, the journey from preclinical success to market approval poses significant challenges, with up to 90% of drug development initiatives failing to proceed from preclinical models to human trials [108].

Conventional models for studying cellular behavior include *in vitro* 2D cultures and *in vivo* mouse models.

In vitro 2D cultures involve growing cells on flat surfaces in controlled laboratory conditions, providing a simplified representation of cellular behavior. They are commonly used for early-stage drug screening, mechanistic studies, and assessing the effects of compounds on isolated cell populations. While offering a cost-effective and easily manipulable platform, they may not fully represent the complexity of the *in vivo* environment. Findings from 2D cultures may not always translate seamlessly to whole organisms.

In vivo studies using mouse models, on the other hand, involve testing potential drug candidates in living organisms to assess systemic effects. These models consider the complexity of the entire organism, including organ systems, intercellular interactions, and systemic responses. Mouse models are crucial for evaluating the efficacy and safety of interventions in a living system before advancing to clinical trials. They provide a more holistic understanding of how drugs may behave in a complex biological environment, considering factors like absorption, distribution, metabolism, and excretion. However, ethical considerations, costs, and potential species-specific differences are challenges associated with *in vivo* studies, especially in the early stages of drug development.

1.6.1 The 3R principle and the need for reliable *in vitro* models in cancer research

In the pursuit of advancing cancer research, understanding the fundamental principles guiding *in vitro* experimentation becomes imperative. The 3R principle, encompassing Replacement, Reduction, and Refinement, emerges as a cornerstone, advocating for ethical and responsible animal research practices [109]. This principle underscores the need to explore alternative methodologies, emphasizing the creation of reliable and ethical *in vitro* models. Such models not only reduce the dependency on animal testing but also enhance the efficiency and ethics of scientific research. Moreover, the refinement aspect of the 3R principle becomes pivotal, ensuring that experiments are not only humane but also yield meaningful and clinically relevant results. *In vitro* models offer several advantages over animal models in biomedical research, especially in the context of:

- ethical considerations, because *in vitro* models eliminate the ethical concerns associated with animal experimentation, providing a humane alternative and ensuring that research does not involve the use of animals for testing purposes [110];
- human relevance, since through *in vitro* models is possible to recapitulate the complexity of human biology, which is even significantly from animal biology, providing a more accurate representation of human physiology using human cells and tissues: this allows researchers to study diseases and test treatments in a context that is directly relevant to humans [111];
- precision and control, with the possibility to create highly controlled environments, where variables can be precisely manipulated, and experiments can be repeated with consistent conditions, reducing the chances of confounding factors [111]; this precision is often challenging to achieve in animal studies due to the inherent biological variability between individual animals;
- cost and time efficiency, since *in vitro* experiments can be set up relatively quickly and can generate results more rapidly, accelerating the pace of research and innovation and turning out as more cost-effective and time-efficient experiments compared to animal studies [110];

- reduction in animal use, because utilizing *in vitro* techniques researchers can significantly decrease the number of animals required for scientific inquiry[109];
- specificity and focus, since *in vitro* models can be tailored to focus on specific cells, tissues, or biological processes relevant to the research question, in order to delve deeply into particular aspects of a disease or treatment and providing detailed insights that might be challenging to achieve in whole animal studies [112];
- drug screening and personalized medicine, using *in vitro* models as platform for drug screening purposes enabling high-throughput screening of potential drug compounds and allowing researchers to identify promising candidates more efficiently [113]; additionally, in the context of personalized medicine, patient-derived cells can be used to create customized *in vitro* models, facilitating the development of treatments tailored to individual patients [112].

Cancer research necessitates *in vitro* models that mimic the phenotype of the target tissue, producing reliable biomedical data [114]. The use of pre-clinical *in vitro* and *in vivo* models remains crucial in cancer research, and they aid in decoding molecular mechanisms of crucial events like tumor growth, metastasis, drug resistance, and immune evasion. They also play a vital role in cancer drug screening and development. [115]. Regrettably, a mere 10% of prospective cancer-fighting medications manage to pass clinical trials due to inadequate effectiveness or insupportable toxicity [116], [117].

In vitro models are commonly based on static and simple 2D cell cultures, which often fail to capture the complex multicellular interactions found *in vivo* [118]. These limitations can significantly impact clinical outcomes, especially when there is a gap between human 2D cell culture and animal models [119], [120]. There is currently a lack of accurate models that can depict the continuous interactions and chemokine signaling between cells in the tumor microenvironment (TME), or effectively evaluate the pre-clinical efficacy of novel and personalized cancer therapeutics. One such model that is missing is an *in vitro* model that describes immune cell trafficking across a human-relevant model of the tumor microvasculature in the TME. To reduce the high attrition rates in drug

development, it is essential to improve the prediction of clinical outcomes during pre-clinical testing of drug candidates.

The transition from traditional 2D cell cultures to the dynamic realm of 3D cell culture technology has brought transformative effects on cellular behavior, offering promising applications across biomedical research [121]. This paradigm shift introduces a multifaceted impact on various aspects of cell biology and drug discovery, shaping the way we understand and manipulate cellular responses. With the advent of self-assembled organoids, tissue engineering and microfluidic technology has been possible to successfully reproduced more reliable and *in vivo*-like, with increasing level of mimicking the TME [122], [123].

In this scenario, the integration of microfluidics into 3D *in vitro* models particularly represents a groundbreaking approach that surpasses traditional methodologies, introducing a new level of precision and versatility to experimental setups.

1.6.2 Introduction to microfluidics

The field of microfluidics emerged in the 1990s thanks to the pioneering work of chemist George Whitesides. Through extensive research on soft-lithography, Whitesides developed a technique that has since become the industry standard for manufacturing microfluidic devices [124]. These devices are capable of precisely manipulating minuscule amounts of fluids within microchannels, offering a range of benefits that have revolutionized *in vitro* research [125]. The main advantages are the following:

- **Precise Spatial and Temporal Control:** Microfluidic platforms excel in providing meticulous control over the spatial distribution and temporal dynamics of crucial factors within the cellular microenvironment [126].
- **High-Throughput Capabilities:** Microfluidic systems are inherently designed for parallel processing and high-throughput screening [127].
- **Mimicking Physiological Gradients:** The ability of microfluidics to establish physiological gradients within 3D cultures is a defining feature. This capacity to create gradients of oxygen, nutrients, and signaling molecules closely mirrors natural *in vivo* conditions [128], [129]. As a result, researchers gain

insights into cellular behaviors under conditions that more faithfully replicate the complexities of living organisms.

- **Cell-Cell and Cell-Environment Interactions:** Microfluidics allows researchers to exert precise control over cell-cell and cell-environment interactions within 3D cultures [130]. This capability is pivotal for studying complex phenomena such as cell signaling, migration, and tissue morphogenesis.
- **Real-Time Monitoring:** Microfluidic devices often support real-time monitoring of cellular responses [131]. Continuous observation of dynamic processes, including cell migration, proliferation, and response to stimuli, provides a time-resolved perspective that is invaluable for capturing transient events and understanding temporal aspects of cellular behavior.
- **Reduction of Reagent Consumption:** Microfluidics operates with small volumes, minimizing reagent consumption. Contributing to more environmentally conscious research methodologies and cost reduction [132].
- **On-Chip Imaging and Analysis:** The integration of on-chip imaging and analysis tools enhances the capabilities of microfluidic devices. Researchers can monitor and analyze cellular processes without the need for sample transfer, reducing the risk of contamination and preserving the physiological conditions under investigation.
- **Tailored Microenvironment Design:** Microfluidics provides the flexibility to design tailored microenvironments with precise control over various parameters. This versatility empowers researchers to investigate specific aspects of cell behavior under well-defined conditions, offering a level of customization that is challenging to achieve with traditional methods.

The convergence of microfabrication and biotechnology has spurred the development of innovative "microfluidic technology" systems. These systems are adept at manipulating small volumes of fluids, typically ranging from microliters to nanoliters, through intricately designed microchannels. The initial applications of microfluidic technology have found resonance across diverse scientific fields.

Chapter I Introduction

Microfluidic devices are fabricated using various techniques, each offering specific advantages and limitations. The choice of fabrication technique depends on factors such as material compatibility, desired features, scalability, and the complexity of the microfluidic device. Researchers often select the most suitable technique based on their specific application requirements. Here are some common fabrication techniques for microfluidic devices (Table 1.1):

Fabrication technique	Overview	Process
Soft lithography [132]	popular technique for fabricating microfluidic devices using elastomeric materials such as polydimethylsiloxane (PDMS).	A master mold is created using photolithography with a photoresist on a silicon wafer. PDMS is then poured onto the master mold, cured, and peeled off to form the microfluidic device.
Photolithography [133]	involves using light to transfer a pattern from a photomask to a light-sensitive material, typically a photoresist.	A photoresist-coated substrate is exposed to light through a photomask, creating a pattern. The exposed or unexposed areas are developed, leaving a pattern on the substrate.
Soft Lithography with Micromolding in Capillaries (MIMIC) [134]	combines soft lithography with capillary forces to mold microfluidic devices.	A PDMS precursor is injected into capillaries on a substrate, and capillary forces fill the channels. After curing, the PDMS replica is peeled off.
Hot embossing [135]	involves pressing a heated mold into a thermoplastic material to create a pattern.	A heated mold is pressed into a thermoplastic substrate, transferring the mold pattern. The material solidifies, and excess material is removed.
Injection molding [135]	high-throughput technique for mass production of microfluidic devices using thermoplastics.	Molten thermoplastic is injected into a mold, and the material takes the mold's shape. After cooling, the molded part is ejected.
3D printing [136]	allows layer-by-layer construction of complex structures, offering design flexibility.	Printers deposit material layer by layer based on a digital model. Various materials, including polymers and resins, can be used.
Micromachining [137]	involves using techniques such as laser ablation or chemical etching to remove material from a substrate.	A substrate is selectively ablated or etched to create microfluidic channels and structures. This technique is often used with materials like glass or silicon.
Thermoplastic Bonding [138]	joins layers of thermoplastic materials to form microfluidic devices.	Layers are heated and pressed together to create a bond. Common methods include thermal or ultrasonic bonding.
Spin coating [138]	technique for creating thin, uniform films on a substrate.	A liquid polymer is dispensed onto a rotating substrate. Centrifugal force spreads the material uniformly, creating a thin film upon curing.

TABLE 1.1 | Fabrication technique used for the design of microfluidic devices from the gold standard to the less common.

1.6.3 *In vitro* SCLC TME modeling using a microfluidic device

Within the context of cancer studies, particularly in Small Cell Lung Carcinoma (SCLC), the complexity of the lung TME demands sophisticated and reliable models that faithfully mimic the complex interactions within the human body. In such scenario, great efforts are focused on developing advanced culture models whose primary goal is to reproduce the key *in vivo* TME interactions, providing a deep understanding of the underlying molecular pathways, and identifying new targeted therapeutic strategies [139].

Micro-physiological platforms feature living cells arranged within compartmentalized single or multiple channels. The primary objective of this model is to replicate essential functional units that mimic tissue- and organ-level functions in a physiologically relevant manner. Key elements of this technology include selecting suitable cell types capable of self-organizing into complex architectures resembling organs or tissues and designing an appropriate ECM composition. This ECM composition facilitates cell polarization and guides their development through intricate morphogenic processes, ultimately culminating in the formation of precise anatomical structures. Moreover, the design of a proper model should guide the process of cell self-organization into 3D multicellular structures [119].

In the particular context of SCLC, using a microfluidic platform with a specific culture represents a considerable opportunity for exploring the interactions between tumor cells and immune cells. As discussed earlier, SCLC cells display diverse characteristics due to their different subtypes, impacting how they respond to immune cells. Unlike conventional 2D cultures, a 3D microfluidic platform enables the incorporation of SCLC cell spheroids: the possibility to incorporate a collagen matrix where cancer cells and stromal cells could preserve their *in vivo*-like phenotypes facilitates a reliable assessment of their sensitivity to immune cells and allows for the evaluation of their migration rate through tumor cells in a manner that closely mimics physiological conditions [140].

Furthermore, as previously mentioned, an essential component of the TME is the Extracellular Matrix (ECM). The unique feature of involving vascular elements in a microfluidic model lies in its ability to emulate the vascular barrier characteristic of solid tumor microenvironments. With a microfluidic device, it becomes feasible

to incorporate vascular components, such as macrovessels or microvascular networks embedding the spheroids, to model the barrier effect of vascularization in the physiological environment. This phenomenon is crucial in promoting tumorigenesis and shielding tumor cells from immune cell interactions.

Another potential aspect of microfluidic systems is their compatibility with external stimulations including drug testing. For instance, applying small drug inhibitors or immunotherapies within these systems allows for observing how immune cells respond to specific stimuli. This feature mirrors real-world conditions and provides a controlled environment for testing the efficacy of various therapeutic compounds [119].

1.6.4 Microfluidic device as a platform for testing anticancer therapies

Microfluidic devices are precisely engineered systems that manipulate small volumes of fluids within microscale channels. These platforms provide a controlled environment for studying cellular behaviors, drug responses, and interactions within intricate tumor microenvironments.

Microfluidic devices offer a unique opportunity to enhance our understanding of cancer biology by mimicking physiological conditions more accurately than traditional methods. Microfluidic devices enable high-throughput drug screening on a microscale, allowing researchers to test multiple compounds simultaneously. This approach aids in the discovery of novel anticancer agents and facilitates personalized medicine by tailoring treatments to individual patients' genetic profiles [141].

Moreover, replicating the complex interactions between cancer cells, stromal cells, and the extracellular matrix by incorporating elements such as vascular networks and immune cells, microfluidic models provide a realistic platform for studying cancer progression and testing therapies that target the tumor microenvironment, with the possibility to include even drug delivery optimization studies since they allow precise control over drug delivery parameters [142].

1.7 Research aims: **study rationale, significance, purposes and objectives**

SCLC remains a difficult challenge in oncology due to its aggressive clinical course and limited treatment options beyond first-line platinum-based chemotherapy [67]. However, subsequent treatment options are plagued by limited efficacy, rapid disease progression, and high rates of hematologic toxicity, emphasizing the urgent need for novel therapeutic approaches [11].

In recent years, researchers have increasingly turned their attention to the SCLC TME due to its critical role in determining treatment outcomes. To develop effective therapeutic strategies, it is essential to understand the complex and diverse nature of the TME, which is constantly evolving and shaped by the interaction between cancer cells, immune cells, stromal cells, and blood vessels [19]. The significance of comprehending the impact of the TME on the immune response has been emphasized by the observation that SCLC lacks immune cells in its tumor bed, suggesting that the TME could play a key role in immune evasion mechanisms [24]. This knowledge can address the development of personalized and highly effective approaches to treating SCLC.

The introduction of targeted therapies represents a paradigm shift in cancer treatment, aiming for a wide therapeutic window with minimal collateral damage [82]. Within this landscape, ADCs have emerged as a potent class of biopharmaceutical drugs. ADCs are designed to leverage the precision of targeted therapy while harnessing the potency of chemotherapy, offering a novel approach to enhance the therapeutic index by selectively delivering cytotoxic payloads into cancer cells expressing specific target antigens [143]. These therapeutic agents are designed to exert potent antitumor effects by selectively delivering the cytotoxic payload into cancer cells expressing the target antigen. The mechanism of action of ADC combines the precision of targeted therapy and the potency of chemotherapy. It aims to enhance the therapeutic index by selectively delivering cytotoxic agents to cancer cells while preserving normal tissues. The identification of the right target antigen is crucial for its success. So far, the success of ADC-based therapies for SCLC is yet to be achieved as no approved treatments are currently available. However, researchers are investigating a few ADC-based therapies in clinical trials.

In this context, Delta-like ligand 3 (DLL3), which is an inhibitory Notch ligand highly expressed in many neuroendocrine tumors such as SCLC but minimally expressed in normal tissues, was identified as a biomarker for SCLC cells and a promising target for ADCs [144]. However, clinical trials for an ADC targeting DLL3 reached advanced stages, but the drug development process failed mostly due to efficacy and toxicity issues [145]. It is imperative to identify the appropriate targets for ADCs. Although the potential of ADCs as a cancer treatment lies in their ability to target tumor cells specifically, the process of accessing tumors and achieving optimal effectiveness can prove to be difficult. This is due to the heterogeneity of tumor cells, the potential loss of antigen expression, and limited accessibility to the tumor bed [85], [146]. Indeed, the entire TME heavily influences these tumors, and understanding its dynamics is key to comprehending tumor growth and evasion mechanisms. It's worth emphasizing that the vasculature plays a pivotal role in protecting the tumor and aiding immune evasion in solid tumors like SCLC [19].

Recent genomic and transcriptomic profiling of SCLC tissue samples has identified B7-H3, which is (also known as CD276) and part of the B7 family of immune checkpoint proteins, as another interesting antigen that is highly expressed by tumor cells and is related to poor prognosis [104]. Currently, an ADC that targets B7-H3 for the treatment of Extensive Stage (ES) SCLC is being investigated in a phase II clinical trial and is expected to move to phase III in the near future [147].

Moreover, previous studies conducted on mouse models have provided convincing evidence that employing an ADC targeting B7-H3 can have a dual effect on both tumor cells and tumor-associated vasculature, preserving healthy tissues [101].

In the context of the drug development process, the utilization of 2D assays in the initial phases of drug screening serves as a foundational step, offering essential insights into a compound's efficacy and laying the groundwork for subsequent exploration [148]. While 2D assays provide valuable information, they often fall short in replicating the intricate complexities of *in vivo* environments. Recognizing this limitation, researchers have turned to the integration of 3D culture within microfluidic devices, marking a pivotal advancement in drug screening and tumor microenvironment (TME) analysis [126], [127]. The incorporation of 3D culture in microfluidic platforms represents a significant breakthrough, effectively bridging

the gap between traditional *in vitro* and *in vivo* models and allowing cells to grow in a three-dimensional arrangement to mimic the architecture and dynamics of tissues within the human body, making them particularly useful in the study of drug responses and the modeling of the TME[126], [149]. Providing a more realistic representation of *in vivo* conditions, microfluidics is a promising tool, potentially streamlining the identification of promising candidates and reducing the reliance on more resource-intensive *in vivo* models. Moreover, the application of 3D culture in microfluidic devices has facilitated a deeper understanding of the mechanisms underlying tumor immune evasion, where studying these interactions in a 3D context allows for a more accurate reflection of the challenges faced by the immune system in the presence of cancer[118], [120].

In particular, the vascular system of the human body is a complex network that needs to be replicated on a microscale to study organ-specific responses to drugs, diseases, and therapeutic interventions. By closely mimicking the vascular microenvironment, microfluidic devices introduce critical elements such as fluid flow, shear stress, and cell-cell interactions, fostering an environment that better mirrors *in vivo* conditions. This increased physiological relevance enhances the accuracy and predictability of experimental outcomes, making microfluidic organs-on-chip invaluable tools for drug screening, toxicity testing, and personalized medicine.

In this thesis we aim to investigate the interactions between immune cells and cancer cells in the landscape of SCLC TIME, focusing on replicate a reliable model of this tumor microenvironment to use for testing targeted therapies against SCLC. Starting from the rationale that different immunological subtypes show different sensitivity to NK cell-mediated control, the presence of stromal barriers, such as vasculature, in the SCLC TIME may prevent NK cells from accessing their target cells. Overcoming these barriers is crucial to enhancing the effectiveness of NK cell-mediated immunotherapy in SCLC.

In this study, we aim to determine the effects of an B7H3-ADC therapy on an *in vitro* microphysiological system (MPS) of the SCLC TME. The main aims of the work can be resumed as following:

- Test B7H3-ADC direct tumoricidal effect (Figure 1.10): the primary objective of this part of the study was to comprehensively evaluate the B7-H3 expression on SCLC immunologic subtypes and on vascular components, in order to consequently investigate their susceptibility to B7H3-ADC-mediated cytotoxicity independent of immune effector, investigating its potential direct tumoricidal effect.
- Examine B7H3-ADC toxic effect on 3D vascular models (Figure 1.10): to assess the therapy's effectiveness in a more *in vivo*-like environment, we aimed to extend the investigation of B7H3-ADC's toxicity to a vascular model developed within our 3D microfluidic model. Administering the treatment on a microvascular network structure would yield more reliable results regarding what occurs *in vivo*. Moreover, our objective was to delve into the dynamics of vascular integrity following the treatment. This investigation aims to evaluate the disruption and permeability increase of vascular barrier, potentially shedding light on novel strategies to enhance immune cell infiltration in tumor microenvironments that are classified as immune-cold.
- Model the interactions between SCLC cells and immune cells in the TME in a 3D MPS: the first part of this objective was focused on understanding how the vascular impacts on immune cells infiltration and its role as a barrier. Then, we aimed to investigate the ability of the NK cells to target and kill the tumor cells according to SCLC different immunological subtypes if they would be able to cross the barrier and come into contact with the target cells. To assess this aim, we first evaluated NK cell-mediated cytotoxicity in 2D assays, and then we wanted to replicate this interplay in a more physiological way by using a microfluidic system.

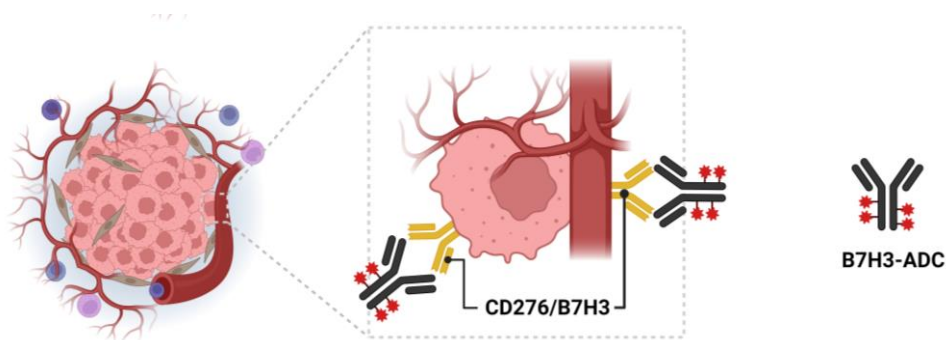


FIGURE 1.10 | Schematic of the aim of the study: simultaneous targeting of SCLC cells and the tumor-associated vasculature expressing B7H3 (yellow antibody) by B7H3-ADC compound. (Schematic created with BioRender.com)

Chapter II

Materials and methods

2.1 Cell culture

Cell culture comprises a set of methods employed to cultivate and maintain cells under controlled and sterile conditions.

Cell culture techniques are diverse, and the choice of method is dependent on the type of cells being studied. The two-dimensional (2D) cell culture on plastic dishes is the most common method. However, cells can also be grown in suspension or adherent cultures. Suspension cultures, such as spheroids, permit higher-density growth, while adherent cultures, such as mesenchymal or endothelial cells, necessitate specific surfaces like collagen for optimal adhesion and differentiation signals. The choice of culture method and surface coating significantly influences cell behavior and experimental outcomes.

Cell culture takes place in a biological hood and incubator is used to control and monitor cell conditions, including temperature (37°C), CO₂ (5%), O₂ (5%) concentration, and humidity (maintained at over 80%). After expansion, cell vials are frozen using -80°C freezers or nitrogen tanks.

Cell culture relies heavily on the composition of the culture medium, which is a combination of nutrients, vitamins, amino acids, and growth factors that are

essential for cell survival, growth, and proliferation. The medium is categorized into basal media containing only nutrients and supplements containing FBS, growth factors, amino acids, and antimicrobials. Supplements help to maintain stability, promote growth, and prevent contamination. It is critical to tailor the composition of the culture medium to the specific cell type being studied.

Sterile conditions must be consistently maintained during cell culture. Adherence to quality system rules for research laboratories, along with good laboratory practices, is crucial to ensuring consistent, reliable, and reproducible results. These practices not only preserve the integrity of the samples but also ensure the safety of laboratory workers. Non-sterile manipulations can lead to contamination, which can compromise the validity of experiments and hinder scientific advancements.

When working with cells, specific protocols must be selected based on the cell type and their response to techniques such as spinning or enzymatic trypsinization. For instance, adherent cells are detached from the culture dish using agents like Trypsin EDTA or TRYPLE. The choice of detachment solution, whether gentle or strong, is dependent on the enzymatic method employed and the characteristics of the cells.

CELL COUNTING

Counting cells is a fundamental technique that is necessary to determine the number of cells and the volume of cell suspension required to obtain a precise cell density. Counting was performed using Countess automated cell counters. Countess Cell Counting Chamber Slides that are designed for it.

Countess automated cell counters works in three simple steps:

1. Mix 10 μ L of sample with 10 μ L of desired reagent: in this study was used Trypan Blue. Trypan blue will seep through the cell membranes of the dead cells, dyeing them blue. The live cells are counted.
2. Fill one side of the *Countess Cell Counting Chamber Slides* (Invitrogen, Catalog #C10283) with 10 μ L of the mix solution.
3. Place the slide into the instrument.

Chapter II

Materials and methods

4. The screen shows the preview and it's possible to adjust the focus in order to highlight cells boundaries: live cells appear white, while dead cells appear black as result of debris accumulation.
5. Press "Count".

The instrument returns the concentration per mL of the total amount of cells, the concentration per mL and percentage of live ones, as well as of the dead ones. Graphically, live cells appear green circled, while dead cells red circled.

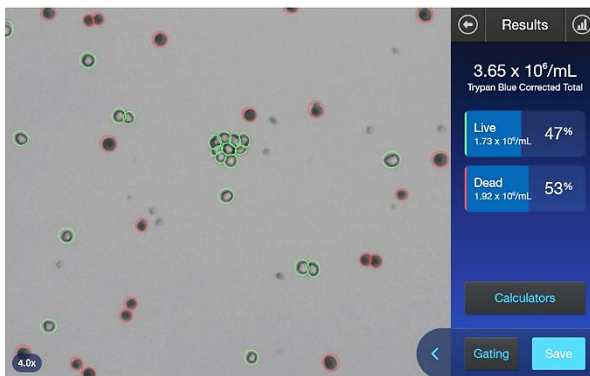


FIGURE 2.1 | Screenshot from Countess Cell Counter. Live cells are circled in green and appear with clear core, while the dead cells are circled in red and appear fully dark. The total number of the cells, as well as the percentages of live and dead, appear on the right box. (Reproduced with permission from Termofisher.com)

All the cell counting intended for experiments was performed considering the number of Live cells and represents the C_1 of the following step.

To calculate the right number of cells to get from the stock it's important to consider the amount of solution (in terms of Volume) required for the experiment, always considering an excess if it's possible, and the desired final density:

C_2 = concentration/density desired

V_2 = volume desired

C_1 = concentration/density of the stock

V_1 = volume to take from the stock in order to have the desired volume (V_1) at the desired concentration (C_1).

From the equation:

$$C_1V_1 = C_2V_2$$

Chapter II
Materials and methods

Has been inversely calculated the only unknown quantity V_1 , which is the volume to take from the starting solution (stock), to which the remaining $V_2 - V_1$ must be added to obtain the final volume required.

CELL SOURCES AND CULTURE CONDITIONS

SCLC cell lines NCI-H69 and NCI-H196 were originally obtained from ATCC. The SCLC mesenchymal-like cell lines H69M, H69EZ-G1 and H69EZ-GV were previously derived from the H69 cell line by CRISPR/Cas9 gene editing and lentiviral infection as described in earlier work [24]. The SCLC cell line CORL47 was kindly provided by Dr. M. Oser. NK cells were kindly provided by Dr. M. Tarannum and Dr. R. Romee after isolation from healthy donors as previously described [150]. The source for HUVECs and NHLF- human Lung Fibroblasts was Lonza company (#C2519AS), #CC-2512). The culture conditions for each cell lines are described in the table below (Table 2.1).

SCLC cell lines	NE	H69 CORL47 H82	RPMI-1640 Medium ATTC modification (Thermo Fisher Scientific, #A1049101) supplemented with 10% fetal bovine serum (FBS) (Gemini Bio-products, #100-106), 1% penicillin/streptomycin (P/S) (Thermo Fisher Scientific, #15140122) and 0.2% plasmocin (2.5 mg/mL, Invivogen, ant-mpp)
	NON-NE	H69M H69EZ-G1 H69EZ-GV	DMEM (Thermo Fisher Scientific, 11965-118) supplemented with 10% FBS and 1% P/S
		H196	Vasculife® VEGF Endothelial Medium Complete Kit (Lifeline Cell Technology, #LL-0003)
Primary stromal cells		Human Umbilical Vein Endothelial Cells (HUVEC)	FibroLife® S2 Fibroblast Medium Complete Kit (Lifeline Cell Technology, #LL-0011)
		Human Lung Fibroblasts (hLFs)	NK MACS media (Miltenyi Biotec, #130-114-429) supplemented with 500 U/mL IL-2 (R&D systems, #202-IL-500)
Human immune cells		Natural Killer (NK) cells	RPMI-1640 Medium ATTC modification (Thermo Fisher Scientific, #A1049101) supplemented with 10% FBS (Gemini Bio-products, #100-106), 1% P/S (Thermo Fisher Scientific, #15140122) supplemented with 50 µM β-Mercaptoethanol (ThermoFisher, #21985023)
		THP1	DMEM (Thermo Fisher Scientific, 11965-118) supplemented with 10% FBS and 1% P/S
Epithelial cells		293T	

Chapter II

Materials and methods

NOTES:

*During coculture experiments, cells were cultured in RPMI-1640 containing 10% FBS, 1% P/S.

*During coculture experiments involving immune cells, cells were cultured in RPMI-1640 Medium ATTC modification supplemented with 10% FBS and 1% P/S, supplemented with 50 μ M β -Mercaptoethanol

*During co-culture involving immune cells and HUVECs the media used was RPMI-1640 containing 10% FBS, 1% P/S and Vasculife at 1:1 ratio.

TABLE 2.1 | Panel of the cell lines used in this study: types, names and culture conditions.

All the SCLC cell lines can proliferate indefinitely under certain conditions, offering several advantages in scientific research, such as reproducibility, genetic stability, cost-effectiveness, standardization, versatility, ethical considerations and long-term studies. However, it is important to note that immortalized cell lines also have limitations, such as potential genetic alterations and differences from primary cells. Researchers must carefully consider these factors and validate their findings in relevant biological contexts to draw meaningful conclusions from experiments involving immortalized cell lines.

In this study, both stromal and immune cells are primary cell lines directly derived from living tissues or organs. The main advantage of using primary cells in scientific research is that they closely resemble *in vivo* conditions, making them biologically relevant for studying normal cellular processes, diseases, and drug responses. Primary cells maintain the physiological characteristics and genetic makeup of the tissue or organ from which they originated, making them biologically relevant. Additionally, primary cells offer functional accuracy, heterogeneity, and *in vitro-in vivo* correlation, which make them valuable for drug screening, toxicity testing, and evaluating the efficacy of therapeutic interventions. They also exhibit physiological responses to external stimuli.

CRISPR/Cas9 Gene Editing and Lentiviral Infection

Oligonucleotides encoding guide RNAs specific to the target gene were selected from both the Avena and Brunello libraries (reference 54). As a control, a non-targeting single-guide RNA (sgRNA) from the Gecko library v2 was utilized (reference 55). The construction of LentiGuide vectors followed previously established protocols (references 55 and 56). Detailed sgRNA target sequences can be found in Tab. Transduction of 293T cells was carried out using X-treme Gene 9 (Roche), following the manufacturer's guidelines. The supernatant from transduced 293T cells, collected after 72 hours through a 0.45 μ m filter, was then introduced to the target cells*. Subsequently, the cells and virus were centrifuged at 2,000 rpm

for 30 minutes at 37°C over a 2-hour period. On the fifth day, puromycin and blasticidin were introduced to facilitate the selection of infected cells.

2.2 2D Viability assay

2.2.1 NK cell-mediated cytotoxicity

CellTiter Glo (CTG) viability assay

The CTG assay is a tool for measuring ATP levels within cells. ATP is a molecule that plays a critical role in cellular processes, serving as a fundamental unit of energy. As a marker of cell viability and metabolic activity, ATP is essential to the functioning of cells. The CTG assay generates a luminescent signal that is directly proportional to the amount of ATP present in the cells. This allows for an indirect assessment of the number of viable and metabolically active cells in a given sample. The main steps of the assay are the following (Figure 2.2 A,C):

1. Target cells were seeded at a density of 10,000 cells per well onto a 96-well black Polystyrene Microplate (Corning #CLS3904) and left to incubate overnight to allow for cell adherence.
2. Following this, NK cells were added in triplicate at different Effector : Target (E:T) ratios ranging from 2:1 to 0:1 and were stimulated with final concentration 500 U/mL Interleukin-2 (IL-2) (R&D systems #202-IL-500), that is classically used cytokine for the expansion of NK cells. The final volume of medium per well was 100 µL. To account for the eventual medium background signal, we plated the same volume of culture medium in other wells.
3. After 4 hours of coculture, CellTiter-Glo® 3D Luminescent Cell Viability Assay reagent (Promega, #G9681) was added to the samples in a 1:10 ratio and allowed to incubate for 30 minutes at room temperature (RT) in the dark, gently shaken to induce cell lysis and promote the homogenous distribution of the reagent.
4. ATP levels were then measured through luminescence using a Tecan Infinite M Plex plate reader.

In the quantitative analysis, the first step involved subtracting the elimination of the blank in order to take off the media background. Tumor cell viability was then calculated by subtracting the luminescence values of NK cell-only controls from

corresponding E:T coculture samples. Finally, relative (%) viability was calculated by comparing the decrease in tumor cell viability in coculture to the tumor cell-only sample.

Bright-Glo Luciferase assay

Luciferin is a small molecule that acts as a substrate for the enzyme luciferase. When luciferin reacts with luciferase in the presence of oxygen and ATP (adenosine triphosphate), it undergoes oxidation, producing light. This bioluminescent reaction is widely used in scientific research for various applications such as reporter gene assays, protein interaction studies and detection of ATP levels in cells. The Bright-Glo Luciferase Assay is not a direct measurement of cell viability. However, in cell viability assays, luciferase-expressing cells can be used to monitor changes in gene expression or promoter activity under different experimental conditions.

In bioluminescent assays, luciferin is added to the reaction mixture along with luciferase-expressing cells or samples. Luciferase catalyzes the oxidation of luciferin, leading to the emission of light, which can be measured and quantified using a luminometer. The intensity of the light signal is directly proportional to the amount of luciferase activity present in the sample.

The target cells must be Luciferase-expressing cells. The experimental steps are the same as the just described Cell-Titer Glo assay, except for the reagent that, in this case, is the Bright-Glo™ Luciferase Assay System (Promega, #E2610) and the incubation time that is around 5 minutes. Luciferase levels were then measured through luminescence using a Tecan Infinite M Plex plate reader (Figure 2.2 C).

In the quantitative analysis, since any other cells except for the target cells express luciferase, relative (%) viability was directly calculated by comparing the decrease in tumor cell viability in coculture to the tumor cell-only sample.

2.2.2 B7H3-ADC - mediated cytotoxicity

The evaluation of cytotoxic effect of B7-H3/ADC on target cells was performed by the previously described CTG viability assay (Figure 2.2 B,C). As previously

mentioned, the ADC consists of an antibody specific for an antigen, chemically linked to the cytotoxic drug (payload); the payload is then released inside the target cell after the ADC has bound to the cell surface antigen, which induces cell death.

To ensure that the assay was run properly, the isotype ADC was used as negative control, while the free payload (Dxd) was used as positive control.

Moreover, in the early stages of the study, we had to determine the B7H3-ADC half-maximal inhibitory concentration (IC₅₀), that was performed by this assay considering different concentrations, obtained by serial dilutions:

- 0 to 150 µg/mL in steps of 10 for B7H3-ADC
- 0 to 150 µg/mL in steps of 10 for Isotype-ADC
- 0 to 150 nM in steps of 10 for Dxd

The main steps of the assay are the following:

1. Target cells were seeded at a density of 5,000 cells per well onto a 96-well Clear Round Bottom Ultra-Low Attachment Microplate (Corning #7007).
2. Previously obtained treatments at all different concentrations were added in triplicate. The final volume per well was 200 µL. To account for the eventual medium background signal, we plated the same volume of culture medium in other wells.
3. After 6 days of incubation, CellTiter-Glo® 3D Luminescent Cell Viability Assay reagent (Promega, #G9681) was added to the samples in a 1:10 ratio and allowed to incubate for 30 minutes at room temperature (RT) in the dark, gently shaken to induce cell lysis and promote the homogenous distribution of the reagent.
4. Before proceeding to the measurement, the samples were transferred onto a 96-well black Polystyrene Microplate (Corning #CLS3904).¹
5. ATP levels were then measured through luminescence using a Tecan Infinite M Plex plate reader.

¹ As in luminescence measurements the signal is very weak and emitted photons can travel in any direction, the clear plates are not suitable for the purpose, because they allow photons to pass through adjacent wells travelling in any direction: it is essential to use in the reader white/black opaque plates to obtain accurate and reliable results.

In the quantitative analysis, after subtracting the elimination of the blank to take off the media background, the relative (%) viability was calculated by comparing the decrease in tumor cell viability in coculture to the tumor cell-only sample.

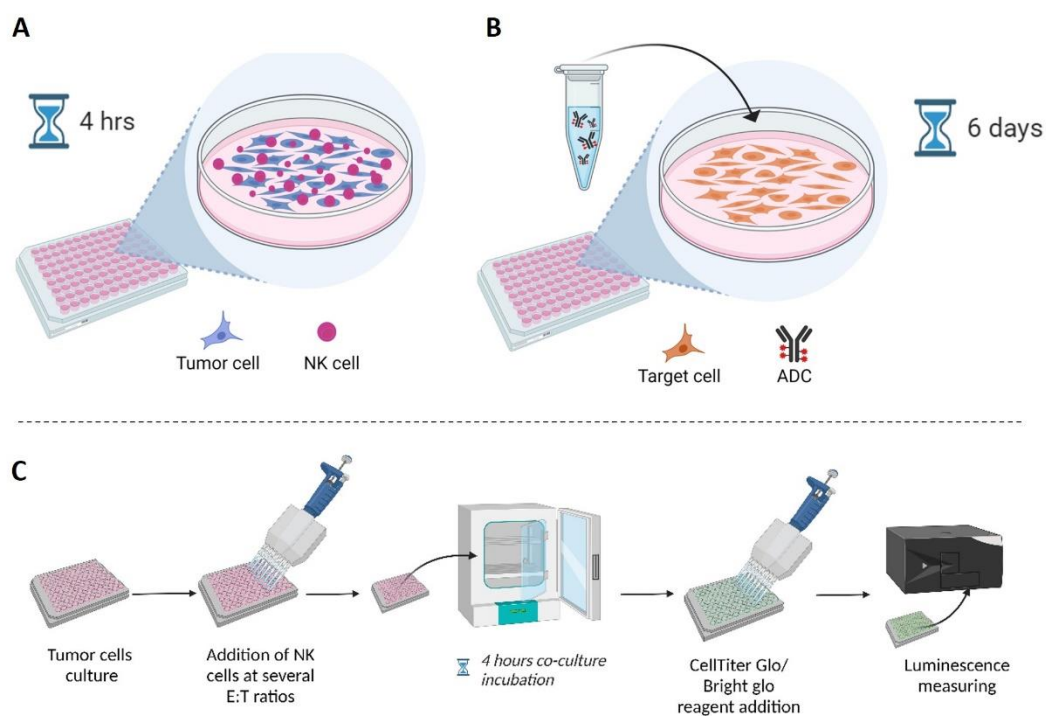


Figure 2.2 | 2D viability assay. (A) Schematic of Tumor cells – NK cells 4 hours co-culture in a 96 well plate. (B) Schematic of generic target cells under a 6 days ADC-based therapeutic treatment. (C) Fundamental steps of a 2D viability assay CellTiter Glo or Bright Glo-based. (Schematics created with BioRender.com)

2.3 ELISA

The detection of human IFN- β (Thermo Fisher Scientific, Cat.# 414101) and human CXCL10 (R&D systems, Cat.# DIP100) was performed using ELISAs as per the manufacturer's protocol. The conditioned media from each cell line were collected after 24 hours co-culture.

The conditioned media (CM) of the SCLC-NK cells coculture were collected after 24 hours of culture. The quantitative analysis was performed considering the average of two/three replicates from at least two independent experiments.

The CM from 3-D cell culture devices were collected at the final time point of the experiment at hand. The quantitative analysis was performed considering the average of three replicates from at least two independent experiments (biological replicates).

2.4 Flow-cytometry

To perform extracellular staining, the single-cell suspensions were first stained for viability using the Zombie NIR Fixable Viability Kit (cat. 423106; Biolegend) following the manufacturer's instructions. Then, the cells were stained with fluorophore-conjugated primary antibodies at a concentration of 2 $\mu\text{g}/\text{mL}$ in PBS containing 2% FBS. Following washing, the cells were incubated with fluorophore-conjugated anti-target (Table 2) at a 1:100 dilution. After washing again, the cells were resuspended in PBS containing 2% FBS and analyzed on a LSRFortessa flow cytometer (Becton Dickinson). The levels were compared to isotype control antibodies and untreated cells. Approximately 20,000 events were collected for each sample, and mean fluorescence intensity (MFI) was normalized to untreated controls and quantified. The data analyses were performed using FlowJo software (TreeStar). The antibodies used for flow cytometry and FACS in this study are listed in Table 2.2.

Target	Clone	Fluorophore	Supplier	Catalog number
HLA-ABC	W6/32	FITC	Biolegend	311403
B7-H3/CD276	MIH42	PE	Biolegend	351007

TABLE 2.2 | List of antibodies used for flow cytometry and FACS.

2.5 Design and fabrication of microfluidic device

The development of microphysiological systems involved the use of a commercial microfluidic chip, specifically the 3-D cell culture chip DAX-1 by AIM Biotech. The chip, which comes in a single-layer slide format measuring 75 mm by 25 mm, features three microfluidic chambers. Each chamber contains a central gel channel that is 1.3 mm wide, flanked by two media channels that are 0.5 mm wide, as well as four reservoirs. To ensure optimal performance, the microfluidic device was

designed and fabricated by AIM Biotech using cyclic olefin polymer (COP). The microfluidic chambers have a height of 0.25 mm, while the media channels were designed with larger reservoirs to prevent over-aspiration (Figure 2.3). The volume considered to fill the gel channel was 10 μL , while the amount of medium to hydrate the device was around 90 μL per each media reservoir.

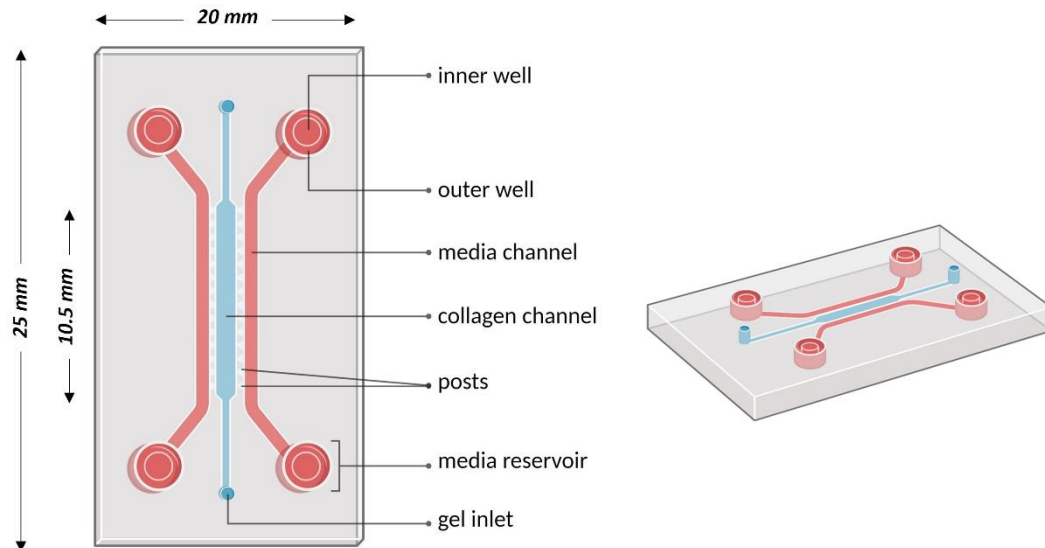


FIGURE 2.3 | Schematic of the microfluidic device used in this study (AIM Biotech 3D Cell Culture Chip). Left side: top view with regions labeled and characteristic dimensions. (Schematic created with BioRender.com)

2.6 3D TME models

2.6.1 Tumor spheroids culture

To generate cancer cell spheroids, we seeded 5×10^5 cells in suspension in a 6-well Clear Flat Bottom Ultra-Low Attachment dish (Corning, Cat.#3471) for 4 to 24 hours (depending on the cell line). After pelleting the samples, we resuspended them in collagen hydrogel as described previously. To ensure each device had around 20,000 cancer cells and taking into account 10 μL of the suspension volume to load into the central channel, we resuspended the pelleted spheroids in 250 μL of collagen hydrogel. We then injected the spheroid-collagen suspension into the central gel region of the microfluidic device through the collagen port and incubated it for 30 minutes at 37 $^{\circ}\text{C}$ in sterile humidity chambers to encourage collagen polymerization (Figure 3.4 A). This model was used to evaluate the effect of B7H3-

ADC on the SCLC cell lines. To ensure that the experiment was performed properly, the isotype ADC was used as negative control, while the free payload (Dxd) was used as positive control. Moreover, a device just hydrated with culture medium consisted of another negative control, while a 2'3'cGAMP (Invivogen, Cat.#tirl-nacga23-1) at the concentration of 1 µg/mL consisted as positive control.

The treatments were added once the collagen was polymerized at the following concentrations:

- 0.1 and 10 µg/mL for B7H3-ADC
- 0.1 and 10 µg/mL for Isotype-ADC
- 0.1 and 1 µg/mL for Dxd
- 1 µg/mL for 2'3'cGAMP

The target cells viability measurement was performed after 6 days treatments, during which the medium (comprising of the treatments) was refreshed daily.

2.6.2 Tumor spheroids – NK cells coculture

In this co-culture we decided to evaluate the tumor cells viability when in co-culture with the same number of NK cells (1:1 ratio). After NK cells counting, they were labeled following the manufacturer's instructions and depending on Live/Dead immunofluorescence staining chosen for the final time point imaging, following the manufacturer's instructions (Table 2.3):

NK CELL TRACKER	Acquisition channels	Incubation time	Concentration	Source
Cell tracker red	TRITC (red)	20 minutes at 37°C	1:1000 in PBS	Thermo Fisher Scientific, Cat.# C34552
Cell Proliferation Dye eFluor 450. - 500 ug	Pacblue			Thermo Fisher Scientific, Cat.# C65-0842-90

TABLE 2.3 | NK cell tracker reagents used in this study and experimental conditions: acquisition channel, incubation time, concentration, and source of the product.

The NK cells and spheroids suspensions in collagen hydrogel was formed separately as just described above, with the difference that we calculated the resuspension volume in order to have twice the concentration of each cell component: this allowed us to have a consistent 20,000 cancer cells per device in 1:1 ratio with NK cells once the suspensions were mixed together.

As control conditions, we considered to have devices loaded with tumor cells alone as well as NK cells alone in collagen hydrogel suspension.

We then injected the spheroids alone, NK cells alone, and spheroids-NK collagen suspensions into the central gel region of the microfluidic devices and incubated for 30 minutes at 37 °C in sterile humidity chambers to encourage collagen polymerization (Figure 3.4 B). Next, devices were hydrated with culture medium (RPMI-1640 Medium ATTC modification with 10% FBS and 1% P/S, supplemented with 500 U/mL IL-2) (Figure 2.7). The coculture was performed for 24 hours to evaluate the tumor cells viability (section 2.10).

2.7 Blood vessel formation: 3D macrovessel

To generate the 3D macrovessel model, the first step was the formation of collagen hydrogel by a Type I rat tail collagen (Corning, Cat.# 354236) following the addition of 10× PBS with phenol red with pH adjusted using NaOH. the amount of the parts was calculated in order to obtain a final collagen concentration of 3 mg/mL. The achievement of the desired physiological pH of 7.0 to 7.5 was confirmed using PANPEHA Whatman paper (Sigma-Aldrich).

The hydrogel was then injected into the center gel region of the 3D microfluidic device (10–15 mL per microfluidic chamber). After incubation for 30 minutes at 37°C in sterile humidity chambers, the side wall of one flanked channel (media channel) was coated with 25 µL of 0.1 mg/mL collagen solution in PBS to allow for better adhesion of endothelial cells to the channel and incubated for 20 minutes.

To create the 3D vessel, 25 µL cell suspension of 3×10^6 cells/mL HUVECs were injected in the collagen precoated media channel. To allow the cells to attach to the media–gel interface and form a monolayer, the chip was incubated 90° tilted for 20 minutes, with cells facing down toward the central channel. Next, 25 µL cell

suspension was reinjected, and the chip was placed upside-down to cover the upper part of the 3D vascular channel. The double rotation is important to create a confluent hollow-lumen 3D vessel. Moreover, between the two injections, the suspension was gently aspirated to remove the unattached endothelial cells.

After 2 hours of incubation in the humidity chamber at 37°C, cell culture media was gently added to both channels and further incubated to form a confluent monolayer. A fully formed 3D macrovessel was obtained after 48 hours culture, during which the culture medium was refreshed daily (Figure 2.4 C1).

This model was used to evaluate the effect of the B7H3-ADC on the endothelial cells. To ensure that the experiment was performed properly, the isotype ADC was used as negative control, while the free payload (Dxd) was used as positive control (Figure 2.4 C2).

Moreover, a device just hydrated with culture medium consisted of another negative control, while a 2'3'cGAMP (Invivogen, Cat.#tirl-nacga23-1) at the concentration of 1 µg/mL consisted as positive control. The treatments were added after macrovessel was formed at the following concentrations:

- 0.1 and 10 µg/mL for B7H3-ADC
- 0.1 and 10 µg/mL for Isotype-ADC
- 0.1 and 1 µg/mL for Dxd
- 1 µg/mL for 2'3'cGAMP

To evaluate the vessel integrity, we performed a permeability assay after 6 days treatments, during which the medium (including treatments) was refreshed daily.

2.7.1 Tumor spheroids culture - vascular barrier – NK cells

To simulate the physiological process of natural killer cell extravasation from blood vessels towards tumor cells, we began by culturing the tumor spheroids as previously described.

In the cases where we included the vascular barrier, once the collagen hydrogel had polymerized, we proceeded with blood vessel formation in one of the flanked channels using the procedure explained in section 2.8. The devices were hydrated

filling medium reservoirs with the proper culture medium. We can consider the macrovessel formed after 48 hours incubation at 37°C, during which the media was refreshed daily (Figure 2.4 C1).

In the experiment without the vascular barrier, after collagen hydrogel polymerization, we skipped the previous step and proceeded as below.

In order to achieve a 1:1 ratio of NK cells with the tumor cells, the NK cells were labeled as instructed in section 2.7.2 and counted. The current model involved injecting the NK cells into the macrovessel side channel (Figure 2.4 D1,D2): in order to inject 20,000 NK cells in 25 µL of medium culture, NK cell suspension was prepared at a density of 8×10^5 cell/mL.

We then filled the media reservoirs with the proper medium culture and incubated at 37°C. The coculture was performed for 48 hours or 72 hours to evaluate the tumor cells viability (section 2.10) and the NK cells migration or, if in presence of the side macrovessel, extravasation (section 2.11).

2.8 Blood vessel formation: vasculogenesis model

Microvascular networks (MVN) were created by detaching HUVEC and hLFB cells from cell culture flasks using TrypLE Express Enzyme (ThermoFisher, Cat.#12604039) as detaching reagent, and spun down at 1500 rpm for 3 min; cell pellet was resuspended in cold vascular medium (Vasculife, Lifeline #LL-0003) with 2 U/ml thrombin from bovine plasma (Millipore Sigma, #T7326). The two cell types were combined with cell densities of 24×10^6 cells/ml endothelial cells and 8×10^6 /ml hLFB. Cell suspensions were mixed 1:1 volume ratio with 6 mg/ml fibrinogen (Millipore Sigma, #341573) and gently injected into the center gel region of the 3D microfluidic device (10–15 mL per microfluidic chamber). The devices were placed upside-down in sterile humidity chamber and incubated at 37°C for 15 minutes to promote fibrin polymerization. Next, warm vascular medium was added to the flanking media channels and refreshed each day of culture. MVN self-assembled over several days refreshing media daily for 7 days.

To create microvascular networks (MVN), HUVEC and hLFB cells were detached from cell culture flasks using TrypLE Express Enzyme as the detaching reagent.

The cells were then spun down at 1500 rpm for 3 minutes and resuspended in cold vascular medium with 2 U/ml thrombin from bovine plasma. Endothelial cells and hLFB were combined at cell densities of $24 \times 10^6/\text{ml}$ and $8 \times 10^6/\text{ml}$ respectively, in order to obtain a 3:1 ratio. The cell suspensions were mixed in a 1:1 volume ratio with 6 mg/ml fibrinogen and gently injected into the center gel region of the 3D microfluidic device (10–15 mL per microfluidic chamber). Afterward, the devices were placed upside-down in a sterile humidity chamber and incubated at 37°C for 15 minutes to promote fibrin polymerization.

Next, we added warm vascular medium to the surrounding media channels and refreshed it daily during the culture period of 48 hours. This allowed the cells to form the microvascular network (MVN) spontaneously (Figure 2.4 E1).

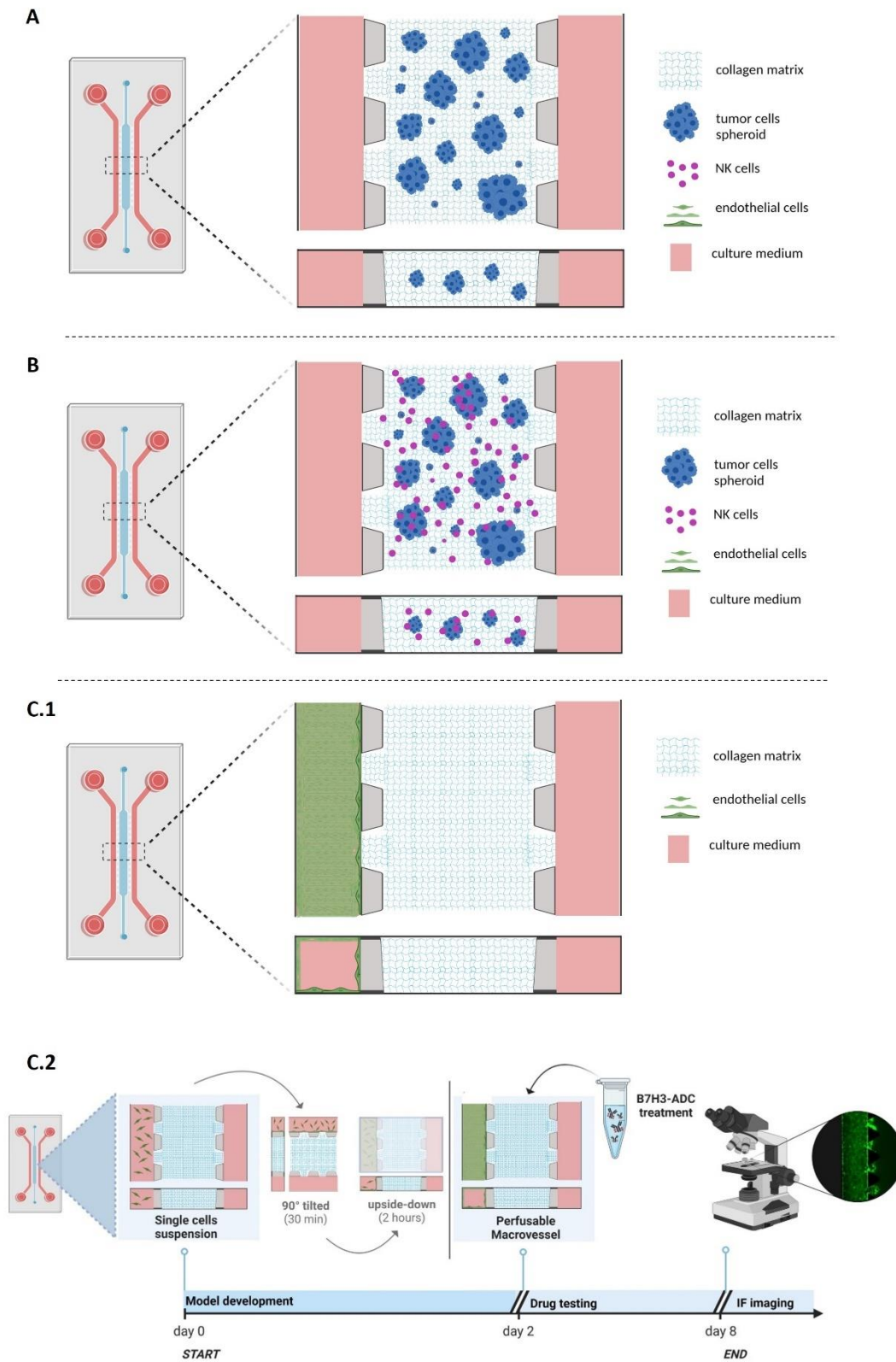
After the MVN was established, we created the macrovessel in the adjacent channel, using the same procedure outlined in the previous paragraph.

The vasculogenesis model was considered formed after three more days of culture, at which point treatments could be added for testing.

As the previous model, even the current one was used to evaluate the cytotoxic effect of the B7H3-ADC on the endothelial cells, at the same treatment conditions used for the blood vessel model (section 2.7.1), which were added after the MVN was formed (Figure 2.4 E2).

To evaluate the vessel integrity, we performed a viability assay after 6 days treatments, during which the medium (including treatments) was refreshed daily (section 2.10).

Chapter II Materials and methods



Chapter II Materials and methods

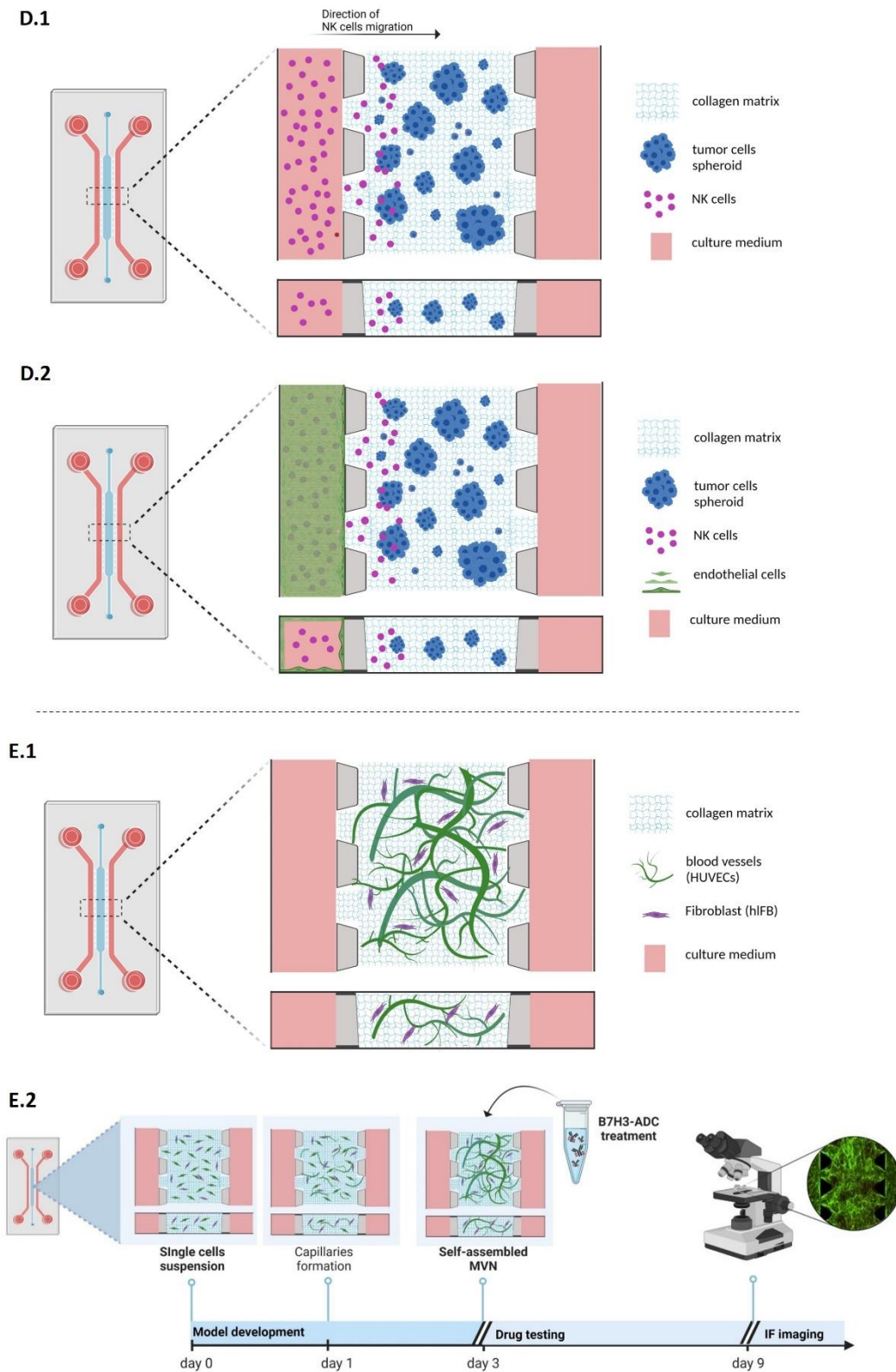


FIGURE 2.4| Schematics of 3D culture models in microfluidic device. (A) Tumor spheroids alone culture (B) Tumor spheroids co-culture with NK. (C.1) Perfusable macrovessel model. (C.2) Timeline experiment of the viability assay after ADC-based treatment. (D.1) Tumor spheroid model with NK cells injected on the side channel to perform 3D migration assay. (D.2) Tumor spheroid model with NK cells injected in the macrovessel model on the side channel to perform 3D migration assay in presence of the vascular barrier. (E.1) MVN model. (E.2) Timeline experiment of the viability assay after ADC-based treatment. (Schematics created with BioRender.com)

2.9 Immunofluorescent (IF) microscope imaging

Whole-chip images were captured with a 4X lens of a Nikon Eclipse 80i fluorescence microscope with an automated motorized stage (Proscan), Z-Stack (Prior) and a Zyla 5.5 sCMOS camera (Andor). Image capture and analysis were done using the Nikon NIS-Elements AR software package.

In the following table (Table 2.4) there's a summary of the IF staining reagents that we used for the experiment in this work, comprising of their characteristics but even of the viability measurement that we performed according to the reagents chosen.

The quantitative measurements were performed considering the intensity of the signals content within specific Regions of Interest (ROIs), properly designed according the aim of the experiment

Chapter II

Materials and methods

IF STAINING REAGENTS		
AO/PI <small>(Acid Orange/Propidium Iodide)</small>	Description	Acquisition channels
	AO stains for live cells	FITC (green)
	PI stains for dead cells	TRITC (red)
	Incubation time	Concentration
	5 minutes at RT	1:1 in PBS
	Viability quantification	
	without NK cells	$Live\ target\ cells\ (\%) = \frac{FITC}{(FITC + TRITC)} \times 100$
with NK ² (Cell Proliferation Dye eFluor 450 traced)	$Live\ target\ cells\ (\%) = \frac{FITC - PacBlue}{(FITC + TRITC)} \times 100$	
DAPI or Hoechst / Draq7 or PI	Description	Acquisition channels
	Hoechst stains for all nuclei	Pacblue/DAPI (blue)
	Draq7 stains for dead cells	Cy5 (Far-red)
	Incubation time	Concentration
	Hoechst: 30 min at RT DAPI: 5 min at RT Draq7: 10min at RT PI: 10-15 min at RT	1:800 in PBS 1:1000 in PBS 1:200 in PBS 1:1000 in PBS
	Viability quantification	
	$Dead\ cells\ (\%) = \frac{Cy5}{Pacblue} \times 100$ $Live\ cells\ (\%) = 100 - Dead\ cells\ (\%)$	
Lectin <small>Ulex Europaeus (Gorse) Agglutinin I (UEA I)</small>	Description	Acquisition channels
	Stains for endothelial cells ³	FITC (green)
	Incubation time	Concentration
15 min	1:200 in culture medium	

TABLE 2.4 | IF staining reagents used in this study and experimental conditions: description, acquisition channels, incubation time and concentration.

² We assumed that the NK cells can be considered 100% alive, hypothesis supported by both representative images and viability quantification on NK cell-only device controls.

³ In all assays involving macrovessels on the side channels, Lectin staining was utilized except in the case of the vasculogenesis model: for this model, the viability assay utilized AO/PI staining, with the FITC signal designated for imaging live cells.

2.10 3D Viability assay using a microfluidic device

The 3D viability measurement was performed through immunofluorescence imaging. Depending on the experiment under consideration, starting from the model, we gently removed the culture media from the side channels⁴. Following this step, we injected 25 μL of a staining reagent (Table 2.4) into the side channels, and let devices incubate in the dark at RT for the appropriate incubation time.

For imaging acquisition, devices were imaged through the employment of the fluorescence microscope (section 2.9)

The quantification of tumor cell viability within the 3D tumor microenvironment was accomplished by measuring the Binary Area (μm^2) of the different channels and the viability was quantified according to the staining used (Table 2.4).

In the 3D viability assays performed on the 3D TIME models we considered 3 different ROIs of the central gel region, where the target cell spheroids are located (Figure 2.5 A).

During the vasculogenesis model's 3D viability assay, we analyzed 3 distinct regions of interest (ROIs) within the entire device, including the side channels: our aim was to assess the response of endothelial cells to the treatments, regardless of whether they were part of the macrovessels on the sides or the microvasculature in the center (Figure 2.C B).

2.11 3D Migration assay: measurements and quantification

The 3D migration measurement was performed through immunofluorescence imaging. The first step is always the gentle removal of the culture media from the side channels reservoirs: when NK cells were injected in the side channel, it is important to aspirate the media from the outer well of the media reservoirs, in order to avoid interfering with the location of the cells.

⁴ During the experiment where NK cells were embedded in the central gel region, the media was carefully aspirated from the inner well of the media reservoirs. However, when NK cells were initially injected in the side channel, it is important to aspirate the media from the outer well to avoid interfering with the location of the cells.

As mentioned above (section 2.6.2), the NK cells were previously labeled with Cell Tracker Red or Cell Proliferation Dye eFluor450 (Table 2.3).

The NK cell migration or, if in presence of vascular barrier, extravasation within the 3D tumor microenvironment was quantified by measuring the Binary Area (μm^2) of the channel corresponding at the cell-tracker used (Table 2.3).

In the 3D migration assays performed on the 3D TIME models we considered 3 different ROIs of the upper part of the central gel region, in order to not taking into account unspecific diffusion from the side channel through the central region (Figure 2.5 C).

2.12 3D permeability assay using a microfluidic device

In 3D the blood vessel model (section 2.8), the macrovessel integrity and barrier function of the vessel model was evaluated through a permeability assay using FITC-Dextran 70 kDa concentration (Dextran, Texas Red™, 70,000 MW, Neutral - ThermoFisher, Cat.#D1830).

After 6 days treatment, culture media were gently removed from the inner well of the media reservoirs. To visualize the structure of the vessel, endothelial cells were Lectin-stained as previously described (Table 2.4).

Before proceeding with the imaging, Lectin-staining solution was gently removed, and the opposite side channel was filled with 25 μl of PBS avoiding the formation of a gradient and Dextran-solution diffusion through the empty channel.

The Dextran solution was prepared at concentration 1:200 in culture medium. Before injecting the solution, the devices have been located on the microscope support, in order to not interfere with the flux of solution. We then perfused each macrovessel side channels with 25 μl Dextran 70 kDa solution, and 3D z-stacks of the gel channel have been imaged from 0 to 20 minutes at 5-minute steps interval.

For the measurements, we considered 3 different ROIs of the central gel region to evaluate the flux, and 3 corresponding ROIs on the vessel side, in order to relate the

currently present flow in the collagen region (area of interest) to the solute injected into the vessel (Figure 2.5 D).

Vascular permeability will be measured as the flux of solute across the walls of the macrovessel (in the central gel region). Using mass conservation, the quantity of FITC-dextran crossing the vascular network equals the rate at which it accumulates outside the vessels as permeability coefficient (cm/s).

The quantification was performed by considering the increase in fluorescence intensity within the gel between the different time points using the following equation:

$$P = \frac{1}{(I_V^{t_1} - I_T^{t_1})} \left(\frac{I_T^{t_2} - I_T^{t_1}}{\Delta t} \right) \frac{A_T}{p_V}$$

$P = \text{permeability} \left[\frac{\text{cm}}{\text{s}} \right]$

$I_V^{t_1} = \text{intensity of the vessel at time point 1}$

$I_T^{t_1} = \text{intensity of the tissue at time point 1}$

$I_T^{t_2} = \text{intensity of the tissue at time point 2}$

$A_T = \text{area of the tissue}$

$p_V = \text{perimeter of the vessel}$

$\Delta t = t_2 - t_1$

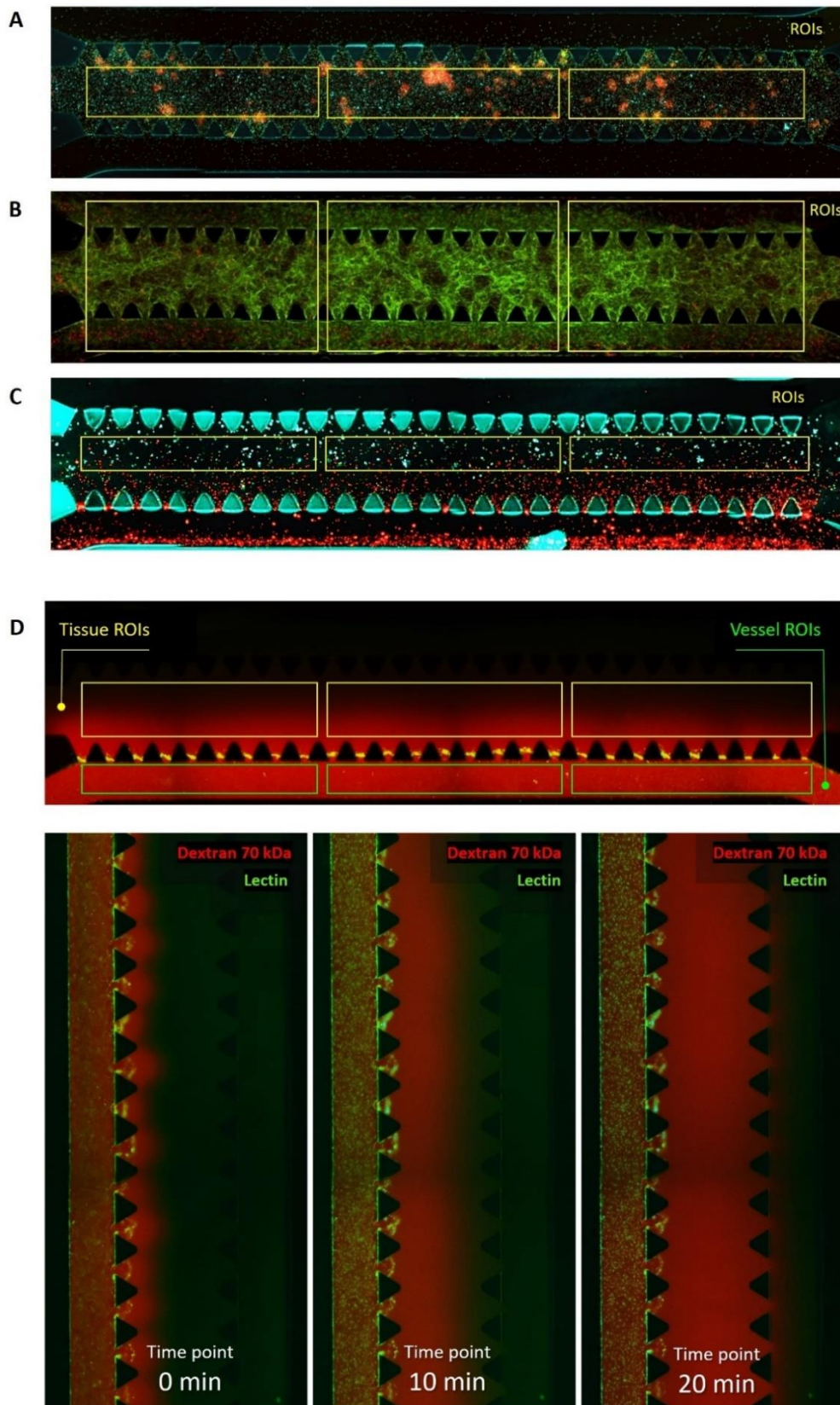


FIGURE 2.5 | Region of interest (ROIs = yellow bordered rectangles) of the IF images considered in the quantification analysis. (A) ROIs for viability assay of 3D tumor spheroids – NK cells co-culture (B) ROIs for viability assay of the MVN model. (C) Upper part: ROIs for the permeability assay on macrovessel model; bottom part = representative IF images at different time point of the flux of solute (Dextran 70 kDa) across the central gel region.

Chapter III

Results

3.1 Evaluation of B7H3 expression in SCLC TME:

B7H3 is mainly upregulated on Non-Neuroendocrine SCLC and vasculature

Currently, a clinical trial is testing an Antibody-Drug Conjugate (ADC) that targets B7-H3 for the treatment of Extensive Stage (ES) SCLC [107], while previous studies on mice have shown that using an ADC targeting B7-H3 can have a dual effect on both tumor cells and tumor-associated vasculature [105].

To validate this observation in a human SCLC model and test the effectiveness of a B7H3-ADC-based therapy, we firstly evaluated B7H3 expression in our cell line models. We profiled by flow cytometry the B7-H3 expression on some representative lines of both NE and Non-Ne subtypes. Interestingly, we found that MHC I low H69 SCLC line had low expression of B7H3, whereas the isogenic MHC I^{hi}/Non-NE SCLC cell lines (H69M, H69-EZG1, H69-EZGV) and the MHC I^{hi}/Non-NE H196 expressed high levels of B7H3. The H82 cell line model shows a

moderate expression of B7H3 (Figure 3.1 A). As we hypothesized, the expression of B7H3 on SCLC cells mirrored the immunologic subtypes.

As previously mentioned, the TME plays a pivotal role especially in terms of protecting the tumor, promoting its growth and creating an intricate ecosystem that is unfavorable for immune cells trafficking. Moreover, there are evidences from several studies that B7H3 is overexpressed by the tumor vasculature components, making them distinctive compared to the healthy vasculature. By flow cytometry, we found that B7H3 is highly expressed on our primary cell lines vascular endothelial cells (HUVEC) and human lung fibroblasts (hLFB) (Figure 3.1 B).

To ensure reliable control for our experiments involving H196 (that at baseline we just demonstrated that overexpress B7-H3), we obtained an H196 B7-H3 negative line (H196.B7H3KO) by knocking out the gene for B7H3 expression. We confirmed by flow cytometry the success of the editing, showed no B7H3 expression in the H196.B7H3KO. (Figure 3.1 C) and we could use this new cell line as negative control for H196.

3.2 Evaluation of the B7H3-ADC's ability to selectivity bind the target: B7H3-ADC selectively binds to B7H3⁺ cells

To confirm the target specificity of B7H3-ADC, we assessed its binding activity to B7H3 protein by incubating CORL47 and H82 and H196 with two different doses of B7H3-ADC. As control, we performed the same experimental condition with the Isotype and without treatment as well. After a short-time incubation (2 hours) the binding was evaluated by flow cytometry, and it resulted as positive only in the condition with B7H3-ADC treatments (Figure 3.2 A). The assay was repeated at 24 hours incubation to confirm what previously obtained and to check for any other unspecific bindings at longer-term culture (Figure 3.2 B). Moreover, it's notable that the positive shift of the signal indicating the binding it's proportional to the number of bindings, mirroring the different expression of B7H3 on each cell line emerged in the previous assay. We could assert that B7H3-ADC specifically bound to B7-H3 expressing cancer cells, but not that of B7-H3-negative cancer cells *in vitro*.

3.3 Evaluation of B7H3-ADC's tumoricidal effect: B7-H3 is cytotoxic on Non-NE SCLC and vascular components in 2D viability assay

Since MHC I^{hi} SCLC specifically upregulates B7-H3 expression, we hypothesize that these cells should be susceptible to ADC-mediated cytotoxicity independent of immune effector function. To investigate the direct tumoricidal effects of the ADC on immunologic SCLC subtypes, we treated CORL47 as representative of NE and B7-H3 negative SCLC and H196 as representative of Non-NE and B7-H3 positive SCLC cell line with different concentrations dose of B7H3-ADC from 0 to 150 µg/mL.

Cells viability was quantified by a CTG viability assay after 6 days treatment: H196 showed growing sensitivity to the ADC with increasing dose concentration, with an IC50 at around 10 µg/mL concentration (Figure 3.3 A,B,C), while CORL47 exhibited resistance to ADC up to 15 µg/mL concentration dose (Figure 3.3 B). We hypothesized that the sensitivity that the B7-H3 negative-cell line showed at concentrations above 15 µg/mL was related to an unspecific cytotoxic effect. Including in the assay the treatment with Isotype as negative control, as expected, we found no toxic effect on both B7-H3 positive and B7-H3 negative cell lines up to 15 µg/mL, but above it the cells started to show decreasing viability: this confirmed our hypothesis of unspecific cytotoxicity above around 15 µg/mL. To ensure the reliability of our results, we included the treatment with free payload as a positive control that showed increasing cytotoxic effect at increasing concentration dose on both B7-H3 positive and negative cell lines (Figure 3.3 B).

Similarly, the assay was performed on H196 B7-H3 positive (H196.scr) and H196 B7-H3 negative (H196.B7H3 KO): under B7H3-ADC treatments the two cell lines' trend was overlapped up to 0.015 µg/mL, after which the H196 B7-H3 negative showed to be resistant compared to the B7-H3-expressing H196, with an evident gap in the viability up to our concentration of interest (Figure 3.3 C).

At the light of the B7-H3 upregulation characterizing even vascular components, we performed the same 2D viability assay on HUVEC and hIFB to evaluate B7H3-ADC cytotoxic effect. In the same assay we included B7-H3 negative representative B7-H3 negative SCLC cell lines that, as the previously data related to CORL47, showed to be resistant up to our concentration of interest. Surprisingly, despite the

overexpression of B7-H3 of the vascular components, both hIFB and HUVEC exhibited relative resistance up to the highest concentration dose (Figure 3.3 D,E). Same behavior for the fibroblasts has been observed under free payload treatment, while the Isotype control turned to be relatively toxic, but following a constant trend from the lowest to the highest concentration (Figure 3.3 D). The endothelial cells, instead, exhibited increasing sensitivity to the payload free treatment, with a similar trend observed to all the SCLC cell lines (Figure 3.3 E).

All the data obtained from the viability quantification was consistent with the observations under the microscope, where the increasing of cytotoxic effect corresponds to the disruption of the cells spheroid: the cytotoxic effect manifested as a shrinkage in the size of the cells spheroid and accumulation of cell debries, becoming more evident the greater the effect (Figure 3.4).

3.4 Evaluation of B7H3-ADC's effect on *in vivo*-like vasculature: B7H3-ADC is effective on microvascular network in a 3D viability assay

To assess the impact of B7H3-ADC on endothelial cells and fibroblasts in the context of a more physiological vasculature-like structures, we utilized a 3D viability assay with a small-caliber MVN. The MVN was generated through a self-assembled vasculogenesis process that involved the co-culture of HUVEC and hIFBs in a fibrin gel for six days, resulting in the presence of macrovessels on both side channels (Figure 3.5 A). We exposed the MVN models to two different concentrations of B7H3-ADC (0.1 and 10 $\mu\text{g}/\text{mL}$) for six days, as well as isotype and free payload as negative and positive controls, respectively. An untreated model served as an additional negative control, while another positive control was represented by STING agonist 2'3' cGAMP (1 $\mu\text{g}/\text{mL}$) treatment. Indeed, there are evidences from previous studies that 2',3'-cGAMP plays an important role in activating STING signaling in endothelial cells and increasing vascular permeability. The activation of STING is related to TBK1-IRF3-dependent signaling process, which leads to the production of pro-inflammatory cytokines [60], [150]. In order to maintain optimal culture condition for these types of cells, we carefully refreshed the culture medium daily including all the different treatments. After 6 days of treatments, we evaluated both HUVEC and hIFBs viability. The results showed that, while at the lower concentration of treatments

there's no evidence of significant differences between the treatments, B7H3-ADC had a cytotoxic effect at a concentration of interest of 10 $\mu\text{g}/\text{mL}$ (identified in previous assays as the IC50 for the H196), quantitatively reducing the total amount of cells forming the network by 40% (Figure 3.5 B), a toxic effect that resulted much more significant if we compare it with what previously obtained in 2D viability assay on both HUVECs and hIFBs. All the negative controls confirmed the preservation of cells viability, while free Payload turned out to be extensively cytotoxic on the MVN suggesting that while the Isotype is not able to target any antigens on endothelial cells or fibroblasts, the compound is able to selectively target and be internalized by B7H3⁺ cells, leading them to death through apoptosis caused by the release of the payload in the cytosol. Since all the cells of the model were B7H3⁺, the difference between the ADC treatment condition and the free payload one statistically non-significant, as we hypothesized (Figure 3.5 B, 3.6).

3.5 Evaluation of the B7H3-ADC effect on the vascular structure: B7H3-ADC enhances vascular permeability in a 3D permeability assay

At the light of the results observed on the toxic effect that the B7H3-ADC had on vascular components, we wanted to investigate how this would impact the vascular permeability. Firstly, we exposed the model to the same treatments and concentration of the previous assay: B7H3-ADC, Isotype and free Payload at 0.1 and 10 $\mu\text{g}/\text{mL}$, untreated negative control, while STING agonist 2'3' cGAMP (1 $\mu\text{g}/\text{mL}$) as positive control. After 6 days exposure we evaluated the vascular permeability as the flux of solute across the walls of the vascular network. To assess the aim, we performed a permeability assay using a FITC-Dextran 70 kDa on a macrovessel model (Figure 3.7 A). The results showed an increase in the permeability coefficient under B7H3-ADC treatment compared to the negative controls, overall comparable with the one measured for both positive controls (Figure 3.7 B,C). Together with the previous findings, it confirms the ability of the B7H3-ADC to target and be cytotoxic to the vascular components, and that this impacts the integrity of the vascular structure.

Chapter III Results

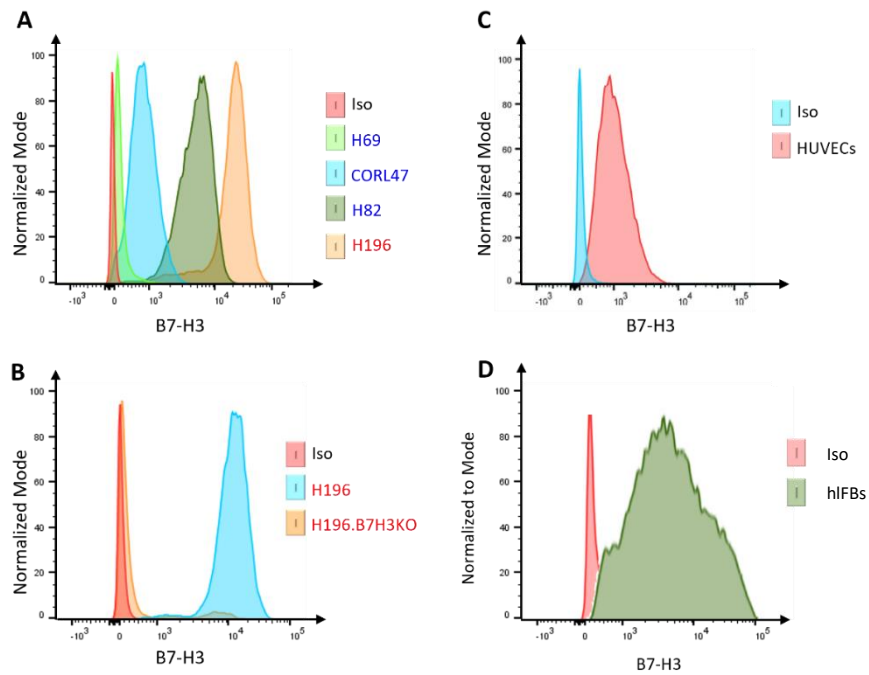


FIGURE 3.1 | Flow cytometry of the B7-H3 expression. (A) B7-H3 expression on our representative NE (blue) and Non-NE (red) cell lines. (B) B7-H3 expression on our stromal cells components endothelial cells (HUVECs) and fibroblasts (hIFB). (C) B7-H3 expression on Non-NE H196 and its corresponding after the knocking-out of the gene for B7-H3 expression.

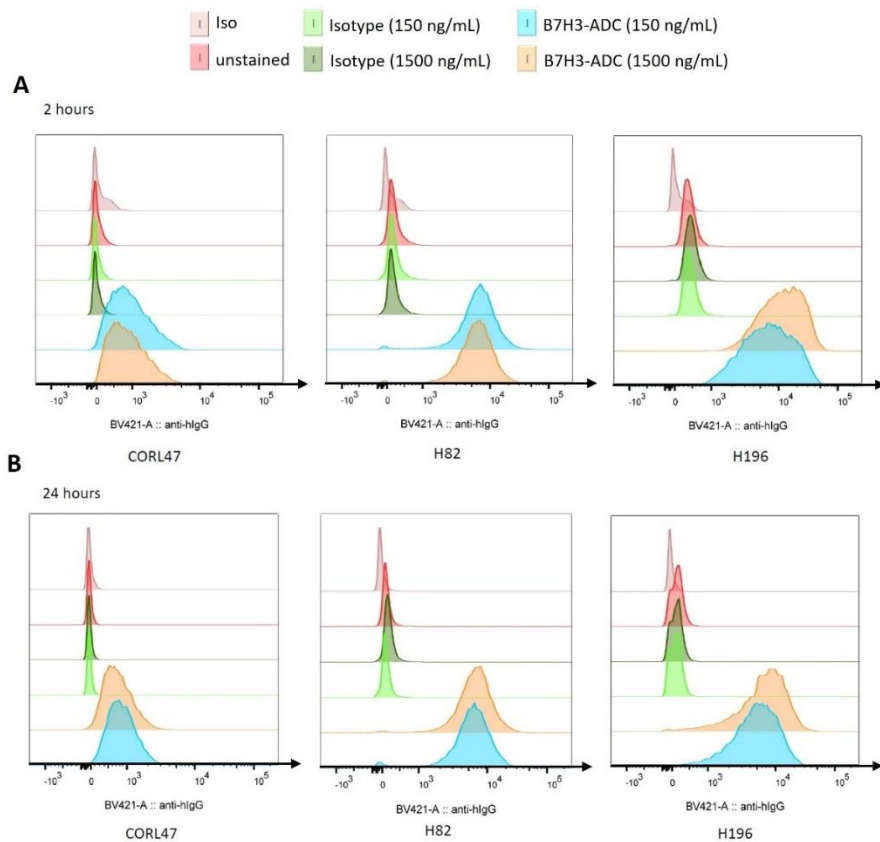


FIGURE 3.2 | Flow cytometry of anti-hlgG expression for the binding assay: the anti-hlgG specifically binds B7H3-ADC. The positive signal of the anti-hlgG is an indirect measure of the B7H3-ADC binding to the B7H3⁺ cells. The amount of the shift on the x axis is reflecting the B7H3 expression by the target cells (Figure 3.1). (A) Incubation time: 2 hours. (B) Incubation time: 24 hours.

Chapter III Results

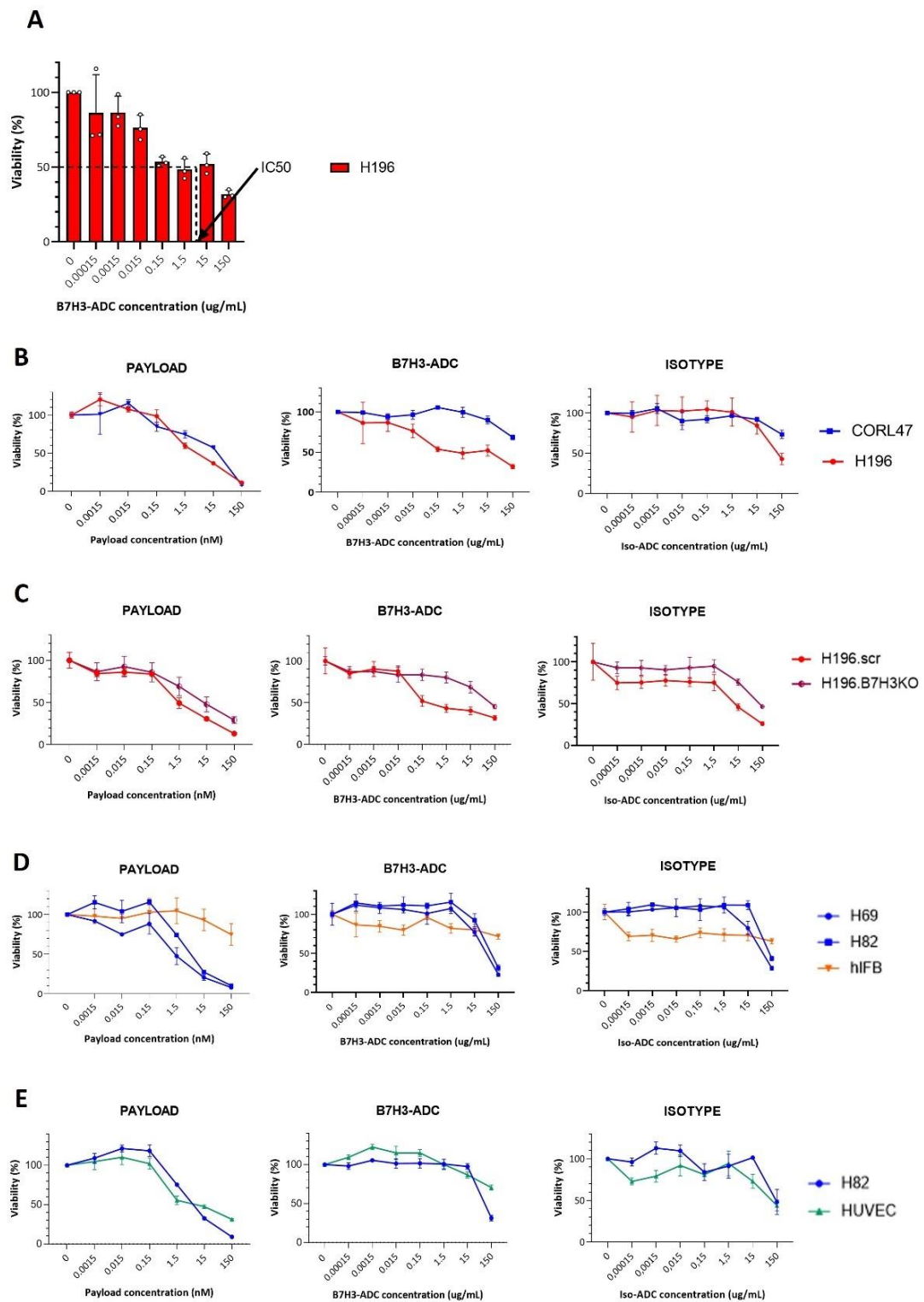
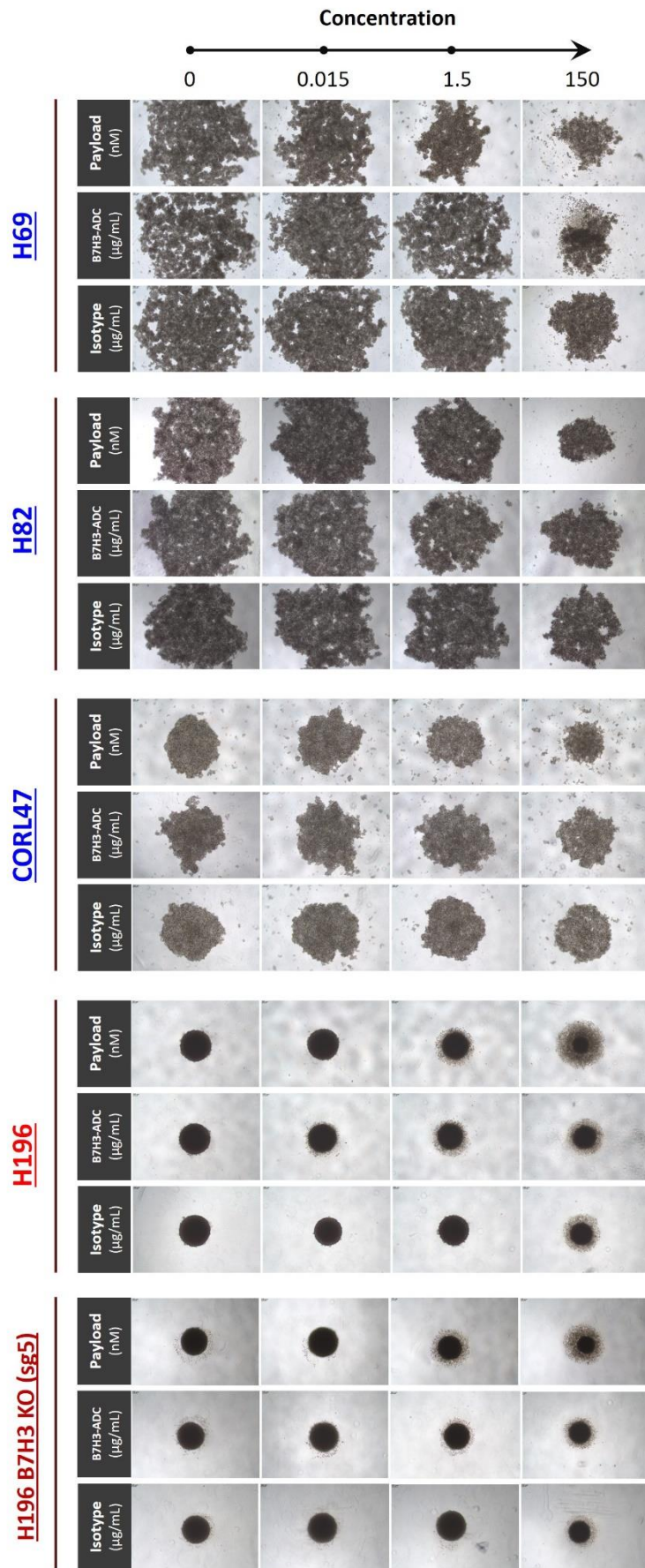


FIGURE 3.3 | Plots of the CTG viability assay quantification analysis. (A) Bar plot of CTG viability assay quantification on H196 after 6 days B7H3-ADC treatment at increasing concentration doses. IC50 individualized at 10 $\mu\text{g}/\text{mL}$ concentration dose. (B, C, D, E) Line charts of the CTG assay quantification performed on target cells after 6 days treatments at increasing concentration doses: free payload treatment on left sides, B7H3-ADC treatment in the center, Isotype treatment on the right side.

Chapter III Results



Chapter III Results

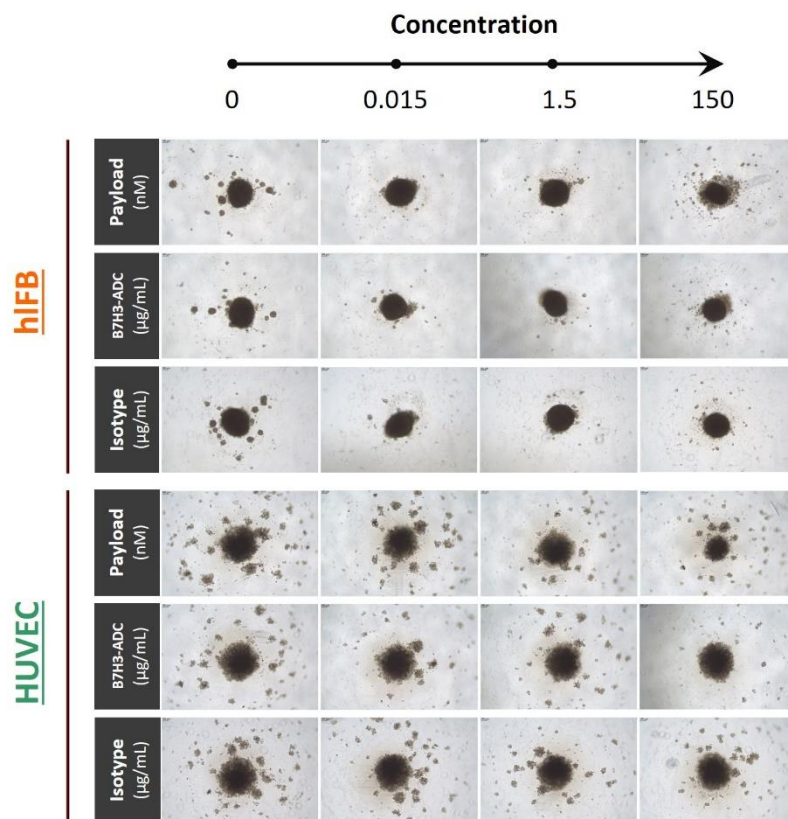


FIGURE 3.4 | Optical microscope representative images of the different target cells cultures (labeled on the left) after 6 days treatments at increasing concentration doses. For each cell line: Payload treatment on the first row, B7H3-ADC treatment in the central row, Isotype treatment in the third row.

Chapter III Results

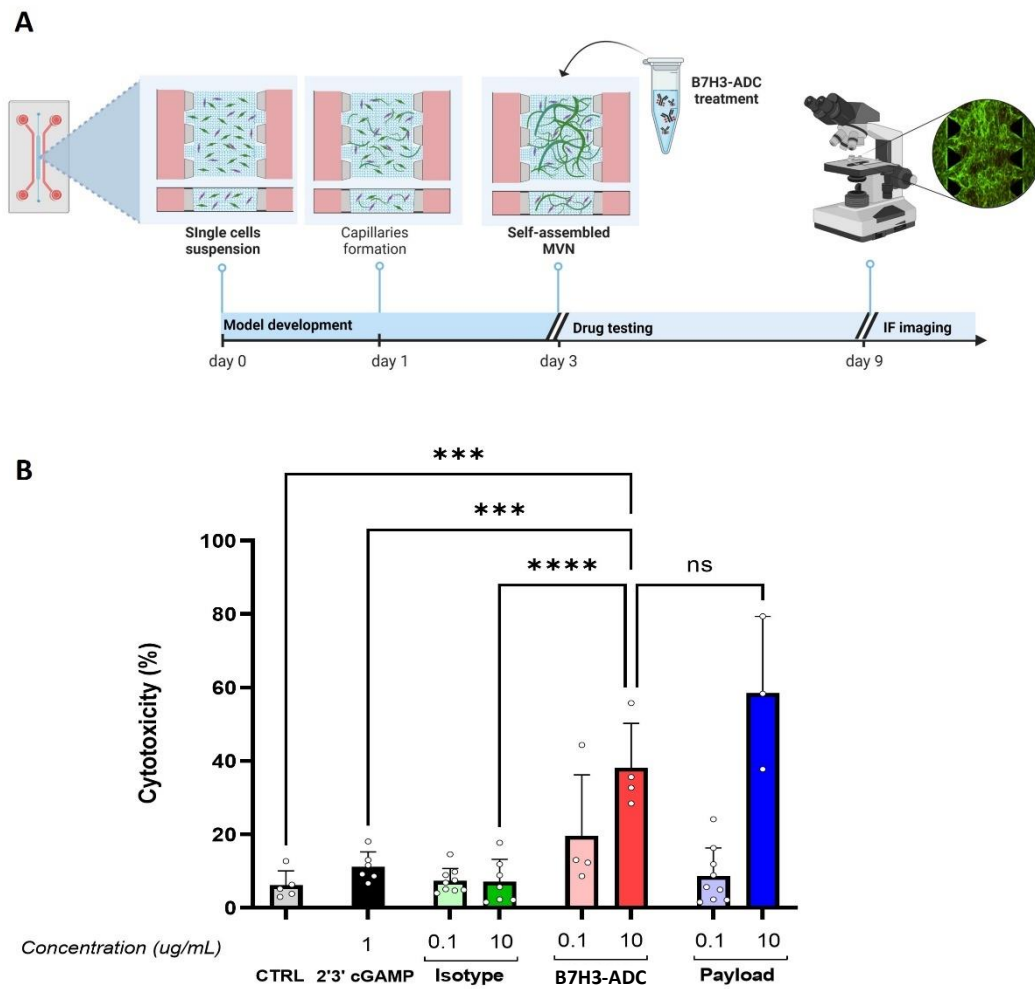


FIGURE 3.5 | 3D Viability assay on the MVN model after 6 days treatments. (A) Timeline experiment of the 3D viability assay on MVN from the model development to final IF imaging. (B) Treatment cytotoxicity (%) of the target cells under the different treatment conditions quantified by the signal of PI (dead) channel quantification relative to the total amount of cells in the device (AO+PI).

Chapter III
Results

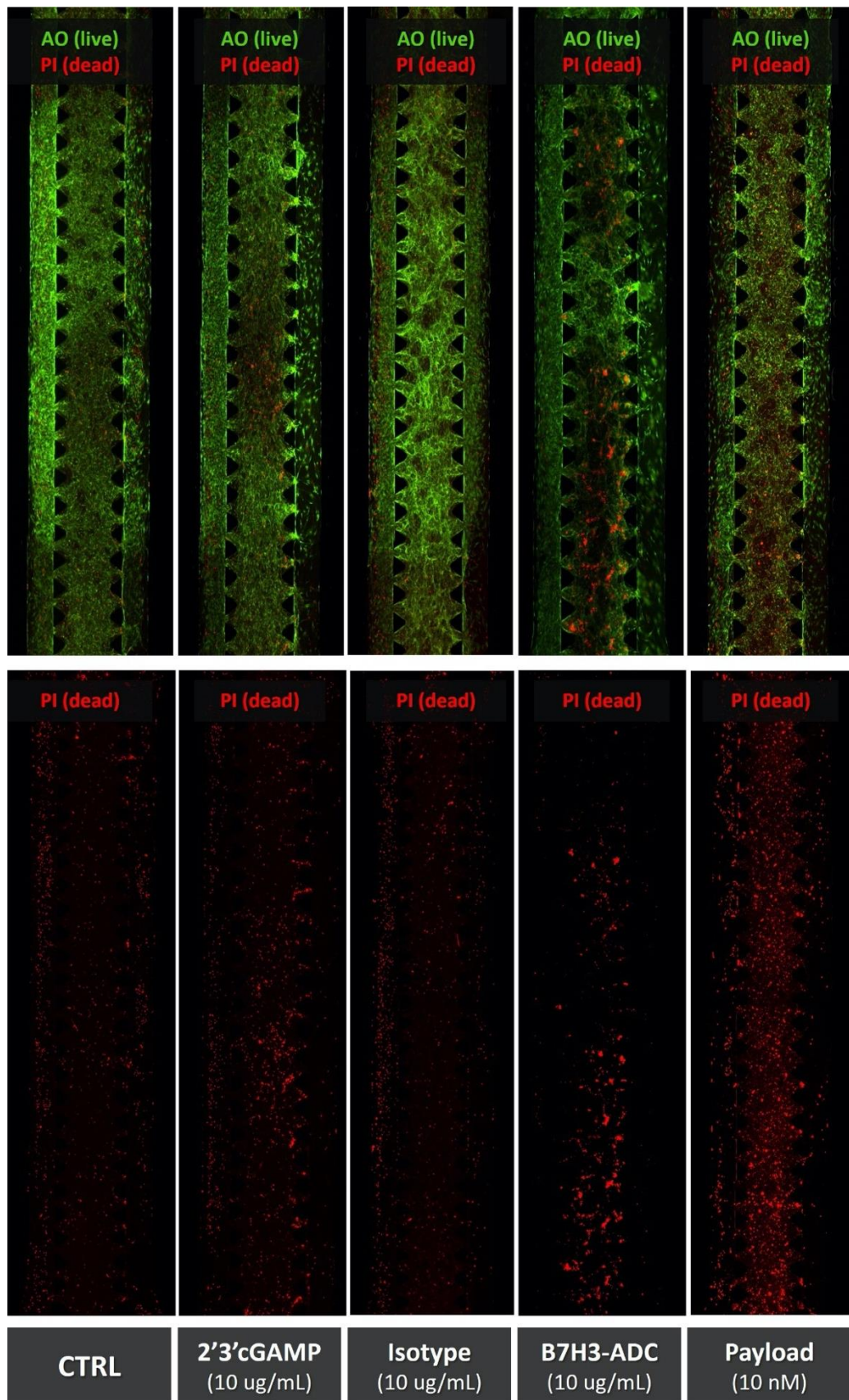


FIGURE 3.6 | IF representative images of the MVN models after 6 days under the different treatments (comparison at the same concentration dose of interest). Top side: all channels (FITC – green = live cells; TRITC – red = dead cells). Bottom side: TRITC – red = dead cells.

Chapter III Results

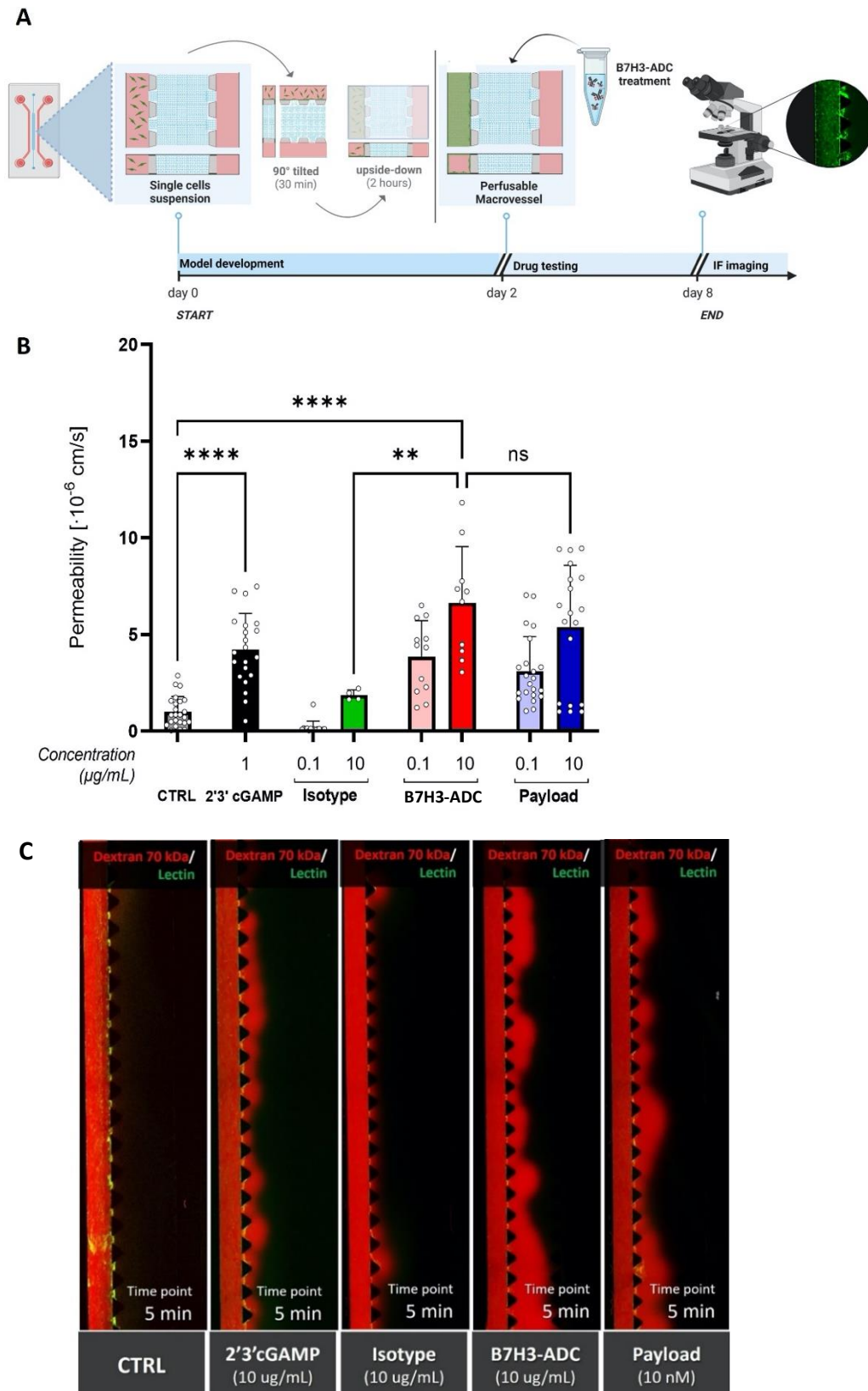


FIGURE 3.7 | 3D permeability assay on the macrovessel model after 6 days treatments (A) Timeline experiment of the 3D permeability assay on macrovessel from the model development to final IF imaging. (B) Cells cytotoxicity (%) under the different treatment conditions quantified by the signal of PI (dead) channel quantification relative to the total amount of cells in the device (AO+PI). (C) IF representative images of the flux of solute across the macrovessel toward the central gel region (Dextran 70kDa) at the same time point after 6 days treatments at the concentration doses of interest

3.6 Investigation of the role of the vasculature in immune cell trafficking: the vasculature acts as a barrier to NK cell infiltration in a 3D migration assay

As previously described, the SCLC TME is characterized by the absence of infiltrated immune cells within the tumor bed. In order to dissect the mechanisms responsible for immune evasion, we started to investigate the role of the vasculature. The presence of vasculature within the TME creates an intricate ecosystem, that could act as a physical obstacle for the immune cell infiltration. To investigate how this barrier impacts the extravasation and infiltration NK cells into the TME, we conducted a 3D migration assay.

In our experimental setup, CORL47 spheroids were embedded in the central collagen gel, and we generated a hollow lumen within one of the side channels, emulating a perfusable blood vessel located in close proximity of the tumor. Firstly, we examined the ability of NK cells, injected into the macrovessel, to extravasate and migrate toward the tumor spheroids. After allowing the system to culture for 48 hours, we quantified the ability of NK cells to migrate (Figure 3.8 A) The extravasation rate measured resulted significantly reduced compared to the infiltration measured in the control condition without the macrovessel, suggesting that the presence of the vascular barrier led to a significant decrease in NK cell migration (Figure 3.8 B). We then measured even the tumor cells viability and, from the quantification analysis, was observed that the cytotoxicity measured in the culture involving the presence of the vessel was significantly lower than the one measured in the condition without the vessel (Figure 3.8 B). This result allowed us to confidently assess that the vasculature is acting as an obstacle to immune cells trafficking.

3.7 Evaluation of NK cells' cytotoxic effect on SCLC molecular subtypes in a 2D co-culture: Neuroendocrine-SCLC is sensitive to NK-cell mediated cytotoxicity in a 2D viability assay

Considering the assumption that the complex vasculature acts as an obstacle for immune cells to infiltrate, our next objective was to explore the potential outcomes if immune cells could come into contact with tumor cells. At the light of the knowledge that 70% of SCLC cases are characterized by downregulation of MHC-

I, according to the mechanisms of action characterizing the immune cells these cells, these tumor cells should be undetectable by T cells, but might be susceptible to NK cell-mediated cytotoxicity [24]. Current studies in our lab focus on examination of the regulators influencing sensitivity to NK cell-mediated cytotoxicity: interestingly, it was demonstrated that HLA-ABC molecules played a significant role in mediating resistance to NK cell-mediated cytotoxicity in MHC I^{hi} SCLC cell lines. Consequently, we conducted experiments to assess the susceptibility of our SCLC cell line panel to primary NK cells using a short-term 2D viability assay. Firstly, we confirmed HLA-ABC expression on several SCLC lines, representative of the MHC I expression: by flow cytometry we confirmed the downregulation of MHC I of our NE-SCLC cell lines and the upregulation of MHC I in our Non-NE SCLC cell lines from our panel (Figure 3.9 A). Co-culturing SCLC cells with primary NK cells at increasing effector to target ratios (E:T ratios) revealed that MHC I^{lo/neg} SCLC cell lines displayed sensitivity to NK cell-mediated cytotoxicity, whereas MHC I^{hi} SCLC cell lines were relatively resistant, although they exhibited moderate sensitivity at high E:T ratios (Figure 3.9 B). Through the elimination of the B2M gene, the correct formation of the MHC I complex was disturbed, resulting in the absence of operative MHC I molecules on the cellular surface (Figure 3.9 C). Upon conducting the viability assay on MHC I^{hi} cells following the knock-out of B2M, we observed heightened sensitivity comparable to that of intrinsically MHC I^{lo/neg} cell lines (Figure 3.9 D). We refer to SCLC MHC I^{hi} cells as NE, while to MHC I^{lo/neg} as Non-NE.

3.8 Evaluation of NK cells' cytotoxic effect on SCLC molecular subtypes in a 3D MPS: Neuroendocrine-SCLC is sensitive to NK-cell mediated cytotoxicity in a 3D viability assay

At the light of the results obtained from the previous result, we translated the 2D viability assay in a 3D MPS in order to evaluate the NK-mediated cytotoxicity in a more physiologically relevant model of the TIME. We performed the viability assay on tumor spheroids of some representative NE-cell lines subtype and on some representatives of the Non-NE subtype, previously formed in ultra-low attachment, embedded in collagen gel hydrogel with primary NK cells at 1:1 E:T ratio (Figure 3.10 A).

Chapter III Results

At 24 hours co-culture, we observed a significant difference in the sensitivity of the MHC I^{lo/neg} cell lines to NK cell-mediated cytotoxicity when compared to the MHC I^{hi} cell lines, and resulted relatively more resistant (Figure 3.10 B), coherently with what previously shown in 2D viability assay (Figure 3.10 B) and confirming our hypothesis that NE SCLC are, at baseline, susceptible at the NK cells action, and the reason why this doesn't happen *in vivo* is to be found in the TME.

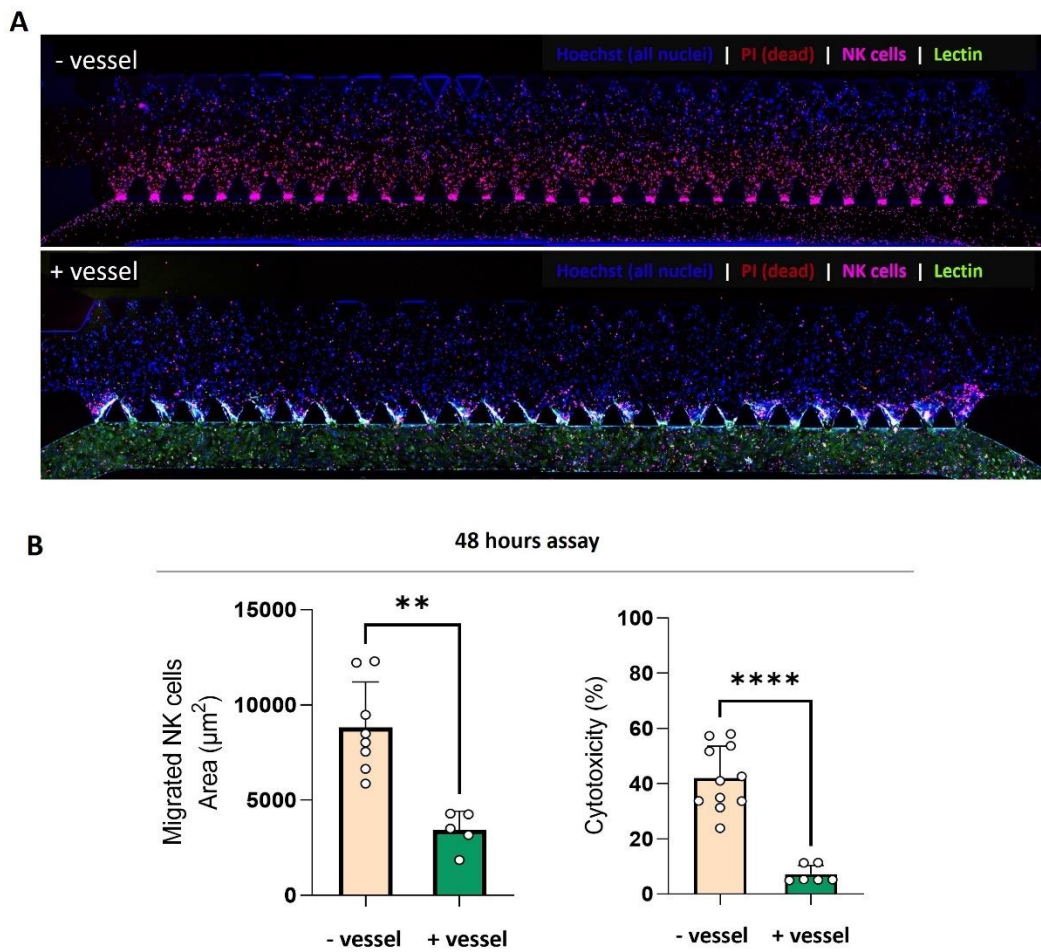


FIGURE 3.8 | 3D migration assay. (A) IF representative images of the devices after 48 hours culture in absence or presence of the macrovessel on the side. The NK cells are pink labeled. (B) NK cell migration (left bar graph) and NK cell mediated-cytotoxicity (%) quantification (right bar graph) at the final time point with and without macrovessel barrier.

Chapter III
Results

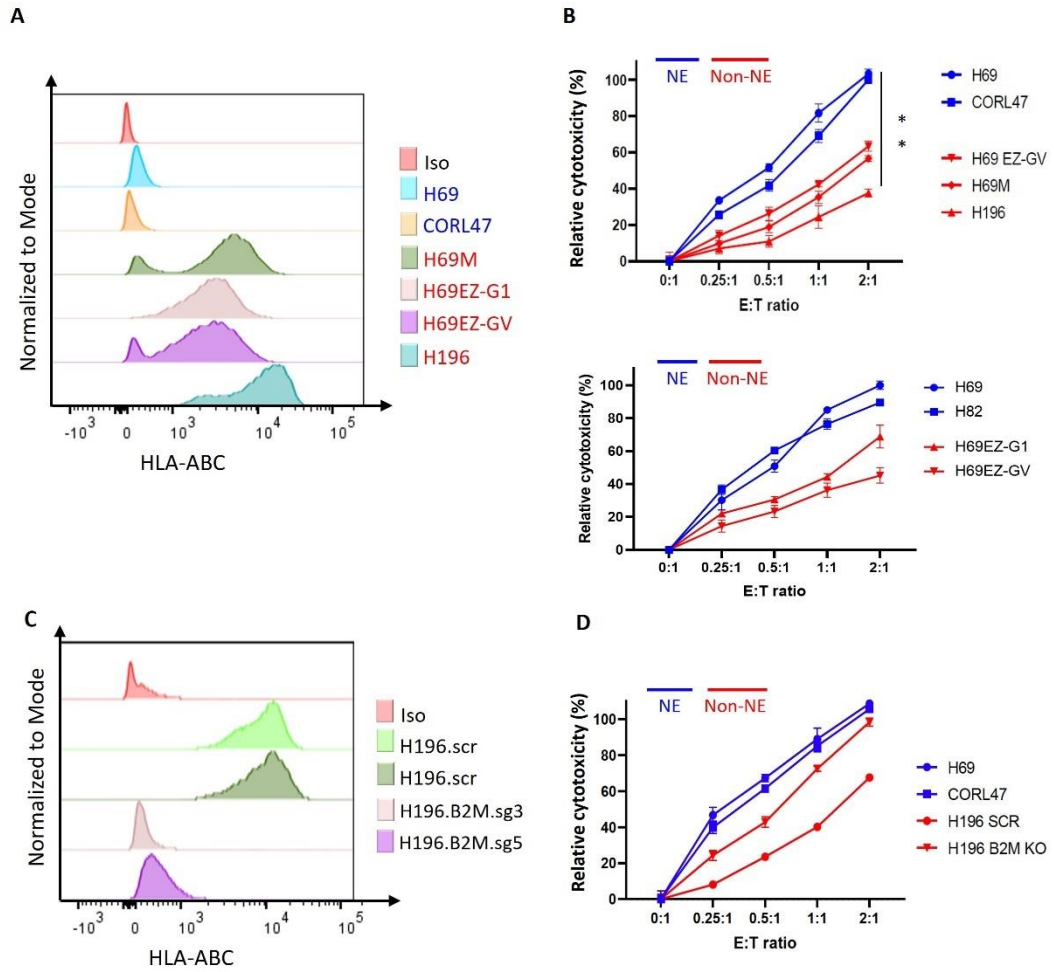


FIGURE 3.9 | HLA-ABC expression (representative of the MHC I) on our cell lines panel and 2D viability assay quantification analysis. (A) Flow cytometry of the HLA-ABC expression on our cell lines panel. (B) CTG viability assay quantification analysis from 4 hours 2D co-culture of target cells with NK cells at increasing E:T ratio: the NK cell-mediated cytotoxicity measured is related to the control condition (0:1)

Chapter III
Results

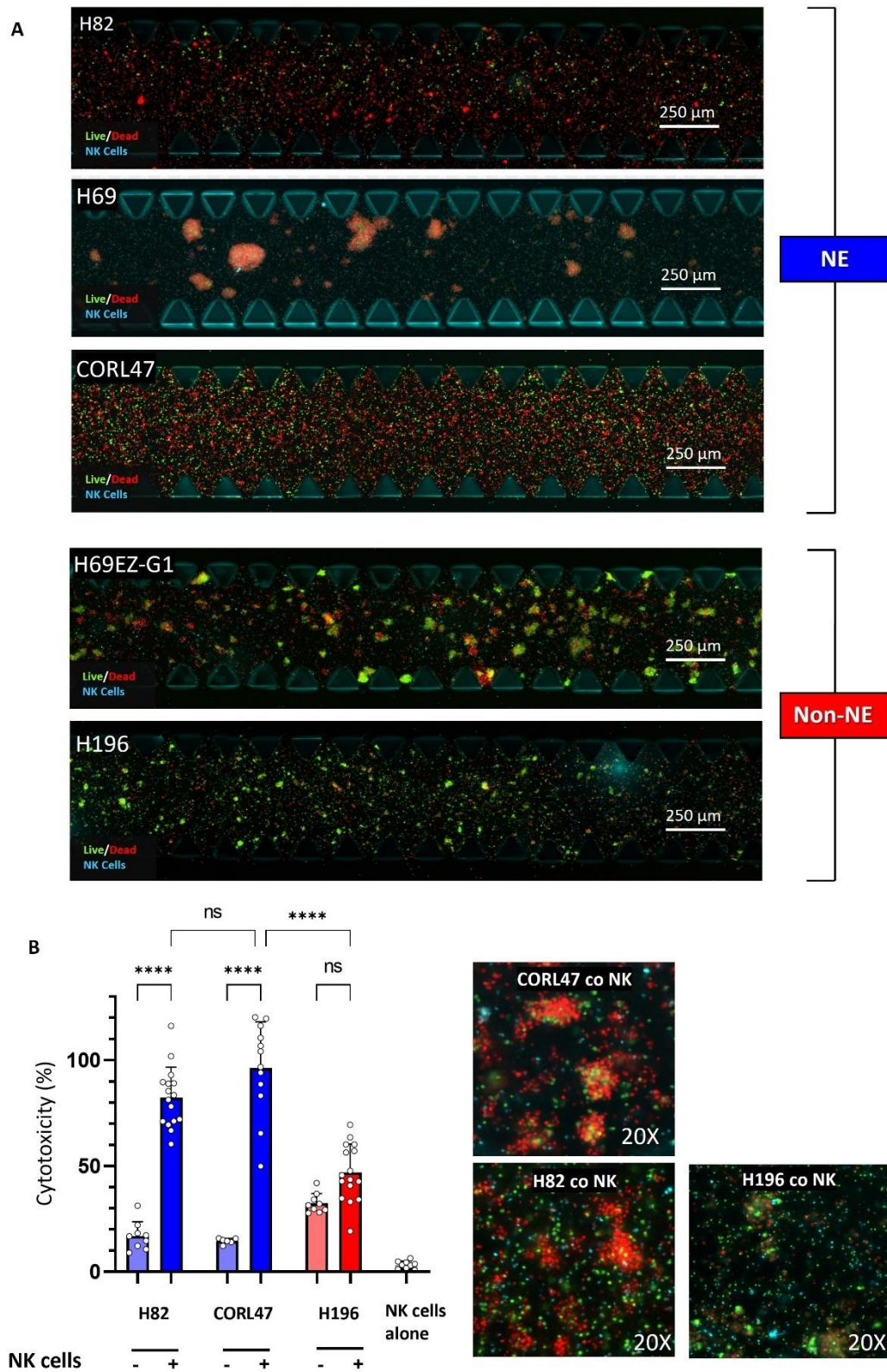


FIGURE 3.10 | 3D viability assay on Tumor cells – NK cells co-culture: (A) IF representative images of tumor spheroids and NK cells in the central gel region after 24 hours co-culture (AO/PI live/dead staining and NK cells blue traced). (B) Left side: Bar graph of NK cell-mediated cytotoxicity (%) on the target cells under the different treatment conditions quantified by the signal of PI (dead) channel quantification relative to the total amount of cells in the device (AO+PI). Right side: IF representative images at 20X of the 3D co-cultures (AO/PI staining).

Chapter IV

Discussion

Results discussion: insights and implications

In this thesis, we first aim to determine if the previous observation conducted on mouse models that employing an ADC targeting B7-H3 can have a dual effect on both tumor cells and tumor-associated vasculature[101] holds in a human SCLC model, and to validate a B7H3-ADC-based therapy to simultaneously target B7H3⁺ tumor cells and vasculature.

We initially aimed to profile the expression of B7-H3 on our SCLC cell lines panel and vasculature components. These SCLC cell lines were selected to represent the different immunological subtypes of SCLC (section 3.1). By flow cytometry, we found that H69 and CORL47 cell lines had low levels of B7H3 expression, while H82 showed moderate levels. On the other hand, the H196 cell lines exhibited an upregulation of B7-H3 expression. Moreover, we found that B7-H3 is expressed on the stromal components vascular endothelial cells (HUVEC) and human lung fibroblasts (hLFB), confirming them as potential targets for B7H3-ADC treatment.

The direct tumoricidal effect and the impact on vascular components was evaluated prior determining the target specificity of the compound. The target specificity of B7H3-ADC was confirmed by testing its ability to bind to B7H3 protein (section 3.2). After a short-term incubation of SCLC cell lines CORL47, H82, and H196 with B7H3-ADC treatment, the number of bindings was measured by flow cytometry, which showed positive shifts only in the B7H3-ADC treatment group, which indicates that B7H3-ADC selectively targets B7-H3 expressing cancer cells *in vitro*. Moreover, the number of bindings was consistent with the different levels of B7H3 expression previously observed on the cell lines used for the assay. The reliability of the result was confirmed by incubating the same cell lines with Isotype as the negative control, and the assay was repeated with a longer incubation time. Based on these results, we confidently conclude that B7H3-ADC specifically binds to B7-H3 positive cancer cells.

This led us to confidently move to the evaluation of the direct cytotoxic effect of the compound on SCLC cell lines, endothelial cells, and fibroblasts. CORL47 as representative of B7-H3 negative SCLC and H196 as representative of B7-H3 positive SCLC cell line were treated with B7H3-ADC in 2D culture (section 3.3). Cell viability was quantified by measuring ATP levels after 6 days of treatment. Coherently with their characterizing B7-H3 upregulation, H196 showed growing sensitivity to the ADC at increasing dose concentration, with an Half maximal Inhibitory Concentration (IC₅₀) of around 10 µg/mL concentration, while B7-H3 low/negative cell lines exhibited resistance, due to the impossibility to be targeted by the compound. However, all cell lines showed relative sensitivity at the treatment above 15 µg/mL, which we assumed was related to an unspecific cytotoxic effect, due to the similar effect with the isotype control. This result shows that B7-H3+ cell lines are susceptible to B7H3-ADC cytotoxicity, independent of immune effector function.

At the light of the B7-H3 upregulation on vascular components, we conducted the same viability assay on endothelial cells (HUVEC) and fibroblasts (hIFB) to examine the effect of B7H3-ADC (section 3.3). Surprisingly, both hIFB and HUVEC cells showed relative resistance up to the highest concentration dose, but since the 2D culture wasn't replicating the physiological architecture of the stromal

cells *in vivo*, we considered this result inconsistent and decided to translate the experiment in a 3D microphysiological system using microfluidic device.

As anticipated, in order to evaluate the effects of B7H3-ADC on endothelial cells and fibroblasts within a more realistic vasculature-like structure, we conducted a 3D viability assay using a small-caliber MVN model developed in a microfluidic device (section 3.4). Upon testing at a concentration of 10 $\mu\text{g}/\text{mL}$, which we had previously determined to be the IC50 for H196, B7H3-ADC exhibited cytotoxic effects that led to a 40% reduction in the overall number of cells forming the network. This marked disparity in results as compared to the 2D viability assay conducted on stromal components affirmed the unreliability of the 2D culture in evaluating vasculature's sensitivity to the treatment.

Considering the results observed on the toxic effect that the B7H3-ADC had on vascular components, we wanted to further investigate how this would impact vascular permeability (section 3.5). By a FITC-Dextran 70 kDa permeability assay on our 3D macrovessel model treated with B7H3-ADC, we demonstrated an increase in the permeability coefficient. Together with the previous assay, it confirms the ability of the B7H3-ADC to target and be cytotoxic to the vascular components, and that this impacts the permeability of the vascular structure. The enhancement of vascular permeability by B7H3-ADC has opened up new perspectives and potential implications for our study, particularly in light of the lack of infiltration of immune cells characterizing the *in vivo* SCLC parenchyma.

Extending the focus to the entire TME, our study moved into the investigation on the role of the vasculature, and how it impacts on the ability of immune cells to infiltrate. In this work, we demonstrate that the presence of vasculature within the TME creates a formidable obstacle for immune cell infiltration by quantifying the migration of the NK cells toward the tumor cells in presence and absence of a vascular barrier (section 3.6). Again, microfluidics was necessary to assess this aim in order to have spatial and temporal control, as well as to model a 3D perfusable macrovessel in which we could mimic the immune cells trafficking. By culturing CORL47 spheroids embedded in the central collagen gel, we evaluated the ability of NK cells to extravasate from the macrovessel. This design aimed to mimic the physiological conditions encountered by immune cells circulating in the bloodstream *in vivo*, allowing us to better replicate what occurs within the TME

during the natural immune response to tumors. After allowing the system to culture for 48 hours, we analyzed the results quantitatively. What emerged from our analysis was that the presence of the vascular barrier led to a significant decrease in the ability of NK cells to migrate, confirming our hypothesis that the vasculature acts as a physical barrier to immune cells infiltration. This result could explain the inability of the immune cells *in vivo* to reach and kill SCLC cells, and it posed a new question about how they would impact SCLC cells viability if they would be able to overcome this barrier.

As previously described, the identification of SCLC immunological subtypes raises the question of how their difference in MHC I expression affects immune cells' ability to target and kill tumor cells. The absence of an immune response *in vivo* in the MHC I^{lo/neg} SCLC TIME is apparent [24]. Nevertheless, the decrease in tumor MHC I expression implies that these cells may be vulnerable to NK cell-mediated cytotoxicity. MHC I is the primary inhibitory ligand for NK cells, so we conducted experiments to evaluate the sensitivity of our SCLC cell line panel to primary NK cells via short-term co-culture.

By evaluating the expression of MHC I in our SCLC cell lines and relating it with the previous results on B7-H3 expression, we observed that, interestingly, B7-H3 upregulation was observed in MHC I^{hi} cell lines: this double positivity of the NE-SCLC is associated with the poorest prognosis (section 3.7).

Furthermore, HLA-ABC molecules appear to play a significant role in mediating resistance to NK cell-mediated cytotoxicity in MHC I^{hi} SCLC cell lines. This suggests that MHC I^{lo/neg} SCLC cells may be responsive to NK cell-mediated cytotoxicity. In this study, we evaluated SCLC subtypes sensitivity to NK cells action by short-term 2D co-cultures, which confirmed that MHC I^{lo/neg} SCLC cell lines are very sensitive to, while MHC I^{hi} SCLC cell lines were relatively resistant (section 3.7).

The results of the study demonstrated that the mechanism of NK cell targeting in SCLC is based on non-self-recognition by the lack of MHC I on target cells. This suggests that NK cells can be highly effective against NE SCLC cells upon contact. Through the elimination of the B2M gene, the correct formation of the MHC I complex was impaired, resulting in the absence of operative MHC I molecules on

the cellular surface. Upon conducting the viability assay on MHC I^{hi} cells following the knock-out of B2M, we observed enhanced sensitivity comparable to that of intrinsically MHC I^{lo/neg} cell lines.

To investigate SCLC cell's sensitive to the NK cell's action in a more physiological manner, we translated the assay in a 3D Microphysiological System (MPS) (section 3.8). A 3D culture is more representative of the interaction between tumor and immune cells in the TIME. In this culture, solid tumors usually appear in a spheroid-like structure. Spheroid-shaped cells are more protected from the action of immune cells due to several factors related to their three-dimensional structure. Firstly, spheroid cells have a more compact and dense arrangement, which creates a physical barrier that hinders the infiltration of immune cells. The dense packing of cells in spheroids limits the accessibility of immune effectors, such as cytotoxic T cells and natural killer cells, to the inner layers of the spheroid, making it difficult for these immune cells to reach and attack the cells within. Furthermore, spheroid cells often have a hypoxic microenvironment, meaning there is a reduced oxygen supply in the inner regions of the spheroid. Hypoxia can induce changes in gene expression, leading to the upregulation of factors that promote immune evasion and resistance to immune-mediated cytotoxicity. In addition to this, spheroid cells frequently exhibit altered cell surface molecule expression and signaling pathways, which can modulate their interaction with immune cells. These changes might include modifications in the expression of adhesion molecules or immune checkpoint proteins, allowing spheroid cells to evade immune recognition and attack. Lastly, the collagen matrix in which the cells are embedded in the device represents a physical barrier to cell transit, which is another factor to consider when deciding the experiment duration.

The viability quantification after 24 hours of co-culture resulted in a significant difference in the sensitivity of the MHC I^{lo/neg} cell lines to NK cell-mediated cytotoxicity when compared to the MHC I^{hi} cell lines, coherently with what previously obtained in 2D viability assay. These results led us to assert that NE-SCLC subtype is sensitive to NK cell-mediated cytotoxicity.

Strengths, limitations and future perspectives of the study

The use of a microfluidic device in this study proved to be pivotal in modeling the vasculature, whether as a macrovessel or microvascular network, for the purpose of validating the efficacy of ADC-based therapy on vascular components. Additionally, the precise spatial and temporal control provided by this method was critical in exploring the NK cells trafficking.

Despite the potential of these models, our next objective is to advance beyond the current capabilities by fully replicating the complex *in vivo* TME tumor microenvironment, that comprises multiple cell types, extracellular matrix components, and gradients of nutrients and signaling molecules. In the future, we plan to introduce other immune cell components, such as monocytes, macrophages, and T cells, as well as cytokines and chemokines, to explore their effect on the immune response. Moreover, to model the vasculature in this study, HUVECs have been used HUVECs as representative endothelial cells and h1FB as representative of fibroblasts, which are both primary cell lines derived from healthy tissues. To ensure accuracy, we plan to replace them with tumor-associated vasculature cells (tumor-derived endothelial cells and CAFs). This will give us greater confidence in screening for B7H3-ADC on stromal cells, especially since murine models have shown that tumor vasculature overexpresses B7H3 compared to healthy vasculature. Investigating whether similar results are observed in our human TME model could have significant and promising implications in terms of preserving the healthy tissue in the translation of the therapy in humans.

In this scenario, another step forward would be enhancing the complexity of the ecosystem by merging the model used for the tumor and the model of MVN with the objective of replicating the tumor-infiltrating blood vessels by designing a vascularized tumor model [151].

Although microfluidic devices show great potential, they may not fully capture the complexity of drug transport and metabolism as it occurs in living organisms. This could ultimately impact drug pharmacokinetics, as factors like rapid diffusion and the absence of systemic circulation can alter drug behavior [149]. To ensure that *in vivo* relevance is achieved, further studies examining drug behavior in more

complex models, such as *in vitro* human-on-chip and then animal models are imperative.

Our ultimate future goal of the study is to validate the combination of B7H3-ADC therapy NK cell therapy, combining the ability of ADC to target and deliver potent cytotoxic drugs with NK cell therapy harnessing the innate immune system's ability to recognize and eliminate abnormal cells by NK cell therapy. The synergy between these two modalities has the potential to significantly enhance the efficacy of cancer treatment. While ADC ensures the precise delivery of cytotoxic drugs directly to the tumor site, this targeted approach is complemented by NK cell therapy, which contributes to the destruction of cancer cells through direct cytotoxicity and the release of cytotoxic granules. One notable advantage of combining ADC therapy and NK cell therapy is the potential to address intratumoral heterogeneity, highly observed in SCLC, potentially reaching the different coexisting subtypes of SCLC. Getting into the details, our hypothesis is based on the result that ADC-B7H3 can target and kill Non-NE SCLC which upregulate B7H3 and MHC-I, making them undetectable by NK cells. Additionally, the impact of B7H3 on vasculature would result in increased permeability, thereby facilitating the infiltration of NK cells. This holds great promise for augmenting their role as an additional layer of targeting against NE SCLC, proven to be sensitive to NK cell-mediated cytotoxicity. The dual precision and potency offered by the combination of ADC therapy and NK cell therapy could represent a cutting-edge strategy that stands out as a promising and innovative approach in the realm of SCLC treatment.

Looking to the future, a promising approach in SCLC treatment could involve the use of nanoparticles (NPs), overcoming some limitations characterizing of ADCs. NPs have proven to be versatile and effective carriers for delivering therapeutic agents to cancer cells [152]. This has made a significant impact in the realm of cancer treatment, with a focus on their unique characteristics and potential applications. The NPs functionalization with specific antibodies, such as B7H3, could be a promising advancement in cancer treatment, Functionalized NPs are versatile carriers that can encapsulate various therapeutic payloads, from traditional drugs to nucleic acids and imaging agents [153]. This adaptability is the cornerstone of a sophisticated and targeted therapeutic strategy, which is a significant departure from conventional one-size-fits-all approaches. One of the key features of this

development is the controlled release mechanism inherent in functionalized NPs: this precision could ensure a more accurate delivery of therapeutic payloads to SCLC cells while minimizing off-target effects [154]. While ADCs have demonstrated remarkable success, concerns persist regarding the potential instability of linkers connecting antibodies to drug payloads, leading to unanticipated releases [155]. Indeed, the linker, responsible for attaching the drug to the antibody, is susceptible to degradation, potentially resulting in premature drug release before reaching the targeted cancer cells. This limitation poses a hurdle in achieving the desired therapeutic concentration within the tumor while minimizing systemic exposure. In contrast, utilizing nanoparticles (NPs) for internalizing and encapsulating therapeutic payloads introduces a robust mechanism for controlled drug release [154]. The encapsulation of therapeutic payloads within NPs acts as a protective shield, safeguarding the payload until it reaches the intended destination. This strategy not only mitigates the risks associated with linker instability but also opens avenues for tailoring drug release profiles based on the unique characteristics of the tumor microenvironment. This approach also paves the way for combination therapies that delve into the intricate landscape of cancer biology. By incorporating multiple therapeutic payloads within a single NP-based delivery system, the strategy aligns seamlessly with the growing understanding of cancer heterogeneity and the need for comprehensive, multi-pronged therapeutic interventions [154]. In comparison to the B7H3-ADCs strategy proposed in this study, the introduction of B7H3-functionalized NPs could potentially enhance the versatility and sophistication of the SCLC treatment, and the challenges associated with the design complexity and potential immunogenicity of NPs could be embraced as opportunities for innovation.

Conclusion

The connection between the *in vitro* findings and the potential clinical application is well-established, as the study not only identifies the target specificity of B7H3-ADC but also emphasizes its relevance for SCLC treatment. The use of 2D assays for early-stage drug screening provides a foundational understanding of the compound's efficacy, setting the stage for further exploration and potential translation to more complex *in vivo* models. The integration of 3D culture in microfluidic devices has been a crucial development in terms of drug screening and tumor microenvironment analysis. This technique has successfully bridged the gap between *in vitro* and *in vivo* models and has provided valuable insights into the complexities of the Tumor Microenvironment (TME). By enhancing the predictive value of preclinical testing, this technique has opened up new avenues for this study. Furthermore, it has enabled to gain a deeper understanding of the mechanisms underlying tumor mechanism of immune evasion.

Our research presents compelling evidence that B7H3 is a potential therapeutic target for SCLC, particularly in the Non-NE subtype, which has the worst prognosis. This sheds light on the diverse functions of B7H3 within the tumor microenvironment, contributing to a deeper investigation of its potential as a therapeutic target. These findings offer valuable insights for screening a B7H3-ADC-based therapy. We have also shown that B7H3's potential as a therapeutic target extends beyond its role in tumor cells to its influence on the tumor vasculature. This provides a unique opportunity for a comprehensive approach to treating SCLC. Additionally, our research demonstrates the cytotoxic effects of a B7H3-ADC specifically on Non-NE SCLC, highlighting its promising application as a targeted therapeutic strategy.

Notably, the expression of B7H3 on stromal components underscores its involvement in the vasculature. This dual expression, both on tumor cells and within the vascular network further emphasizes its potential to enhance vasculature permeability.

In addition, our study delves into the implications that this could lead in terms of dynamics of natural killer (NK) cells within the TME. Our findings elucidate that the vasculature functions as a formidable barrier hindering the infiltration of NK

Conclusion

cells into the tumor parenchyma. This observation underscores the intricate relationship between the tumor vasculature and immune cells, shedding light on potential challenges in harnessing the full cytotoxic potential of NK cells within the context of SCLC.

Moreover, we have compelling evidence that indicates the sensitivity of NE SCLC to NK cell-mediated cytotoxicity. This perspective not only encompasses the proof of a direct tumoricidal effect on Non-NE SCLC and tumor vasculature, but also highlights the potential for enhancing the permeability of this barrier, as well as the sensitivity of NE-SCLC to NK cell activity. This opens the door to investigate a combination therapy of B7H3-ADC and NK cell therapy, which would offer a powerful synergic strategy to enhance the efficacy of the treatment. This approach could be particularly effective in addressing intratumoral heterogeneity and immune evasion, hallmarks of this type of cancer, and would represent a revolutionary step in the realm of SCLC treatment.

References

- [1] H. Sung *et al.*, 'Global Cancer Statistics 2020: GLOBOCAN Estimates of Incidence and Mortality Worldwide for 36 Cancers in 185 Countries', *CA Cancer J Clin*, vol. 71, no. 3, pp. 209–249, May 2021, doi: 10.3322/caac.21660.
 - [2] M. Zheng, 'Classification and Pathology of Lung Cancer', *Surg Oncol Clin N Am*, vol. 25, no. 3, pp. 447–468, Jul. 2016, doi: 10.1016/j.soc.2016.02.003.
 - [3] A. Saltos, M. Shafique, and A. Chiappori, 'Update on the Biology, Management, and Treatment of Small Cell Lung Cancer (SCLC)', *Front Oncol*, vol. 10, Jul. 2020, doi: 10.3389/fonc.2020.01074.
 - [4] R. Govindan *et al.*, 'Changing epidemiology of small-cell lung cancer in the United States over the last 30 years: Analysis of the surveillance, epidemiologic, and end results database', *Journal of Clinical Oncology*, vol. 24, no. 28, pp. 4539–4544, Oct. 2006, doi: 10.1200/JCO.2005.04.4859.
 - [5] A. S. Jain *et al.*, 'Everything Old Is New Again: Drug Repurposing Approach for Non-Small Cell Lung Cancer Targeting MAPK Signaling Pathway', *Front Oncol*, vol. 11, Oct. 2021, doi: 10.3389/fonc.2021.741326.
 - [6] W. D. Travis *et al.*, 'The 2015 World Health Organization Classification of Lung Tumors: Impact of Genetic, Clinical and Radiologic Advances since the 2004 Classification', *Journal of Thoracic Oncology*, vol. 10, no. 9. Elsevier Inc, pp. 1243–1260, Sep. 26, 2015. doi: 10.1097/JTO.0000000000000630.
 - [7] E. Brambilla, W. D. Travis, T. V. Colby, B. Corrin, and Y. Shimosato, 'The new World Health Organization classification of lung tumours', *European Respiratory Journal*, vol. 18, no. 6, pp. 1059–1068, Dec. 2001, doi: 10.1183/09031936.01.00275301.
 - [8] S. N. Waqar and D. Morgensztern, 'Treatment advances in small cell lung cancer (SCLC)', *Pharmacol Ther*, vol. 180, pp. 16–23, Dec. 2017, doi: 10.1016/j.pharmthera.2017.06.002.
 - [9] L. A. Pikor, V. R. Ramnarine, S. Lam, and W. L. Lam, 'Genetic alterations defining NSCLC subtypes and their therapeutic implications', *Lung Cancer*, vol. 82, no. 2, pp. 179–189, Nov. 2013, doi: 10.1016/j.lungcan.2013.07.025.
 - [10] Q. Wang *et al.*, 'SCLC: Epidemiology, Risk Factors, Genetic Susceptibility, Molecular Pathology, Screening, and Early Detection', *Journal of Thoracic Oncology*, vol. 18, no. 1, pp. 31–46, Jan. 2023, doi: 10.1016/j.jtho.2022.10.002.
 - [11] A. F. Gazdar, P. A. Bunn, and J. D. Minna, 'Small-cell lung cancer: what we know, what we need to know and the path forward', *Nat Rev Cancer*, vol. 17, no. 12, pp. 725–737, Dec. 2017, doi: 10.1038/nrc.2017.87.
 - [12] A. Keogh, S. Finn, and T. Radonic, 'Emerging Biomarkers and the Changing Landscape of Small Cell Lung Cancer', *Cancers*, vol. 14, no. 15. MDPI, Aug. 01, 2022. doi: 10.3390/cancers14153772.
-

- [13] S. Wang, S. Zimmermann, K. Parikh, A. S. Mansfield, and A. A. Adjei, 'Current Diagnosis and Management of Small-Cell Lung Cancer', *Mayo Clin Proc*, vol. 94, no. 8, pp. 1599–1622, Aug. 2019, doi: 10.1016/j.mayocp.2019.01.034.
- [14] N. Roper *et al.*, 'Notch signaling and efficacy of PD-1/PD-L1 blockade in relapsed small cell lung cancer', *Nat Commun*, vol. 12, no. 1, p. 3880, Jun. 2021, doi: 10.1038/s41467-021-24164-y.
- [15] C. Belli *et al.*, 'Targeting the microenvironment in solid tumors', *Cancer Treat Rev*, vol. 65, pp. 22–32, Apr. 2018, doi: 10.1016/j.ctrv.2018.02.004.
- [16] M. G. Raso, N. Bota-Rabassedas, and I. I. Wistuba, 'Pathology and classification of SCLC', *Cancers*, vol. 13, no. 4. MDPI AG, pp. 1–11, Feb. 02, 2021. doi: 10.3390/cancers13040820.
- [17] K. Khalaf, D. Hana, J. T.-T. Chou, C. Singh, A. Mackiewicz, and M. Kaczmarek, 'Aspects of the Tumor Microenvironment Involved in Immune Resistance and Drug Resistance', *Front Immunol*, vol. 12, May 2021, doi: 10.3389/fimmu.2021.656364.
- [18] R. Nooreldeen and H. Bach, 'Current and Future Development in Lung Cancer Diagnosis', *Int J Mol Sci*, vol. 22, no. 16, p. 8661, Aug. 2021, doi: 10.3390/ijms22168661.
- [19] Y. Chen, H. Li, and Y. Fan, 'Shaping the tumor immune microenvironment of SCLC: Mechanisms, and opportunities for immunotherapy', *Cancer Treatment Reviews*, vol. 120. W.B. Saunders Ltd, Nov. 01, 2023. doi: 10.1016/j.ctrv.2023.102606.
- [20] A. Keogh, S. Finn, and T. Radonic, 'Emerging Biomarkers and the Changing Landscape of Small Cell Lung Cancer', *Cancers*, vol. 14, no. 15. MDPI, Aug. 01, 2022. doi: 10.3390/cancers14153772.
- [21] M. Binnewies *et al.*, 'Understanding the tumor immune microenvironment (TIME) for effective therapy', *Nat Med*, vol. 24, no. 5, pp. 541–550, May 2018, doi: 10.1038/s41591-018-0014-x.
- [22] N. R. Mahadevan *et al.*, 'Intrinsic immunogenicity of small cell lung carcinoma revealed by its cellular plasticity', *Cancer Discov*, vol. 11, no. 8, pp. 1952–1969, Aug. 2021, doi: 10.1158/2159-8290.CD-20-0913.
- [23] A. G. Nicholson *et al.*, 'The 2021 WHO Classification of Lung Tumors: Impact of Advances Since 2015', *Journal of Thoracic Oncology*, vol. 17, no. 3, pp. 362–387, Mar. 2022, doi: 10.1016/j.jtho.2021.11.003.
- [24] N. R. Mahadevan *et al.*, 'Intrinsic immunogenicity of small cell lung carcinoma revealed by its cellular plasticity', *Cancer Discov*, vol. 11, no. 8, pp. 1952–1969, Aug. 2021, doi: 10.1158/2159-8290.CD-20-0913.
- [25] M. D. Borromeo *et al.*, 'ASCL1 and NEUROD1 Reveal Heterogeneity in Pulmonary Neuroendocrine Tumors and Regulate Distinct Genetic Programs', *Cell Rep*, vol. 16, no. 5, pp. 1259–1272, Aug. 2016, doi: 10.1016/j.celrep.2016.06.081.
- [26] J. M. Chan *et al.*, 'Signatures of plasticity, metastasis, and immunosuppression in an atlas of human small cell lung cancer', *Cancer Cell*, vol. 39, no. 11, pp. 1479–1496.e18, Nov. 2021, doi: 10.1016/j.ccell.2021.09.008.
-

- [27] C. M. Rudin *et al.*, 'Molecular subtypes of small cell lung cancer: a synthesis of human and mouse model data', *Nature Reviews Cancer*, vol. 19, no. 5. Nature Publishing Group, pp. 289–297, May 01, 2019. doi: 10.1038/s41568-019-0133-9.
- [28] D. Hanahan and L. M. Coussens, 'Accessories to the Crime: Functions of Cells Recruited to the Tumor Microenvironment', *Cancer Cell*, vol. 21, no. 3. Cell Press, pp. 309–322, Mar. 20, 2012. doi: 10.1016/j.ccr.2012.02.022.
- [29] M. R. Junttila and F. J. De Sauvage, 'Influence of tumour micro-environment heterogeneity on therapeutic response', *Nature*, vol. 501, no. 7467. pp. 346–354, 2013. doi: 10.1038/nature12626.
- [30] U. M. Polanska and A. Orimo, 'Carcinoma-associated fibroblasts: Non-neoplastic tumour-promoting mesenchymal cells', *J Cell Physiol*, vol. 228, no. 8, pp. 1651–1657, Aug. 2013, doi: 10.1002/jcp.24347.
- [31] D. Johnson, R. O'Keefe, and J. Grandis, 'Targeting the IL-6/JAK/STAT3 signalling axis in cancer', vol. 8, Feb. 2018, doi: <https://doi.org/10.1038/nrclinonc.2018.8>.
- [32] J. W. Franses, A. B. Baker, V. C. Chitalia, and E. R. Edelman, 'Stromal Endothelial Cells Directly Influence Cancer Progression', *Sci Transl Med*, vol. 3, no. 66, Jan. 2011, doi: 10.1126/scitranslmed.3001542.
- [33] K. J. O'Byrne *et al.*, 'Vascular endothelial growth factor, platelet-derived endothelial cell growth factor and angiogenesis in non-small-cell lung cancer', *Br J Cancer*, vol. 82, no. 8, pp. 1427–1432, Apr. 2000, doi: 10.1054/bjoc.1999.1129.
- [34] K. Hida, N. Maishi, D. Annan, and Y. Hida, 'Contribution of Tumor Endothelial Cells in Cancer Progression', *Int J Mol Sci*, vol. 19, no. 5, p. 1272, Apr. 2018, doi: 10.3390/ijms19051272.
- [35] T. Tomita, M. Kato, and S. Hiratsuka, 'Regulation of vascular permeability in cancer metastasis', *Cancer Sci*, vol. 112, no. 8, pp. 2966–2974, Aug. 2021, doi: 10.1111/cas.14942.
- [36] P. Lu, V. M. Weaver, and Z. Werb, 'The extracellular matrix: A dynamic niche in cancer progression', *Journal of Cell Biology*, vol. 196, no. 4. pp. 395–406, 2012. doi: 10.1083/jcb.201102147.
- [37] N. K. Altorki *et al.*, 'The lung microenvironment: an important regulator of tumour growth and metastasis', *Nature Reviews Cancer*, vol. 19, no. 1. Nature Publishing Group, pp. 9–31, Jan. 01, 2019. doi: 10.1038/s41568-018-0081-9.
- [38] H. Salmon *et al.*, 'Matrix architecture defines the preferential localization and migration of T cells into the stroma of human lung tumors', *Journal of Clinical Investigation*, vol. 122, no. 3, pp. 899–910, Mar. 2012, doi: 10.1172/JCI45817.
- [39] N. K. Altorki *et al.*, 'The lung microenvironment: an important regulator of tumour growth and metastasis', *Nat Rev Cancer*, vol. 19, no. 1, pp. 9–31, Jan. 2019, doi: 10.1038/s41568-018-0081-9.
- [40] D. Hanahan and L. M. Coussens, 'Accessories to the Crime: Functions of Cells Recruited to the Tumor Microenvironment', *Cancer Cell*, vol. 21, no. 3, pp. 309–322, Mar. 2012, doi: 10.1016/j.ccr.2012.02.022.
-

- [41] K. Renner *et al.*, 'Metabolic Hallmarks of Tumor and Immune Cells in the Tumor Microenvironment', *Front Immunol*, vol. 8, Mar. 2017, doi: 10.3389/fimmu.2017.00248.
- [42] N. Nagarsheth, M. S. Wicha, and W. Zou, 'Chemokines in the cancer microenvironment and their relevance in cancer immunotherapy', *Nat Rev Immunol*, vol. 17, no. 9, pp. 559–572, Sep. 2017, doi: 10.1038/nri.2017.49.
- [43] Y. Tian *et al.*, 'Single-cell transcriptomic profiling reveals the tumor heterogeneity of small-cell lung cancer', *Signal Transduct Target Ther*, vol. 7, no. 1, p. 346, Oct. 2022, doi: 10.1038/s41392-022-01150-4.
- [44] H. L. Chen, D. Gabrilovich, R. Tampé, K. R. Girgis, S. Nadaf, and D. P. Carbone, 'A functionally defective allele of TAP1 results in loss of MHC class I antigen presentation in a human lung cancer', *Nat Genet*, vol. 13, no. 2, pp. 210–213, Jun. 1996, doi: 10.1038/ng0696-210.
- [45] M. L. Burr *et al.*, 'An Evolutionarily Conserved Function of Polycomb Silences the MHC Class I Antigen Presentation Pathway and Enables Immune Evasion in Cancer', *Cancer Cell*, vol. 36, no. 4, pp. 385–401.e8, Oct. 2019, doi: 10.1016/j.ccell.2019.08.008.
- [46] Y. Sun *et al.*, 'Characterization of PD-L1 protein expression and CD8+ tumor-infiltrating lymphocyte density, and their associations with clinical outcome in small-cell lung cancer', *Transl Lung Cancer Res*, vol. 8, no. 6, pp. 748–759, Dec. 2019, doi: 10.21037/tlcr.2019.10.09.
- [47] S. E. Busch, M. L. Hanke, J. Kargl, H. E. Metz, D. MacPherson, and A. M. Houghton, 'Lung Cancer Subtypes Generate Unique Immune Responses', *The Journal of Immunology*, vol. 197, no. 11, pp. 4493–4503, Dec. 2016, doi: 10.4049/jimmunol.1600576.
- [48] H. Wang *et al.*, 'Prognostic significance of PD-L1 expression and CD8+ T cell infiltration in pulmonary neuroendocrine tumors', *Diagn Pathol*, vol. 13, no. 1, p. 30, Dec. 2018, doi: 10.1186/s13000-018-0712-1.
- [49] D. Carvajal-Hausdorf *et al.*, 'Expression and clinical significance of PD-L1, B7-H3, B7-H4 and TILs in human small cell lung Cancer (SCLC)', *J Immunother Cancer*, vol. 7, no. 1, p. 65, Dec. 2019, doi: 10.1186/s40425-019-0540-1.
- [50] Y. Chen, Y. Jin, X. Hu, and M. Chen, 'Infiltrating T lymphocytes in the tumor microenvironment of small cell lung cancer: a state of knowledge review', *J Cancer Res Clin Oncol*, vol. 148, no. 4, pp. 881–895, Apr. 2022, doi: 10.1007/s00432-021-03895-x.
- [51] R. Yazdani, M. Sharifi, A. S. Shirvan, G. Azizi, and M. Ganjalikhani-Hakemi, 'Characteristics of innate lymphoid cells (ILCs) and their role in immunological disorders (an update)', *Cell Immunol*, vol. 298, no. 1–2, pp. 66–76, Nov. 2015, doi: 10.1016/j.cellimm.2015.09.006.
- [52] A. J. Ozga, M. T. Chow, and A. D. Luster, 'Chemokines and the immune response to cancer', *Immunity*, vol. 54, no. 5, pp. 859–874, May 2021, doi: 10.1016/j.immuni.2021.01.012.
-

- [53] H.-G. Ljunggren and K. Kärre, 'In search of the "missing self": MHC molecules and NK cell recognition', *Immunol Today*, vol. 11, pp. 237–244, Jan. 1990, doi: 10.1016/0167-5699(90)90097-S.
- [54] A. Cerwenka, J. L. Baron, and L. L. Lanier, 'Ectopic expression of retinoic acid early inducible-1 gene (RAE-1) permits natural killer cell-mediated rejection of a MHC class I-bearing tumor *in vivo*', *Proceedings of the National Academy of Sciences*, vol. 98, no. 20, pp. 11521–11526, Sep. 2001, doi: 10.1073/pnas.201238598.
- [55] H. J. Pegram, D. M. Andrews, M. J. Smyth, P. K. Darcy, and M. H. Kershaw, 'Activating and inhibitory receptors of natural killer cells', *Immunol Cell Biol*, vol. 89, no. 2, pp. 216–224, Feb. 2011, doi: 10.1038/icb.2010.78.
- [56] W. Wang, A. K. Erbe, J. A. Hank, Z. S. Morris, and P. M. Sondel, 'NK cell-mediated antibody-dependent cellular cytotoxicity in cancer immunotherapy', *Frontiers in Immunology*, vol. 6, no. JUL. Frontiers Research Foundation, 2015. doi: 10.3389/fimmu.2015.00368.
- [57] A. J. Anandappa, C. J. Wu, and P. A. Ott, 'Directing traffic: How to effectively drive t cells into tumors', *Cancer Discovery*, vol. 10, no. 2. American Association for Cancer Research Inc., pp. 185–197, Feb. 01, 2020. doi: 10.1158/2159-8290.CD-19-0790.
- [58] Y. Tian *et al.*, 'Single-cell transcriptomic profiling reveals the tumor heterogeneity of small-cell lung cancer', *Signal Transduct Target Ther*, vol. 7, no. 1, Dec. 2022, doi: 10.1038/s41392-022-01150-4.
- [59] N. Milošević, M. Rütter, and A. David, 'Endothelial Cell Adhesion Molecules-(un)Attainable Targets for Nanomedicines', *Front Med Technol*, vol. 4, Apr. 2022, doi: 10.3389/fmedt.2022.846065.
- [60] D. Wan, W. Jiang, and J. Hao, 'Research Advances in How the cGAS-STING Pathway Controls the Cellular Inflammatory Response', *Front Immunol*, vol. 11, Apr. 2020, doi: 10.3389/fimmu.2020.00615.
- [61] E. H. Knelson *et al.*, 'Activation of Tumor-Cell STING Primes NK-Cell Therapy', *Cancer Immunol Res*, vol. 10, no. 8, pp. 947–961, Aug. 2022, doi: 10.1158/2326-6066.CIR-22-0017.
- [62] F. Pu, F. Chen, J. Liu, Z. Zhang, and Z. Shao, 'Immune Regulation of the cGAS-STING Signaling Pathway in the Tumor Microenvironment and Its Clinical Application', *Oncotargets Ther*, vol. Volume 14, pp. 1501–1516, Mar. 2021, doi: 10.2147/OTT.S298958.
- [63] N. Samson and A. Ablasser, 'The cGAS–STING pathway and cancer', *Nat Cancer*, vol. 3, no. 12, pp. 1452–1463, Dec. 2022, doi: 10.1038/s43018-022-00468-w.
- [64] M. Campisi *et al.*, 'Tumor-Derived cGAMP Regulates Activation of the Vasculature', *Front Immunol*, vol. 11, Sep. 2020, doi: 10.3389/fimmu.2020.02090.
- [65] K. Krpina, S. Vranić, K. Tomić, M. Samaržija, and L. Batičić, 'Small Cell Lung Carcinoma: Current Diagnosis, Biomarkers, and Treatment Options with Future Perspectives', *Biomedicines*, vol. 11, no. 7, p. 1982, Jul. 2023, doi: 10.3390/biomedicines11071982.
-

- [66] T. Li and T. Qiao, 'Unraveling tumor microenvironment of small-cell lung cancer: Implications for immunotherapy', *Seminars in Cancer Biology*, vol. 86. Academic Press, pp. 117–125, Nov. 01, 2022. doi: 10.1016/j.semcancer.2022.09.005.
- [67] C. M. Rudin, E. Brambilla, C. Faivre-Finn, and J. Sage, 'Small-cell lung cancer', *Nat Rev Dis Primers*, vol. 7, no. 1, p. 3, Jan. 2021, doi: 10.1038/s41572-020-00235-0.
- [68] F. Facchinetti, M. Di Maio, and M. Tiseo, 'Adding PD-1/PD-L1 Inhibitors to Chemotherapy for the First-Line Treatment of Extensive Stage Small Cell Lung Cancer (SCLC): A Meta-Analysis of Randomized Trials', *Cancers (Basel)*, vol. 12, no. 9, p. 2645, Sep. 2020, doi: 10.3390/cancers12092645.
- [69] J. H. Schiller, 'Current Standards of Care in Small-Cell and Non-Small-Cell Lung Cancer', *Oncology*, vol. 61, no. Suppl. 1, pp. 3–13, 2001, doi: 10.1159/000055386.
- [70] J. T. Poirier *et al.*, 'New Approaches to SCLC Therapy: From the Laboratory to the Clinic', *Journal of Thoracic Oncology*, vol. 15, no. 4, pp. 520–540, Apr. 2020, doi: 10.1016/j.jtho.2020.01.016.
- [71] M. Yarchoan, A. Hopkins, and E. M. Jaffee, 'Tumor Mutational Burden and Response Rate to PD-1 Inhibition', *New England Journal of Medicine*, vol. 377, no. 25, pp. 2500–2501, Dec. 2017, doi: 10.1056/NEJMc1713444.
- [72] L. Horn *et al.*, 'First-Line Atezolizumab plus Chemotherapy in Extensive-Stage Small-Cell Lung Cancer', *New England Journal of Medicine*, vol. 379, no. 23, pp. 2220–2229, Dec. 2018, doi: 10.1056/NEJMoa1809064.
- [73] S. F. Nassar, K. Raddassi, B. Ubhi, J. Doktorski, and A. Abulaban, 'Precision Medicine: Steps along the Road to Combat Human Cancer', *Cells*, vol. 9, no. 9, p. 2056, Sep. 2020, doi: 10.3390/cells9092056.
- [74] F. Mosele *et al.*, 'Recommendations for the use of next-generation sequencing (NGS) for patients with metastatic cancers: a report from the ESMO Precision Medicine Working Group', *Annals of Oncology*, vol. 31, no. 11, pp. 1491–1505, Nov. 2020, doi: 10.1016/j.annonc.2020.07.014.
- [75] S. R. Patel and M. Das, 'Small Cell Lung Cancer: Emerging Targets and Strategies for Precision Therapy', *Cancers*, vol. 15, no. 16. Multidisciplinary Digital Publishing Institute (MDPI), Aug. 01, 2023. doi: 10.3390/cancers15164016.
- [76] E. N. Baruch, A. L. Berg, M. J. Besser, J. Schachter, and G. Markel, 'Adoptive T cell therapy: An overview of obstacles and opportunities', *Cancer*, vol. 123, no. S11, pp. 2154–2162, Jun. 2017, doi: 10.1002/cncr.30491.
- [77] M. Mata and S. Gottschalk, 'Engineering for Success: Approaches to Improve Chimeric Antigen Receptor T Cell Therapy for Solid Tumors', *Drugs*, vol. 79, no. 4, pp. 401–415, Mar. 2019, doi: 10.1007/s40265-019-01071-7.
- [78] C. H. June, R. S. O'Connor, O. U. Kawalekar, S. Ghassemi, and M. C. Milone, 'CAR T cell immunotherapy for human cancer', *Science (1979)*, vol. 359, no. 6382, pp. 1361–1365, Mar. 2018, doi: 10.1126/science.aar6711.
- [79] K.-J. Malmberg, M. Carlsten, A. Björklund, E. Sohlberg, Y. T. Bryceson, and H.-G. Ljunggren, 'Natural killer cell-mediated immunosurveillance of human cancer', *Semin Immunol*, vol. 31, pp. 20–29, Jun. 2017, doi: 10.1016/j.smim.2017.08.002.
-

- [80] N. T. Joncker, N. Shifrin, F. Delebecque, and D. H. Raulet, 'Mature natural killer cells reset their responsiveness when exposed to an altered MHC environment', *Journal of Experimental Medicine*, vol. 207, no. 10, pp. 2065–2072, Sep. 2010, doi: 10.1084/jem.20100570.
- [81] J. Xiao *et al.*, 'Natural Killer Cells: A Promising Kit in the Adoptive Cell Therapy Toolbox', *Cancers (Basel)*, vol. 14, no. 22, p. 5657, Nov. 2022, doi: 10.3390/cancers14225657.
- [82] D. M. K. Keefe and E. H. Bateman, 'Tumor control versus adverse events with targeted anticancer therapies', *Nat Rev Clin Oncol*, vol. 9, no. 2, pp. 98–109, Feb. 2012, doi: 10.1038/nrclinonc.2011.192.
- [83] A. Desai, P. Abdayem, A. A. Adjei, and D. Planchard, 'Antibody-drug conjugates: A promising novel therapeutic approach in lung cancer', *Lung Cancer*, vol. 163, Elsevier Ireland Ltd, pp. 96–106, Jan. 01, 2022. doi: 10.1016/j.lungcan.2021.12.002.
- [84] D. Schrama, R. A. Reisfeld, and J. C. Becker, 'Antibody targeted drugs as cancer therapeutics', *Nature Reviews Drug Discovery*, vol. 5, no. 2, pp. 147–159, Feb. 2006. doi: 10.1038/nrd1957.
- [85] A. Thomas, B. A. Teicher, and R. Hassan, 'Antibody–drug conjugates for cancer therapy', *Lancet Oncol*, vol. 17, no. 6, pp. e254–e262, Jun. 2016, doi: 10.1016/S1470-2045(16)30030-4.
- [86] C. H. Chau, P. S. Steeg, and W. D. Figg, 'Antibody-drug conjugates for cancer', 2019. [Online]. Available: www.thelancet.com
- [87] U. J. E. Seidel, P. Schlegel, and P. Lang, 'Natural Killer Cell Mediated Antibody-Dependent Cellular Cytotoxicity in Tumor Immunotherapy with Therapeutic Antibodies', *Front Immunol*, vol. 4, 2013, doi: 10.3389/fimmu.2013.00076.
- [88] M. J. Smyth *et al.*, 'Activation of NK cell cytotoxicity', *Mol Immunol*, vol. 42, no. 4, pp. 501–510, Feb. 2005, doi: 10.1016/j.molimm.2004.07.034.
- [89] A. Poli, T. Michel, M. Thérésine, E. Andrès, F. Hentges, and J. Zimmer, 'CD56^{bright} natural killer (NK) cells: an important NK cell subset', *Immunology*, vol. 126, no. 4, pp. 458–465, Apr. 2009, doi: 10.1111/j.1365-2567.2008.03027.x.
- [90] P. Gogia, H. Ashraf, S. Bhasin, and Y. Xu, 'Antibody–Drug Conjugates: A Review of Approved Drugs and Their Clinical Level of Evidence', *Cancers (Basel)*, vol. 15, no. 15, p. 3886, Jul. 2023, doi: 10.3390/cancers15153886.
- [91] H. Maecker, V. Jonnalagadda, S. Bhakta, V. Jammalamadaka, and J. R. Junutula, 'Exploration of the antibody–drug conjugate clinical landscape', *MAbs*, vol. 15, no. 1, Dec. 2023, doi: 10.1080/19420862.2023.2229101.
- [92] J. Z. Drago, S. Modi, and S. Chandarlapaty, 'Unlocking the potential of antibody–drug conjugates for cancer therapy', *Nat Rev Clin Oncol*, vol. 18, no. 6, pp. 327–344, Jun. 2021, doi: 10.1038/s41571-021-00470-8.
- [93] H. Xie and A. A. Adjei, 'Antibody-Drug Conjugates for the Therapy of Thoracic Malignancies', *Journal of Thoracic Oncology*, vol. 14, no. 3, pp. 358–376, Mar. 2019, doi: 10.1016/j.jtho.2018.11.034.
-

- [94] T. Nakada *et al.*, 'Novel antibody drug conjugates containing exatecan derivative-based cytotoxic payloads', *Bioorg Med Chem Lett*, vol. 26, no. 6, pp. 1542–1545, Mar. 2016, doi: 10.1016/j.bmcl.2016.02.020.
- [95] Y. Ogitani *et al.*, 'DS-8201a, A Novel HER2-Targeting ADC with a Novel DNA Topoisomerase I Inhibitor, Demonstrates a Promising Antitumor Efficacy with Differentiation from T-DM1', *Clinical Cancer Research*, vol. 22, no. 20, pp. 5097–5108, Oct. 2016, doi: 10.1158/1078-0432.CCR-15-2822.
- [96] D. Neri and R. Bicknell, 'Tumour vascular targeting', *Nat Rev Cancer*, vol. 5, no. 6, pp. 436–446, Jun. 2005, doi: 10.1038/nrc1627.
- [97] H.-P. Gerber, P. D. Senter, and I. S. Grewal, 'Antibody drug-conjugates targeting the tumor vasculature', *MAbs*, vol. 1, no. 3, pp. 247–253, May 2009, doi: 10.4161/mabs.1.3.8515.
- [98] A. Abdollahi and J. Folkman, 'Evading tumor evasion: Current concepts and perspectives of anti-angiogenic cancer therapy', *Drug Resistance Updates*, vol. 13, no. 1–2, pp. 16–28, Feb. 2010, doi: 10.1016/j.drug.2009.12.001.
- [99] K. Akiyama *et al.*, 'Tumor Endothelial Cells Acquire Drug Resistance by MDR1 Up-Regulation via VEGF Signaling in Tumor Microenvironment', *Am J Pathol*, vol. 180, no. 3, pp. 1283–1293, Mar. 2012, doi: 10.1016/j.ajpath.2011.11.029.
- [100] V. Gardner, C. O. Madu, and Y. Lu, 'Anti-VEGF Therapy in Cancer: A Double-Edged Sword', in *Physiologic and Pathologic Angiogenesis - Signaling Mechanisms and Targeted Therapy*, InTech, 2017. doi: 10.5772/66763.
- [101] S. Seaman *et al.*, 'Eradication of Tumors through Simultaneous Ablation of CD276/B7-H3-Positive Tumor Cells and Tumor Vasculature', *Cancer Cell*, vol. 31, no. 4, pp. 501–515.e8, Apr. 2017, doi: 10.1016/j.ccell.2017.03.005.
- [102] F. P. Fabrizio, L. A. Muscarella, and A. Rossi, 'B7-H3/CD276 and small-cell lung cancer: What's new?', *Transl Oncol*, vol. 39, Jan. 2024, doi: 10.1016/j.tranon.2023.101801.
- [103] A. A. Getu, A. Tigabu, M. Zhou, J. Lu, Ø. Fodstad, and M. Tan, 'New frontiers in immune checkpoint B7-H3 (CD276) research and drug development', *Mol Cancer*, vol. 22, no. 1, p. 43, Mar. 2023, doi: 10.1186/s12943-023-01751-9.
- [104] F. Kontos *et al.*, 'B7-H3: An Attractive Target for Antibody-based Immunotherapy', *Clinical Cancer Research*, vol. 27, no. 5, pp. 1227–1235, Mar. 2021, doi: 10.1158/1078-0432.CCR-20-2584.
- [105] Y. H. Lee *et al.*, 'Inhibition of the B7-H3 immune checkpoint limits tumor growth by enhancing cytotoxic lymphocyte function', *Cell Res*, vol. 27, no. 8, pp. 1034–1045, Aug. 2017, doi: 10.1038/cr.2017.90.
- [106] T. Doi *et al.*, '453O DS-7300 (B7-H3 DXd antibody-drug conjugate [ADC]) shows durable antitumor activity in advanced solid tumors: Extended follow-up of a phase I/II study', *Annals of Oncology*, vol. 33, pp. S744–S745, Sep. 2022, doi: 10.1016/j.annonc.2022.07.582.
- [107] M. Yamato *et al.*, 'DS-7300a, a DNA Topoisomerase I Inhibitor, DXd-Based Antibody–Drug Conjugate Targeting B7-H3, Exerts Potent Antitumor Activities in
-

- Preclinical Models', *Mol Cancer Ther*, vol. 21, no. 4, pp. 635–646, Apr. 2022, doi: 10.1158/1535-7163.MCT-21-0554.
- [108] D. Sun, W. Gao, H. Hu, and S. Zhou, 'Why 90% of clinical drug development fails and how to improve it?', *Acta Pharm Sin B*, vol. 12, no. 7, pp. 3049–3062, Jul. 2022, doi: 10.1016/j.apsb.2022.02.002.
- [109] J. A. MacArthur Clark and D. Sun, 'Guidelines for the ethical review of laboratory animal welfare People's Republic of China National Standard GB/T 35892-2018 [Issued 6 February 2018 Effective from 1 September 2018]', *Animal Model Exp Med*, vol. 3, no. 1, pp. 103–113, Mar. 2020, doi: 10.1002/ame2.12111.
- [110] N. Franco and I. Olsson, 'Scientists and the 3Rs: attitudes to animal use in biomedical research and the effect of mandatory training in laboratory animal science', *Lab Anim*, vol. 48, no. 1, pp. 50–60, Jan. 2014, doi: 10.1177/0023677213498717.
- [111] J. P. Mather, 'In vitro models', *Stem Cells*, vol. 30, no. 2, pp. 95–99, Feb. 2012, doi: 10.1002/stem.774.
- [112] K. Halfter and B. Mayer, 'Bringing 3D tumor models to the clinic – predictive value for personalized medicine', *Biotechnol J*, vol. 12, no. 2, Feb. 2017, doi: 10.1002/biot.201600295.
- [113] J. Giacomotto and L. Ségalat, 'High-throughput screening and small animal models, where are we?', *Br J Pharmacol*, vol. 160, no. 2, pp. 204–216, May 2010, doi: 10.1111/j.1476-5381.2010.00725.x.
- [114] S. Breslin and L. O'Driscoll, 'Three-dimensional cell culture: the missing link in drug discovery', *Drug Discov Today*, vol. 18, no. 5–6, pp. 240–249, Mar. 2013, doi: 10.1016/j.drudis.2012.10.003.
- [115] M. E. Katt, A. L. Placone, A. D. Wong, Z. S. Xu, and P. C. Searson, 'In Vitro Tumor Models: Advantages, Disadvantages, Variables, and Selecting the Right Platform', *Front Bioeng Biotechnol*, vol. 4, Feb. 2016, doi: 10.3389/fbioe.2016.00012.
- [116] W. N. Hait, 'Anticancer drug development: the grand challenges', *Nat Rev Drug Discov*, vol. 9, no. 4, pp. 253–254, Apr. 2010, doi: 10.1038/nrd3144.
- [117] A. L. Hopkins, 'Network pharmacology: the next paradigm in drug discovery', *Nat Chem Biol*, vol. 4, no. 11, pp. 682–690, Nov. 2008, doi: 10.1038/nchembio.118.
- [118] S. N. Bhatia and D. E. Ingber, 'Microfluidic organs-on-chips', *Nat Biotechnol*, vol. 32, no. 8, pp. 760–772, Aug. 2014, doi: 10.1038/nbt.2989.
- [119] M. Campisi, S. E. Shelton, M. Chen, R. D. Kamm, D. A. Barbie, and E. H. Knelson, 'Engineered Microphysiological Systems for Testing Effectiveness of Cell-Based Cancer Immunotherapies', *Cancers*, vol. 14, no. 15, MDPI, Aug. 01, 2022. doi: 10.3390/cancers14153561.
- [120] A. Sontheimer-Phelps, B. A. Hassell, and D. E. Ingber, 'Modelling cancer in microfluidic human organs-on-chips', *Nat Rev Cancer*, vol. 19, no. 2, pp. 65–81, Feb. 2019, doi: 10.1038/s41568-018-0104-6.
-

- [121] H. Wang, T. Xu, and D. Yin, 'Emerging trends in the methodology of environmental toxicology: 3D cell culture and its applications', *Science of The Total Environment*, vol. 857, p. 159501, Jan. 2023, doi: 10.1016/j.scitotenv.2022.159501.
- [122] Y. Xing *et al.*, 'Engineering organoid microfluidic system for biomedical and health engineering: A review', *Chin J Chem Eng*, vol. 30, pp. 244–254, Feb. 2021, doi: 10.1016/j.cjche.2020.11.013.
- [123] R. Curvello, V. Kast, P. Ordóñez-Morán, A. Mata, and D. Loessner, 'Biomaterial-based platforms for tumour tissue engineering', *Nat Rev Mater*, vol. 8, no. 5, pp. 314–330, Feb. 2023, doi: 10.1038/s41578-023-00535-3.
- [124] G. M. Whitesides, 'The origins and the future of microfluidics', *Nature*, vol. 442, no. 7101, pp. 368–373, Jul. 2006, doi: 10.1038/nature05058.
- [125] A.-G. Niculescu, C. Chircov, A. C. Bîrcă, and A. M. Grumezescu, 'Fabrication and Applications of Microfluidic Devices: A Review', *Int J Mol Sci*, vol. 22, no. 4, p. 2011, Feb. 2021, doi: 10.3390/ijms22042011.
- [126] X. Zhu, K. Wang, H. Yan, C. Liu, X. Zhu, and B. Chen, 'Microfluidics as an Emerging Platform for Exploring Soil Environmental Processes: A Critical Review', *Environ Sci Technol*, vol. 56, no. 2, pp. 711–731, Jan. 2022, doi: 10.1021/acs.est.1c03899.
- [127] P. De Stefano, E. Bianchi, and G. Dubini, 'The impact of microfluidics in high-throughput drug-screening applications', *Biomicrofluidics*, vol. 16, no. 3, May 2022, doi: 10.1063/5.0087294.
- [128] J. M. Ayuso *et al.*, 'Tumor-on-a-chip: a microfluidic model to study cell response to environmental gradients', *Lab Chip*, vol. 19, no. 20, pp. 3461–3471, 2019, doi: 10.1039/C9LC00270G.
- [129] P. Chen, S. Li, Y. Guo, X. Zeng, and B.-F. Liu, 'A review on microfluidics manipulation of the extracellular chemical microenvironment and its emerging application to cell analysis', *Anal Chim Acta*, vol. 1125, pp. 94–113, Aug. 2020, doi: 10.1016/j.aca.2020.05.065.
- [130] J. Farhat, I. Pandey, and M. AlWahsh, 'Transcending toward Advanced 3D-Cell Culture Modalities: A Review about an Emerging Paradigm in Translational Oncology', *Cells*, vol. 10, no. 7, p. 1657, Jul. 2021, doi: 10.3390/cells10071657.
- [131] M. L. Coluccio *et al.*, 'Microfluidic platforms for cell cultures and investigations', *Microelectron Eng*, vol. 208, pp. 14–28, Mar. 2019, doi: 10.1016/j.mee.2019.01.004.
- [132] A. Tony *et al.*, 'The Additive Manufacturing Approach to Polydimethylsiloxane (PDMS) Microfluidic Devices: Review and Future Directions', *Polymers (Basel)*, vol. 15, no. 8, p. 1926, Apr. 2023, doi: 10.3390/polym15081926.
- [133] A.-G. Niculescu, C. Chircov, A. C. Bîrcă, and A. M. Grumezescu, 'Fabrication and Applications of Microfluidic Devices: A Review', *Int J Mol Sci*, vol. 22, no. 4, p. 2011, Feb. 2021, doi: 10.3390/ijms22042011.
- [134] M. A. Rose, J. J. Bowen, and S. A. Morin, 'Emergent Soft Lithographic Tools for the Fabrication of Functional Polymeric Microstructures', *ChemPhysChem*, vol. 20, no. 7, pp. 909–925, Apr. 2019, doi: 10.1002/cphc.201801140.
-

- [135] S. Scott and Z. Ali, 'Fabrication Methods for Microfluidic Devices: An Overview', *Micromachines (Basel)*, vol. 12, no. 3, p. 319, Mar. 2021, doi: 10.3390/mi12030319.
- [136] V. Mehta and S. N. Rath, '3D printed microfluidic devices: a review focused on four fundamental manufacturing approaches and implications on the field of healthcare', *Biodes Manuf*, vol. 4, no. 2, pp. 311–343, Jun. 2021, doi: 10.1007/s42242-020-00112-5.
- [137] Y.-J. Juang and Y.-J. Chiu, 'Fabrication of Polymer Microfluidics: An Overview', *Polymers (Basel)*, vol. 14, no. 10, p. 2028, May 2022, doi: 10.3390/polym14102028.
- [138] K. Giri and C.-W. Tsao, 'Recent Advances in Thermoplastic Microfluidic Bonding', *Micromachines (Basel)*, vol. 13, no. 3, p. 486, Mar. 2022, doi: 10.3390/mi13030486.
- [139] G. Imparato, F. Urciuolo, and P. A. Netti, 'Organ on Chip Technology to Model Cancer Growth and Metastasis', *Bioengineering*, vol. 9, no. 1, p. 28, Jan. 2022, doi: 10.3390/bioengineering9010028.
- [140] J. Skommer, Z. Darzynkiewicz, and D. Wlodkovic, 'Cell death goes LIVE: Technological advances in real-time tracking of cell death', *Cell Cycle*, vol. 9, no. 12, pp. 2330–2341, Jun. 2010, doi: 10.4161/cc.9.12.11911.
- [141] S. Damiati, U. Kompella, S. Damiati, and R. Kodzius, 'Microfluidic Devices for Drug Delivery Systems and Drug Screening', *Genes (Basel)*, vol. 9, no. 2, p. 103, Feb. 2018, doi: 10.3390/genes9020103.
- [142] Y. Li, H. Fan, J. Ding, J. Xu, C. Liu, and H. Wang, 'Microfluidic devices: The application in TME modeling and the potential in immunotherapy optimization', *Front Genet*, vol. 13, Sep. 2022, doi: 10.3389/fgene.2022.969723.
- [143] R. S. Zolot, S. Basu, and R. P. Million, 'Antibody-drug conjugates', *Nature Reviews Drug Discovery*, vol. 12, no. 4, pp. 259–260, Apr. 2013. doi: 10.1038/nrd3980.
- [144] D. H. Owen, M. J. Giffin, J. M. Bailis, M.-A. D. Smit, D. P. Carbone, and K. He, 'DLL3: an emerging target in small cell lung cancer', *J Hematol Oncol*, vol. 12, no. 1, p. 61, Dec. 2019, doi: 10.1186/s13045-019-0745-2.
- [145] D. Uprety, J. Remon, and A. A. Adjei, 'All That Glitters Is Not Gold: The Story of Rovalpituzumab Tesirine in SCLC', *Journal of Thoracic Oncology*, vol. 16, no. 9, pp. 1429–1433, Sep. 2021, doi: 10.1016/j.jtho.2021.07.012.
- [146] A. Desai, P. Abdayem, A. A. Adjei, and D. Planchard, 'Antibody-drug conjugates: A promising novel therapeutic approach in lung cancer', *Lung Cancer*, vol. 163, Elsevier Ireland Ltd, pp. 96–106, Jan. 01, 2022. doi: 10.1016/j.lungcan.2021.12.002.
- [147] L. Paz-Ares *et al.*, '1550TiP Phase II, multicenter, randomized, open-label study of DS-7300 in patients (pts) with pre-treated extensive-stage small cell lung cancer (ES-SCLC)', *Annals of Oncology*, vol. 33, pp. S1255–S1256, Sep. 2022, doi: 10.1016/j.annonc.2022.07.1644.
-

- [148] S. Martinez-Pacheco and L. O’driscoll, ‘Pre-clinical *in vitro* models used in cancer research: Results of a worldwide survey’, *Cancers (Basel)*, vol. 13, no. 23, Dec. 2021, doi: 10.3390/cancers13236033.
- [149] K. E. Sung and D. J. Beebe, ‘Microfluidic 3D models of cancer’, *Adv Drug Deliv Rev*, vol. 79–80, pp. 68–78, Dec. 2014, doi: 10.1016/j.addr.2014.07.002.
- [150] E. H. Knelson *et al.*, ‘Activation of Tumor-Cell STING Primes NK-Cell Therapy’, *Cancer Immunol Res*, vol. 10, no. 8, pp. 947–961, Aug. 2022, doi: 10.1158/2326-6066.CIR-22-0017.
- [151] A. Dellaquila, C. Le Bao, D. Letourneur, and T. Simon-Yarza, ‘*In Vitro* Strategies to Vascularize 3D Physiologically Relevant Models’, *Advanced Science*, vol. 8, no. 19, Oct. 2021, doi: 10.1002/advs.202100798.
- [152] F. Roncato *et al.*, ‘Improvement and extension of anti-EGFR targeting in breast cancer therapy by integration with the Avidin-Nucleic-Acid-Nano-Assemblies’, *Nat Commun*, vol. 9, no. 1, p. 4070, Oct. 2018, doi: 10.1038/s41467-018-06602-6.
- [153] D. Lombardo, M. A. Kiselev, and M. T. Caccamo, ‘Smart Nanoparticles for Drug Delivery Application: Development of Versatile Nanocarrier Platforms in Biotechnology and Nanomedicine’, *J Nanomater*, vol. 2019, pp. 1–26, Feb. 2019, doi: 10.1155/2019/3702518.
- [154] A. Simonazzi, A. G. Cid, M. Villegas, A. I. Romero, S. D. Palma, and J. M. Bermúdez, ‘Nanotechnology applications in drug controlled release’, in *Drug Targeting and Stimuli Sensitive Drug Delivery Systems*, Elsevier, 2018, pp. 81–116. doi: 10.1016/B978-0-12-813689-8.00003-3.
- [155] A. Lucas *et al.*, ‘Factors Affecting the Pharmacology of Antibody–Drug Conjugates’, *Antibodies*, vol. 7, no. 1, p. 10, Feb. 2018, doi: 10.3390/antib7010010.
- [156] N. R. Mahadevan *et al.*, ‘Intrinsic immunogenicity of small cell lung carcinoma revealed by its cellular plasticity’, *Cancer Discov*, vol. 11, no. 8, pp. 1952–1969, Aug. 2021, doi: 10.1158/2159-8290.CD-20-0913.
-